Multilayered Magneto-optical Recording Media for High-speed, High-density Storage

(高速高密度記録用光磁気多層媒体の研究)

Haruhisa Miyamoto

(宮本 晴一)

Multilayered Magneto-optical Recording Media for High-speed, High-density Storage

Harukazu Miyamoto

Abstract

Multilayered magneto-optical (MO) media were studied in order to achieve high-speed, high-density MO recording. The relationship between the recording characteristics and the multilayered MO disk structure was analyzed from the viewpoints of three kinds of physical properties: thermal, magnetic, and optical. The analysis was performed both numerically and experimentally.

Two optical properties, Kerr rotation and reflectivity, were studied through optical simulation and experiment. The experimental results for Kerr rotation in multilayered MO disks were successfully simulated by using a multiple-reflection model of magnetically induced circular dichroism. This led to the most suitable optical structures: a quadrilayered structure with a metal reflective layer, and a magnetic bilayer with a readout magnetic layer.

The thermal properties of MO disks were studied by analyzing the relationship between the recording characteristics and the thermal structure of the media for magnetic-field modulation overwriting. Thermal simulation combined with a domain-formation model showed the relationship between the media structure, the recording characteristics, and the recorded domain shape. This led to the most suitable thermal structure: a quadrilayered structure with a thermal-diffusive metal layer.

Magnetic multilayers for light-intensity modulation overwriting (LMO) were studied. Problems occur in LMO because it requires two levels of laser power for overwriting and because it uses magnetic exchange-coupling between layers. The former results in a narrow power margin and thermal crosstalk. The latter results in initialization noise and degradation after the repetitive overwriting. Domain transfer was applied in order to expand the readout power margin, although a slight increase in the noise level was observed when the readout power was high. The thermal crosstalk was analyzed, then effectively reduced by using comb-shaped laser pulses and a disk with a thick thermal diffusion layer. A noise increase after initialization was detected and eliminated by using a transition-metal dominant memory layer having a large effective coercivity. Arrhenius analysis of overwrite

repeatability revealed the degradation mode characteristics of LMO; the degradation was eliminated by using a memory layer having high domain wall coercivity. Application of mark-edge recording resulted in an LMO disk with 2-GB capacity on an 130-mm-diameter disk.

To achieve high-density recording, small-domain recording and small-domain readout techniques were studied. Magnetic-field modulation with pulsed-laser irradiation was shown to perform well for small-domain recording. Use of a rapid signal change on a magnetic super-resolution medium provided good small-domain readout performance. Combining these two high-density techniques promises to double the recording density of MO disks.

The most suitable form for high-density, high-speed magneto-optical recording is a combination of magnetically induced super-resolution using the readout layer for a short wavelength laser and magnetic-field modulation with pulsed-laser irradiation.

Contents

1 Introduction

In today's information-oriented society, the word "multimedia" has been attracting the attention of people all over the world. In a multimedia system, information, such as audio and video materials, is treated in a digital form. This has led to a dramatic increase in the quantity of information to be handled. Large-capacity storage systems are thus needed to store and to manage this information.

Optical storage is a practical approach to large-capacity storage systems. In optical disk systems, information stored in a small optical spot is accessed. This access can be performed with a relatively large distance between the medium and the head because the optical (laser) beam used is focusable onto a small spot (≤ 1 μm). Therefore, optical disk systems have both high reliability and media-removability.

Optical disks are classified into three types, read-only, write-once, and rewritable. The read-only type, such as compact disks (CDs) and video disks, are widely used in the audio and visual fields. This type of optical disk stores information as physical pits covered with a metal reflection layer. The pits are formed by replication using a master stamper, which enables low-cost mass production. The write-once type of optical disk [1.1] is widely used for archival file systems in libraries and offices because the recorded information is preserved semipermanently. The information is recorded by forming irreversible holes or protuberances on the recording layer, which is made of chalcogenide or organic dye. The rewritable type of optical disk is used in magneto-optical (MO) recording and in phase-change recording. In MO recording, information is recorded as a magnetic domain, the same as on a magnetic disk. Therefore, the recorded information is rewritable, the same as on a magnetic disk. In phase-change recording, information is recorded by reversibly transforming the physical state of the recording layer between crystal and amorphous states.

Among the various optical disk systems, the MO disk has achieved a strong position as a rewritable optical disk. For example, 90-mm (3.5-in) MO disks are used like large capacity floppy disks for personal computers.

But with a capacity of more than 200 MB, they have 100 times more capacity than floppy disks.

Although the MO disk has these advantages, its market share in memory system is still poor. This is mainly due to the high price and poor performance of MO disks compared with other memory systems. Improved performance, i.e., more capacity and faster speed, is thus important.

To improve the MO medium, MO recording mechanism must be analyzed and the relationship between the properties of the disk materials and the recording characteristics must be clarified. In MO recording, not only the optical properties, but also the magnetic and thermal properties of the media play important roles. In conventional MO recording, the thermal and magnetic properties are important for recording, while the optical properties are important for readout. However, in functional media, such as magnetic multilayers, these three properties interact with each other and complicate the recording mechanism.

In this thesis, multilayered MO media were studied in order to achieve high-speed, high-density MO recording. Most of the study focused on analyzing the relationship between the recording characteristics and the structure of the multilayered MO disk from the viewpoints of the three physical properties: thermal, magnetic, and optical. The analysis was performed both numerically and experimentally.

1.1 Background

1.1.1 Principle of magneto-optical (MO) recording

The outline of MO recording is shown in Fig. 1.1. Information is recorded in the form of magnetic domains on an MO film by irradiating a focused laser light under a bias magnetic field. The laser light is irradiated through a transparent substrate made of glass or polycarbonate. The intensity of the irradiated light is modulated with the information to be recorded, as shown in Fig. 1.2. The laser light irradiation increases the temperature of the MO layer, reducing the coercivity of the magnetic film. Therefore, the magnetization of the heated region aligns in the direction of the bias magnetic field, and a magnetic domain representing the recorded

information is formed. The diameter of this magnetic domain is about 0.8 μm for first-generation MO disks [1.2], which went into production in 1988.

To rewrite the information, the recorded information must first be erased. A focused laser beam is continuously irradiated on the medium under a constant magnetic field opposite to that for recording. This aligns the magnetization direction within the laser-irradiated area to that in the blank area, thus, erasing the recorded information.

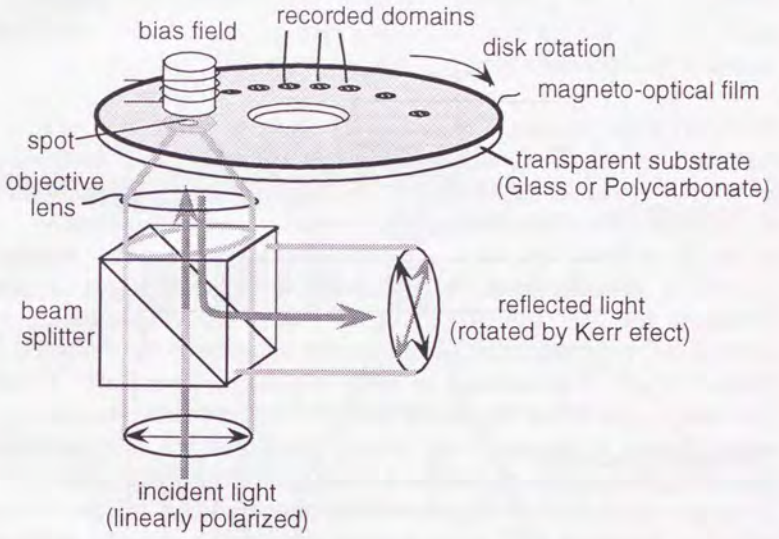

Fig. 1.1 Outline of magneto-optical recording and readout.

To read out the recorded information, a linearly polarized light is irradiated on the MO film, as shown in Fig. 1.1, and the polarization angle of the reflected light is detected. The polarization is rotated by the magnetic Kerr effect. The laser light is focused through a transparent substrate, generally 1.2 mm thick. Using a transparent substrate greatly reduces the effect of dust on the disk surface, a key factor in providing removability and reliability.

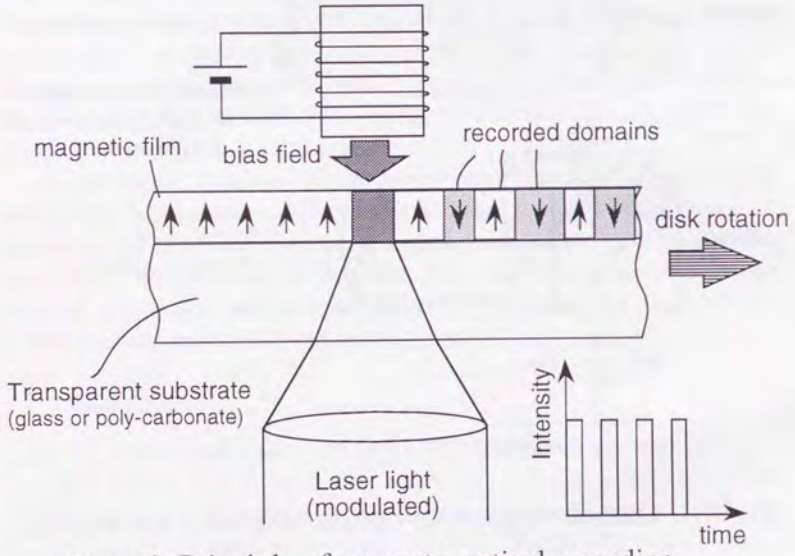

Fig. 1.2 Principle of magneto-optical recording.

1.1.2 MO medium

A typical structure of MO medium is shown in Fig. 1.3(a). The substrate (glass or poly-carbonate) is transparent and pregrooved for tracking. A typical track pitch is about 1.4 μm. The tracking grooves are formed by replication or injection method. On the substrate, an MO layer (TbFeCo), nitride dielectric layers, and an aluminum-alloy reflection layer are formed. The nitride layers are used for protecting the MO layer from oxidation and for enhancing Kerr rotation angle of the MO layer by using multiple-reflection. This disk structure is called quadrilayered structure [1.3].

The MO layer is made of rare-earth transition-metal (RE-TM) amorphous alloy, which has high perpendicular anisotropy ($\geq 1\times10^5$ J/m^3 {1×10^6 erg/cm^3}) and high coercivity (≥1600 kA/m {20 kOe}). In order to record small domain, high coercivity and high perpendicular anisotropy are required. Typical magnetic characteristics of the MO layer are shown in Fig. 1.3(b). Around a room temperature (RT), the coercivity of the MO layer is relatively high (800~1600 kA/m {10~20 kOe}). The coercivity decreases as the temperature increases to a Curie temperature T_C of about 200 °C. This coercivity gradient plays an important role to achieve good recording characteristics. RE-TM alloy is excellent in this point. Since it is ferrimagnetic, the coercivity greatly varies around a compensation temperature, at which the magnetization vanishes and the coercivity becomes infinite ideally. Among various RE-TM alloy, TbFeCo is the most popular material used for an MO film because of its high coercivity and high anisotropy.

In ferrimagnetic materials, magnetic moments of rare-earth (RE) elements always align in the opposite direction of those of transition-metal (TM) elements; this spin arrangement is done by exchange-coupling force. The anti-parallel coupling of RE and TM moments reduces the total magnetization. This results in small demagnetizing field and high effective perpendicular anisotropy.

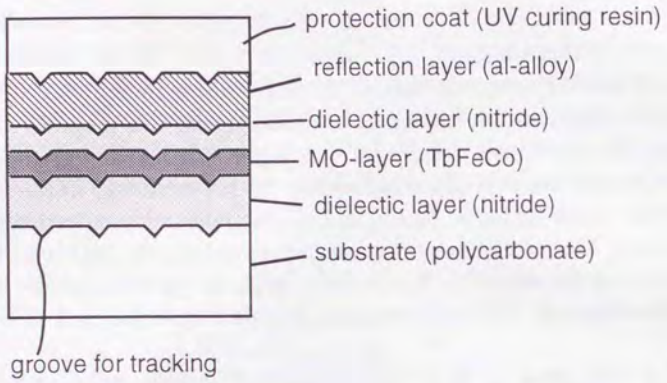

(a) structure of a typical MO medium (quadrilayered)

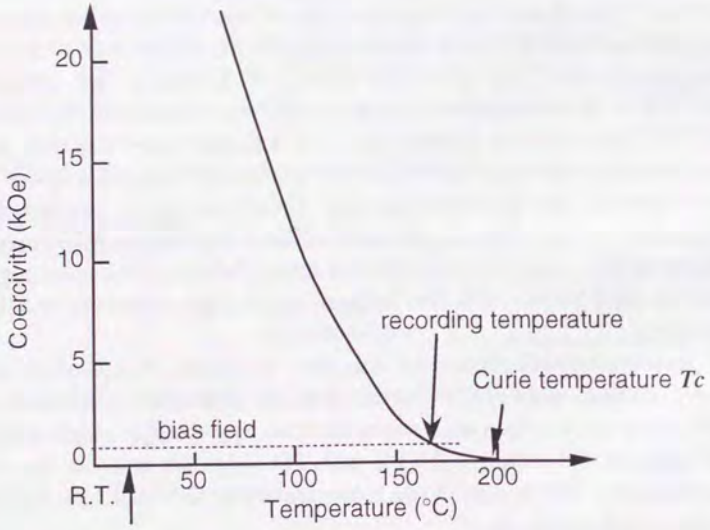

(b) temperature dependance of the coercive forces

Fig. 1.3 Configuration of a typical MO medium.

Since the difference of TM and RE moments determines the amplitude and direction of the magnetization, RE-TM alloy is classified into two types with its composition: TM-dominant and RE-dominant. In TM-dominant alloy, the moment of TM component is greater than that of RE component. In RE-dominant alloy, the moment of RE component is greater than that of TM component. The magnetic properties, such as coercivity and magnetization, greatly depends on the composition of RE and TM elements. That is, the magnetic properties are very sensitive to the variation in the composition. Therefore, precise composition control is very important in RE-TM alloy.

In order to obtain good readout characteristics, both high Kerr rotation angle and high reflectivity are required of the MO medium because the signal intensity is proportional to the product of the Kerr rotation and the reflectivity. The product is called a figure of merit [1.4]. The quadrilayered structure is chosen for high figure of merit.

In addition to the recording and readout characteristics, reliability, such as high corrosion resistance and high write-and-erase repeatability, is required. The quadrilayered structure is excellent in this point also [1.2].

1.1.3 Drive

The optical system of a typical MO recording drive is shown in Fig. 1.4. The laser light radiates from a laser diode, and its spatial profile is circularized by using a beam reformer which consists of a pair of prisms. The circularized light beam is focused onto a recording layer of an MO disk through a polarized beam splitter (PBS), a galvano mirror and an objective lens. The light reflected by the disk is introduced into MO signal detectors through PBSs. The servo signals, such as radial tracking signal and focusing signal, are detected by servo signal detectors.

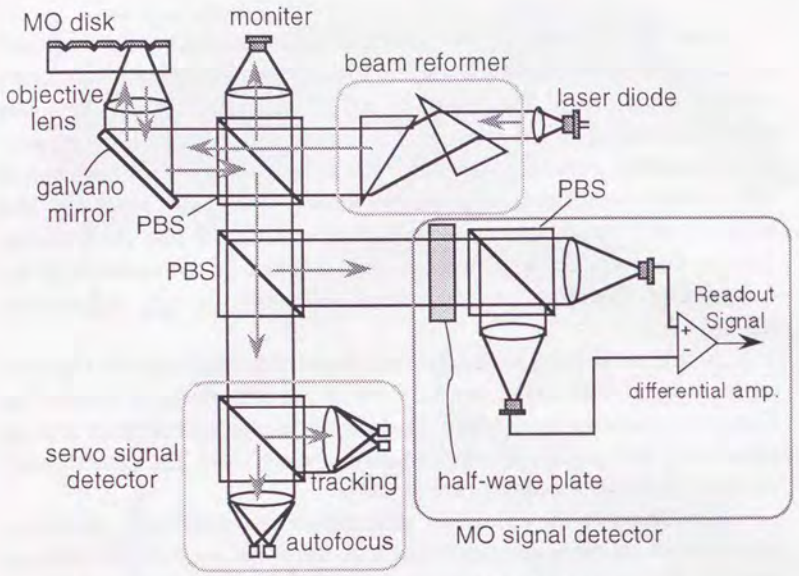

Fig. 1.4 Optical system of MO drive.

Since the Kerr rotation angle of MO media is small (~1°), 45°-differential detection method is used for MO signal detection. In the method, the reflected light is rotated by 45°, then divided into two orthogonal components by the PBS in the MO detector. A half-wave plate is used for rotating the polarization of the reflected light by 45°. Each orthogonal component is detected by the corresponding detector. The detected signals are introduced into a differential amplifier, providing the MO readout signal as the difference of the orthogonal components.

Figure 1.5 shows the principle of the differential detection. The diagonal bold arrow is the electric field vector $\boldsymbol{E}$ of the reflected light. The vector is divided into two orthogonal components $\boldsymbol{P}$ and $\boldsymbol{S}$. The signals detected by the corresponding detectors are proportional to $|\boldsymbol{P}|^2$ and $|\boldsymbol{S}|^2$ since the detector transforms light-intensity into electric current. The MO

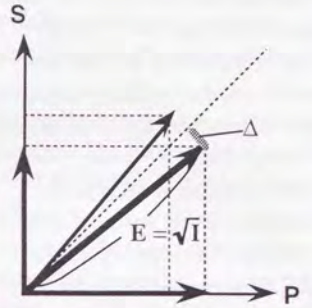

Signal: $|\mathbf{P}|^2 - |\mathbf{S}|^2 = |\mathbf{E}| \cdot \Delta \approx \mathbf{I} \cdot \theta_K$

Fig. 1.5 Principle of differential detection.

readout signal $\boldsymbol{Sig}_{MO}$, the difference of the detected signals, is expressed as follows:

$$\boldsymbol{Sig}_{MO} = \eta \cdot |\boldsymbol{P}|^2 - \eta \cdot |\boldsymbol{S}|^2 = \eta \cdot |\boldsymbol{E}| \cdot \Delta \approx \eta \cdot \boldsymbol{I} \cdot \theta_K \quad \text{.....(1.1)}$$

where $\boldsymbol{I}$, θ_K and η are the intensity of the reflected light, the Kerr rotation angle and the quantum efficiency in the detector. In detail, $\boldsymbol{I}$ and θ_K must be replaced by the effective values considering the reflectivity of the two PBSs.

The noise in the MO readout signal N_{MO} is expressed as the following expression:

$$N_{MO} = \sqrt{N_{amp}^2 + N_{shot}^2 + N_{laser}^2 + N_{disk}^2 + N_{write}^2} \quad \text{.....(1.2)}$$

where, N_{amp}, N_{shot}, N_{laser}, N_{disk} and N_{write} are called amplifier noise, shot noise, laser noise, disk noise and write noise, respectively. The amplifier noise is mainly due to thermal noise in a feed back resistor of the amplifier. The shot noise occurs when photons are converted into electron-hall pairs in

the detector because the conversion is a statistical process. The laser noise results from the fluctuation in the laser intensity. The disk noise is induced by the fluctuation of the reflectivity and the Kerr rotation angle of the MO disk, which originates from the surface roughness of the disk. The write noise occurs due to the inhomogeneity of the recorded domains. Since these kinds of noise are independent of each other, the total noise N_{MO} is expressed as the root sum squares of each noise.

Among the various kinds of noise, the shot noise and the amplifier noise are inevitable because they are quantum noise. If the shot noise is dominant, the readout signal to noise ratio ***SNR*** becomes the following expression.

$$\begin{aligned} SNR &\approx Sig_{MO} / N_{shot}, = \eta I \theta_K / \sqrt{2 e \eta I \Delta f} \\ &\propto \sqrt{I} \cdot \theta_K \\ &\propto \sqrt{R} \cdot \theta_K \end{aligned} \quad \text{.....(1.3)}$$

where, e, Δf and R are the elementary electric charge, the detection frequency width, and the reflectivity of the disk, respectively. If the amplifier noise, which is independent of the signal intensity, is dominant, ***SNR*** is proportional to Sig_{MO} only:

$$SNR \propto Sig_{MO} \propto R \cdot \theta_K \quad \text{.....(1.4)}$$

In Eq. (1.3) and (1.4), R and θ_K are media parameters. Therefore, the value $\sqrt{R} \cdot \theta_K$ or $R \cdot \theta_K$ is called figure of merit of the medium.

1.2 High-speed, high-density technologies

1.2.1 MO disk trends

The first-generation 130-mm (5.25-in) MO disk had a recording speed of 0.3 MB/s and a capacity of 320 MB per side. This performance was poor compared to other recording systems, such as magnetic disks. The recording speed was much slower than that of common magnetic disks, mainly because there was no overwrite capability. Before rewriting the information, erasing

was necessary, which reduced the effective recording speed to about half the readout speed. Magnetic-field modulation overwriting [1.5, 1.6, 1.7, 1.8, 1.9] and light-intensity modulation overwriting [1.10, 1.11, 1.12] have led to high-speed recording.

The capacity of first-generation MO disks was insufficient for both audio and video data recording. For example, a compact disk has about twice the capacity (about 600 MB/side). Digital video recording of two-hour movie requires about 5 GB even if data compression is applied. Therefore, high-density recording was needed to expand the use for MO disks.

To achieve high-density MO recording, a short-wavelength laser diode, which reduces the laser spot size, is needed. However, progress in laser-diode technology has not kept pace with the demand for high-density storage. Therefore, various other high-density MO recording technologies have been investigated.

In second-generation MO disks, which went into production in 1993, the zoned constant-angular-velocity recording technique [1.13] and the mark-edge recording technique [1.14, 1.15, 1.16] were applied. The former technique has enabled more effective use of the recording area on a disk. The latter technique has increased the recording density by correlating the recorded information with the leading- and trailing-edge positions of the recorded domain. Each technique alone increases the recording capacity by about one and half times. Therefore, second-generation MO disks had two or three times more capacity than the first-generation ones.

Magnetic super-resolution, another high-density technology, was first reported in 1991 [1.17, 1.18]. This technique was epoch-making because it broke the optical-resolution barrier.

In the following subsections, these technologies are reviewed.

1.2.2 Magnetic-field modulation overwriting

Figure 1.6 shows the principle of the magnetic-field modulation overwriting (MMO). Unmodulated laser light is irradiated on a medium at such an intensity that a part of the recording film is heated above the Curie temperature. On the heated area, modulated magnetic field is applied, which forms magnetic domains. In the process, the magnetization direction of the

recorded domains follows the direction of the modulated field, independent of the previous domains. Therefore, the information is rewritten without erasing process, that is, the information is overwritten.

A floating type of magnetic head is used for applying high-speed modulated magnetic field. The head is similar to that of a magnetic disk. However, the size of the magnetic head and the floating distance are much larger than those of magnetic disks. This is because the domain width is determined by the laser spot size (heated area size) and is independent of the size of the area where the magnetic field is applied.

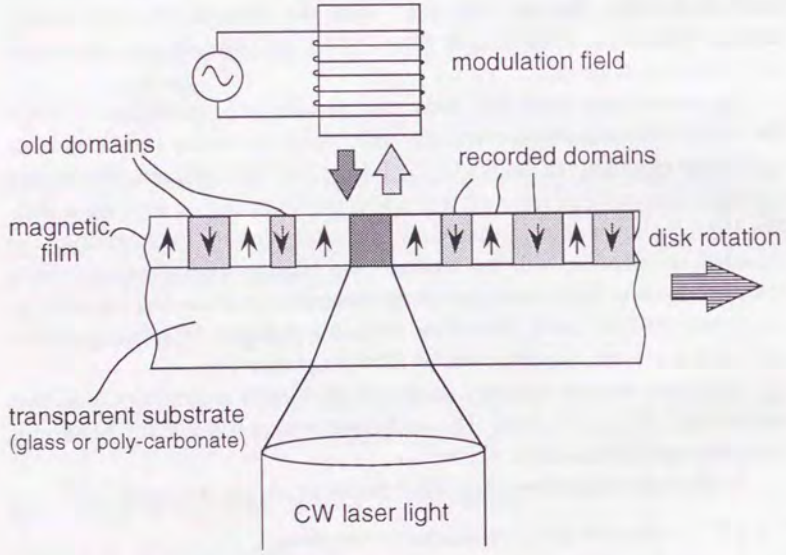

Fig. 1.6 Principle of magnetic field modulation overwriting.

Furthermore, MMO technique is also effective to high-density recording because high-speed modulation enables the easy formation of domains shorter than the optical spot diameter [1.19].

1.2.3 Light-intensity modulation overwriting

Figure 1.7(a) shows a typical MO disk structure for light-intensity modulation overwriting (LMO). The disk has a TbFeCo memory layer (M-layer) and a TbDyFeCo writing layer (W-layer). These two magnetic layers are sandwiched by dielectric layers in order to protect them from oxidation. The magnetic properties of the M-layer and the W-layer are shown in Fig. 1.7(b). The M-layer has higher coercivity than the W-layer at room temperature, and it has lower Curie temperature than the W-layer.

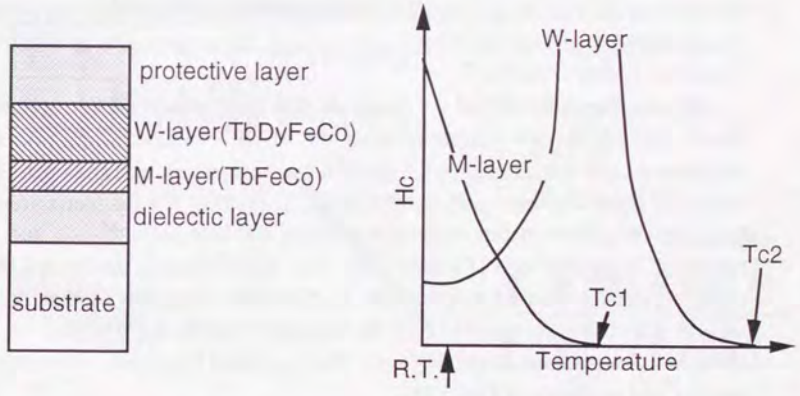

(a) structure of the medium (b) temperature dependance of the coercivity

Fig. 1.7 Configuration of LMO medium.

Figure 1.8 explains the process of LMO. Overwriting is performed by modulating the laser power between a high level (P_H) and a low level (P_L) under a constant bias magnetic field H_{bias}.

Before overwriting, the W-layer is uniformly magnetized by the initializing field (H_{ini}) as shown in Fig. 1.8(a). H_{ini} is applied by a permanent magnet. In the initialization, the magnetization of the M-layer, which represents the information in the form of recorded domains, is not disturbed because the coercivity of the M-layer is higher than H_{ini}.

When P_L is irradiated on the disk, the temperature of the magnetic layers approaches the Curie temperature of the M-layer (T_{C1}). At the temperature, the magnetization of the M-layer is aligned in the same direction as the uniformly magnetized W-layer through the exchange-coupling force between two layers, as shown in Fig. 18(b). Consequently, the M-layer is uniformly magnetized and the recorded domains are erased. This is called L-process or erasing process and, the temperature at which the L-process occurs is called T_L.

When P_H is irradiated on the disk, the temperature of the magnetic layers approaches the Curie temperature of the W-layer (T_{C2}). At that temperature, the magnetization of the M-layer disappears, and the coercivity of the W-layer becomes sufficiently small. Therefore, the magnetization of the W-layer aligns in the same direction of the bias field H_{bias}, and the recorded domains are formed. As the temperature decreases, the magnetization of the M-layer aligns in the same direction as that of the recorded domains on the W-layer. In the other words, the domains on the W-layer is transferred to the M-layer. This is called H-process or recording process and is shown in Fig. 1.8(c).

In summary, P_H forms the recorded domains and P_L erases them. Therefore, overwriting is performed by modulating the laser power between P_H and P_L.

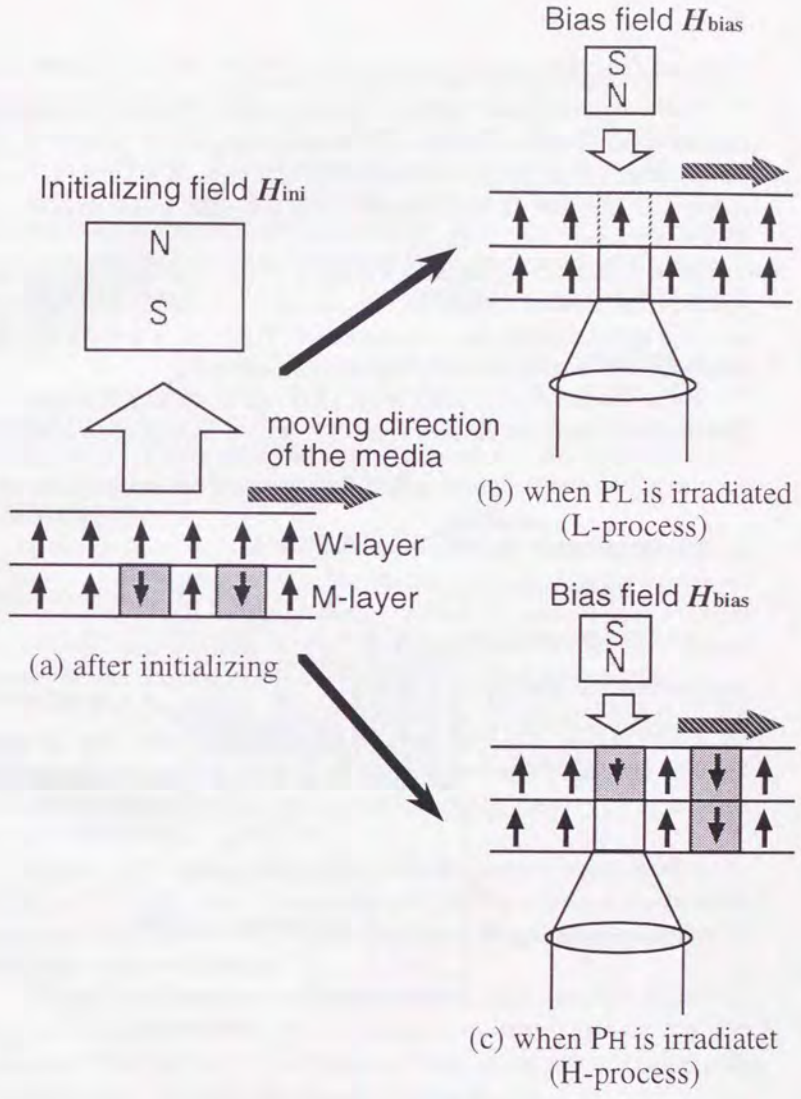

Fig. 1.8 Overwriting process.

1.2.4 *Magnetically induced super-resolution*

For a high-resolution readout method, various types of magnetically induced super-resolution (MSR) have been investigated [1.20, 1.21, 1.22]. Among them, front aperture detection (FAD) type of MSR is the most simple and effective. In this subsection, the principle of the FAD type of MSR is explained.

MSR is induced by masking a portion of the laser spot. The masked region on the medium reflects no information, which reduces the effective spot size and eliminates optical interference. The mask is formed by using temperature difference caused by the readout laser spot.

Figure 1.9 shows the outline of the FAD type of MSR. The medium has three magnetic layers, a memory layer (TbFeCo), a readout layer (GdFeCo)

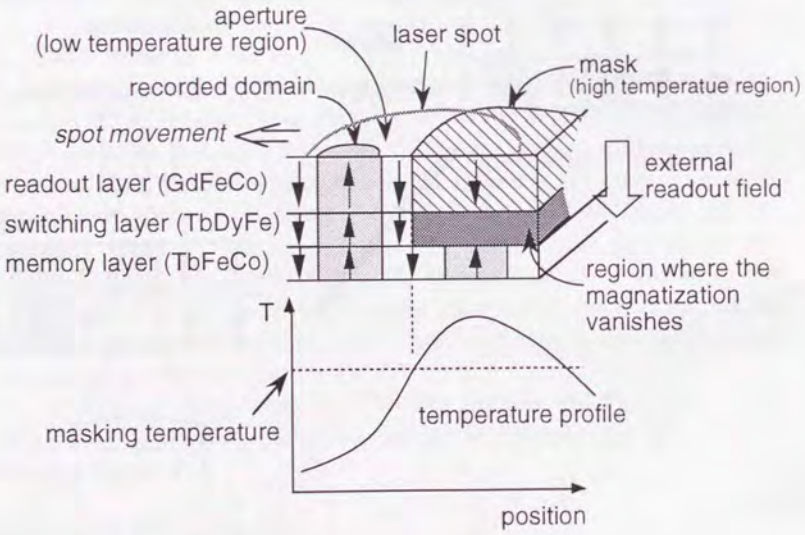

Fig. 1.9 Principle of MSR.

and a switching layer (TbDyFe). The memory layer, which has the same function of the magnetic film of the conventional MO disk (Fig. 1.2), stores the information in the form of magnetic domain. The readout layer is capable of duplicating domain from the memory layer with the exchange-coupling force through the switching layer. Therefore, the recorded information is read through the readout layer by irradiating a readout laser beam. The switching layer has the lowest Curie temperature of the three. It controls the exchange-coupling force between the memory and the readout layers by using its Curie temperature.

When the readout laser beam is irradiated, the magnetic films in the spot are heated. The laser spot is divided into two region with its temperature: an aperture region and a mask region. In the aperture region, the temperature is lower than the Curie temperature of the switching layer. In the mask region, the temperature is higher than the Curie temperature of the switching layer.

In the aperture, the low temperature region, the recorded domain on the memory layer is transferred to the readout layer through the exchange-coupling force. This is because the coercivity of the readout layer is lower than the exchange-coupling force. The recorded information is accessed through the transferred domains on the readout layer in the aperture.

In the mask, the high temperature region, the magnetization of the switching layer vanishes; this magnetically uncouples the readout layer from the memory layer and magnetizes the readout layer in the direction of a bias field. In the mask, therefore, no information on the memory layer is read-out through laser spot.

Because of the spot movement, the high temperature region is shifted to the rear portion of the spot; consequently, the aperture, the low temperature region, is located at the front portion of the spot. This is why the method is called front aperture detection.

Thus, the readout region is limited to the aperture, the front portion of the spot. This improves the effective optical resolution. That is to say, the magnetically induced super-resolution technique is capable of reading and resolving smaller domains than the optical spot size.

1.3 Outline of the thesis

To achieve high-density, high-speed optical disks, the signal-to-noise ratio (SNR) is the most important factor to be improved. The SNR reflects the figure of merit of the medium (FOM), which is proportional to the Kerr rotation angle, and the recorded domain shape. The FOM depends on the optical properties of the medium. The recorded domain shape reflects the thermal and magnetic properties. Therefore, the optical, the thermal, and the magnetic properties play important roles in MO recording. In this thesis, the relationship between the media structure and the write/read characteristics is discussed based on these three physical properties. The experimental results are analyzed with the help of various numerical simulations.

In chapter 2, the optical and thermal structures of MO disks are discussed based on simulation and experimental results. The optical properties (the Kerr rotation angle and the reflectivity) are common properties independent of the recording method. The enhancement of the Kerr effect by using multiple-reflection improves the performance of MO readout. A media structure that provides a large MO readout signal is determined with the help of optical simulations. The thermal properties of MO disks depend on the recording method because the domain formation and the recording laser pulse shape differ with the recording method. In chapter 2, thermal simulation [1.23] shows the shape of the recorded domain precisely. With the help of a magnetic domain formation model [1.24, 1.25], the temperature distribution obtained by the thermal simulation is expanded to the domain shape.

In chapter 3, exchange-coupled magnetic multilayers are studied for light-intensity modulation overwriting (LMO). In a magnetic multilayer, the exchange-coupling force between layers plays a very important role. Therefore, analysis and improvement of the mechanism for the domain formation are needed to achieve good performance. Several problems to be solved are addressed. Some, such as the power margin and the thermal crosstalk, occur because LMO needs three levels of laser power: recording power, erasing power, and readout power. Others, such as the initialization noise and the degradation after overwrite repetition, originate from the

exchange-coupling force between magnetic layers. The causes of three problems are studied experimentally by analyzing the mechanism of domain formation and magnetization with the help of thermal simulation. Ideas for solving these problems are introduced and examined experimentally. In addition, the high-density mark-edge recording technique is applied to LMO media.

In chapter 4, recording and readout techniques for high-density recording are discussed. For high-density recording, both small-domain readout and small-domain recording are important. Magnetic super-resolution, an application of a magnetic multilayer, is studied as a small-domain readout technique [1.26]. Magnetic-field modulation by pulsed-laser irradiation is studied [1.27], as a small-domain recording technique.

In chapter 5, conclusions drawn from the results throughout the thesis are presented. The most suitable form of the MO media and the recording method for high-speed, high-density storage are discussed.

References

[1.1] H. Sugiyama, T. Maeda, A. Saitoh T. Nishida, S. Horigome, S. Arai, K. Shigematsu, H. Watanabe, and, A. Gotoh, Jpn. J. Appl. Phys. **31**, 584 (1992)

[1.2] N. Ogihara, K. Shimazaki, Y. Yamada, M. Yoshihiro, A. Gotoh, H. Fujiwara, F. Kirino, and N. Ohta, Jpn. J. Appl. Phys., **28**, Suppl. **28-3**, 61 (1989).

[1.3] H. Miyamoto, T. Niihara, H. Sukeda, M. Takahashi, T. Nakao, M. Ojima, and N. Ohta, J. Appl. Phys. **66**, 6138 (1989).

[1.4] K. Egashira, T. Yamada, J. Appl. Phys. **45**, 3643 (1974).

[1.5] F. Tanaka, S. Tanaka, and N. Imamura, Jpn. J. Appl. Phys., **26-2**, 231 (1987)

[1.6] H. Sukeda, T. Kaku, T. Niihara, T. Nakao, M. Kasai, H. Miyamoto, K. Akagi, Y. Miyamura, N. Ohta, M. Ojima, F. Tanaka, S. Tanaka, Y. Sasano, K. Ono, and S. Suzuki, Int. Symp. Opt. Memory '89, Post-deadline papers Tech. Digest, 28B-22, Sep. (1989).

[1.7] T. Nakao, M. Ojima, Y. Miyamura, S. Okamine, H. Sukeda, N. Ohta, and Y. Takeuchi, Jpn. J. Appl. Phys., **26**, Suppl. **26-7**, 149 (1987).

[1.8] H. Sukeda, T. Nakao, and M. Ojima, IEEE Trans. on Magn. in Jpn., **3-12**, 848 (1988).

[1.9] M. Ojima, H. Sukeda, T. Niihara, T. Nakao, M. Kasai, T. Kaku, H. Miyamoto, K. Akagi, Y. Miyamura, and N. Ohta, SPIE **1316**, Optical Data Storage '90, 95 (1990).

[1.10] J. Saito, M. Sato, H. Matsumoto, and H. Akasaka, Jpn, J. Appl. Phys. **26**, Suppl. **26-4**, 155 (1987).

[1.11] K. Aratani, M. Kaneko Y. Mutoh, K. Watanabe, and H. Makino, SPIE **1078**, Optical Data Storage '89, 258 (1989).

[1.12] T. Fukami, Y. Nakaki, T. Tokunaga, M. Taguchi, and K. Tsutsumi, Jpn. J. Appl. Phys., **67**, 4415 (1990)

[1.13] T. Maeda, A. Saito, H. Sugiyama, M. Ojima, S. Arai, and K. Shigematsu, SPIE **1499**, Optical Data Storage '91, 414 (1991).

[1.14] H. Sukeda, M. Ojima, and T. Maeda, Jpn. J. Appl. Phys., **26**, Suppl. **26-4**, 243 (1987).

[1.15] T. Maeda, T. Toda, H. Ide, F. Kirino, S. Mita, and K. Shigematsu, IEEE Trans. on Magn., **29**, 3788 (1993).

[1.16] H. Ide, T. Toda, F. Kirino, T. Maeda, F. Kugiya, S. Mita, and K. Shigematsu, Jpn. J. Appl. Phys. **32**, 5342 (1993)

[1.17] K. Aratani, A. Fukumoto, M. Ohta, M. Kaneko, and K. Watanabe, SPIE **1499**, Optical Data Storage '91, 209 (1991)

[1.18] A. Fukumoto, S. Yoshimura, and T. Udagawa, SPIE **1499**, Optical Data Storage '91, 216 (1991)

[1.19] M. Takahashi, H. Sukeda, T. Nakao, T. Niihara, M. Ojima, and N. Ohta, Jpn. J. Appl. Phys. **28**, Suppl. **28-3**, 323 (1989).

[1.20] M. Ohta, A. Fukumoto, K. Aratani, M, Kaneko, and K. Watanabe, J. Magn. Soc. Jpn., **15**, Suppl. **S1**, 319 (1991)

[1.21] A. Fukumoto, and S. Kubota, Jpn. J. Appl. Phys., **31**, 529 (1992)

[1.22] Y. Murakami, N. Iketani, J. Nakajima, A. Takahashi, K. Ohta, and T. Ishikawa, J. Mag. Soc. Jpn., **17**, Suppl. **S1**, 201 (1993)

[1.23] M. Takahashi, H. Sukeda, M. Ojima, and N. Ohta, J. Appl. Phys. **63**, 3838 (1988).

[1.24] B. G. Huth, IBM J. Res. Dev. **18**, 100 (1974).

[1.25] M. Takahashi, T. Niihara, and N. Ohta, J. Appl. Phys. **64**, 262 (1988).

[1.26] H. Miyamoto, K. Andoo, H. Saga, H. Sukeda, and M. Ojima, J. Magn. Soc. Jpn., **19**, Suppl. **S1**, 425 (1995).

[1.27] S. Yonezawa and H. Miyamoto, Digest of Symp. Opt. Memory '94, 65 (1994).

2 Optical and Thermal Design of MO Disks

To achieve high-density, high-speed optical disks, the signal to noise ratio (SNR) is the most important factor to consider. The SNR represents both readout and recording performance. Readout performance mainly depends on the optical properties of the recording medium. Recording performance (recorded domain quality) mainly depends on the thermal and magnetic properties.

The readout signal is detected as the Kerr rotation angle of the reflected light. As discussed in §1.1.3, the figure of merit (FOM) for MO detection, which reflects the SNR, is expressed as $\sqrt{R} \cdot \theta_K$ or $R \cdot \theta_K$. To obtain a high FOM, the multiple-reflection method, which uses dielectric layers and a metal reflection layer, has been investigated [2.1]. The multiple reflection enhances the Kerr rotation angle [2.2]. In this chapter, the FOM for a disk with a single MO film and for a disk with a magnetic multilayer (bilayer) are discussed.

The recorded domain shape directly depends on the thermal properties of the MO media because the domain is formed in the high-temperature region of the disk. The thermal properties of MO disks depend on the recording method because, as mentioned above, domain formation process and recording laser pulse shape are different with the recording method.

The magnetic properties relate to the fluctuations in the recorded domains, which increase the noise level [2.3]. The magnetic properties of magnetic multilayers are discussed in detail in the next chapter.

In this chapter, a suitable optical and thermal structure for MO disks, especially for magnetic-field modulation overwriting (MMO) [2.4], [2.5], is discussed.

2.1 Optical design

2.1.1 Measurement of optical properties

The reflectivity of MO disks was measured using an unfocused light with wavelengths of 780 or 830 nm. The effective reflectivity for the MO-disk drive was obtained from the measured reflectivity considering the reflection at the substrate surface and the diffraction due to the tracking grooves. Since the laser beam is focused onto the MO film surface in an actual MO-disk drive, the light reflected at the substrate surface does not reach the detectors of the drive. The effect of the diffraction was confirmed by comparing the reflectivity for the focused light on the non-grooved and on the grooved areas of the disk. Since the wave front of a focused beam within the focal depth is flat, the reflectivity for focused light is considered to be same as that for unfocused light.

The Kerr rotation angles of the MO disks were measured using a Kerr loop tracer (Nihon Optics Co., J-250). The Kerr rotation angle is half the difference between the polarization angles of two reflected lights, one magnetized in one direction and one in the opposite direction. To magnetize MO disks, a strong magnetic field (about 1200 kA/m {15 kOe}) was applied. The wavelength dependence and the temperature dependence of the Kerr rotation angle were also measured.

2.1.2 Optical simulation

Magnetic material rotates the polarization plane of the linearly polarized reflected light, which is called the magnetic Kerr effect. Physically, this is due to the interaction between an incident photon and an electron with an orbital angular momentum. A circularly polarized photon is absorbed or emitted with a change in the quantum number of the angular momentum. The magnetization induces the population difference between atoms with positive angular momentum and those with negative angular momentum. The population difference causes the difference in the refractive indices for two circular-polarized light, namely, the circular dichroism.

In the simulation, the Kerr effect was treated as a circular dichroism, by which the optical phase shift is caused for two circular-polarized reflected lights. The shift results in the rotation of the linearly polarized light, i.e., the Kerr rotation.

The birefringence causes not only the optical phase shift but also the difference in the absorbance or the reflectivity. This difference results in the Kerr ellipticity, by which reflected light of the linearly polarized incident

light becomes elliptical polarization. The Kerr ellipticity is also a key parameter to be controlled.

The actual magnetic materials have relatively small (~0.2 deg.) Kerr rotation angle. For obtaining higher Kerr rotation, the multilayered structure, which utilizes multiple-reflection [2.6, 2.7] is used. However, the multiple-reflection technique causes the reduction in the reflectivity. Therefore, to obtain an MO media with good optical properties, the figure of merit (FOM), mentioned in §1.1.3, is important.

The numerical simulation is useful to study the relationship between the media structure and the Kerr enhancement effect. The simulation was performed as follows.

First, two interfaces, shown in Fig. 2.1, were considered. By regarding these surfaces as one virtual reflective surface, the reflectivity of the virtual surface is expressed as follows:

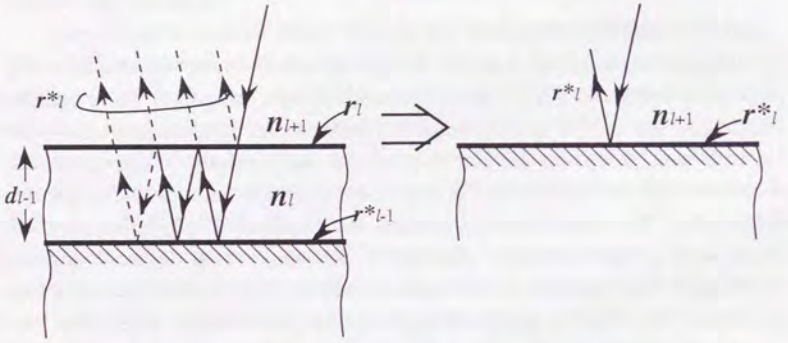

(a) two reflective surfaces (b) virtual reflective surface

Fig. 2.1 Kerr calculation method on multilayer system.

$$r^*_l = r_l + t_l \cdot r^*_{l-1} \cdot \exp(-i\frac{2n_l d_l}{\lambda}) \cdot t_l \cdot \begin{bmatrix} 1+\left\{-r_l \cdot r^*_{l-1} \cdot \exp(-i\frac{2n_l d_l}{\lambda})\right\} \\ +\left\{-r_l \cdot r^*_{l-1} \cdot \exp(-i\frac{2n_l d_l}{\lambda})\right\}^2 \\ +\left\{-r_l \cdot r^*_{l-1} \cdot \exp(-i\frac{2n_l d_l}{\lambda})\right\}^3 \\ +\ldots \end{bmatrix} \quad \ldots\ldots (2.1)$$

where, r_l, r^*_{l-1}, n_l , d_l , t_l and λ are the amplitude reflectivity of the interface between the layers l and l+1, the virtual reflectivity of the interface between layers l-1 and l, the refractive index of layer l , the thickness of layer l , the transmissivity of the interface between layers l and l-1, and the wavelength of the incident light, respectively. By using the relation $t_l^2 = 1 - r_l^2$, Eq. (2.1) is reduced into the following expression.

$$r^*_l = \frac{r_l + r^*_{l-1} \cdot \exp(-i\frac{2n_l d_l}{\lambda})}{1 + r^*_l \cdot \exp(-i\frac{2n_l d_l}{\lambda}) r^*_{l-1}} \quad \ldots\ldots (2.2)$$

By sequentially calculating the virtual reflectivity of Eq. (2.2) at every interface of the multilayer, the reflectivity of the multilayer is obtained. In the MO medium, the refractive indices for the circular-polarized lights are different from each other. The amplitude reflectivity for two circular-polarized light r^*_L and r^*_R is thus calculated. The Kerr rotation angle θ_K, the Kerr ellipticity η_K, and energy reflectivity R are obtained by the following equations.

$$\theta_K = \frac{\arg(r^*_R) - \arg(r^*_L)}{2} \quad \ldots\ldots (2.3)$$

$$\eta_K = \tan^{-1}\left(\frac{|r^*_R| - |r^*_L|}{|r^*_R| + |r^*_L|}\right) \quad \text{.....(2.4)}$$

$$R = \frac{|r^*_R|^2 + |r^*_L|^2}{2} \quad \text{.....(2.5)}$$

The optical constants used for the simulation are summarized in Table 2.1. The refractive indices of the thin films on the MO disks were obtained by ellipsometry. The magneto-optical constants of the MO films, which are expressed as differences in the refractive indices for two circular-polarized lights, were obtained from the literature [2.8]. The double signs in the TbFeCo row indicate the refractive indices for circularly polarized lights. Since the refractive index for SiN greatly depended on the sputtering condition, the index is shown by a range.

Table 2.1 Refractive indices.

material	n	k
TbFeCo±	3.0 ± 0.03	3.6 ±0.035
SiN	1.9 ~ 2.3	0 ~ 0.1
UV-resin	1.53	0
Glass	1.5	0
Al	0.5	7.0
Al-Ti	2.0	5.0

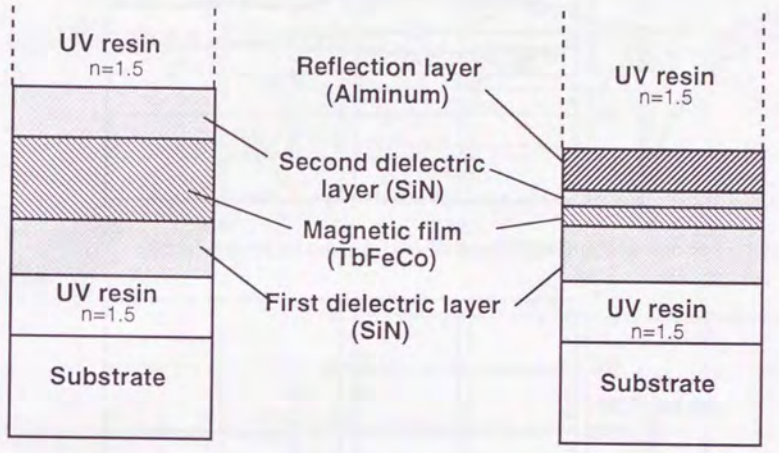

(a) Trilayered disk (b) Quadrilayered disk

Fig. 2.2 Typical disk structures of MO Disk.

2.1.3 Trilayered and quadrilayered disk

The FOM was calculated by the scheme described in §2.1.2 for two kinds of disks, both of which has a single layer MO film. Figure 2.2(a) and 2.2(b) show disk structure for a trilayered disk and a quadrilayered disk, respectively. In the trilayered disk, the first dielectric (SiN) layer located between the substrate and the MO (TbFeCo) film enhances the Kerr effect by multiple reflection. In the quadrilayered disk, both the second dielectric layer and the MO film enhance the Kerr effect in addition to the first dielectric layer. In this structure, therefore, the MO film is so thin that a part of incident light reaches to the reflection layer through it.

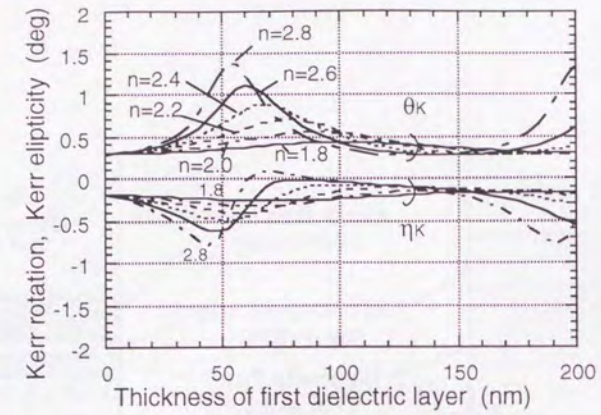

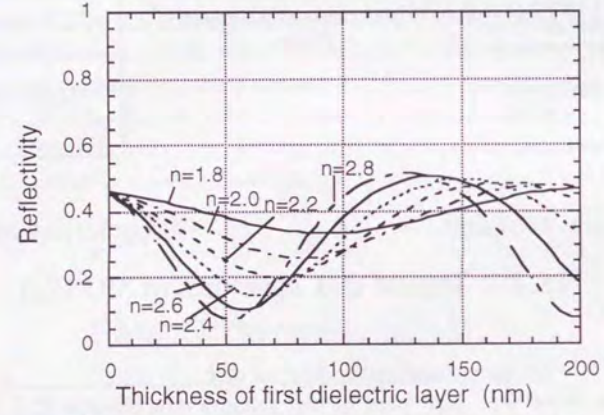

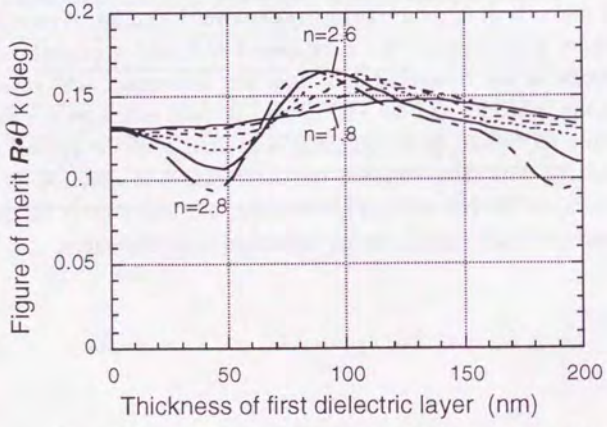

Fig. 2.3 Kerr simulation for trilayered disk.

(a) Kerr rotation

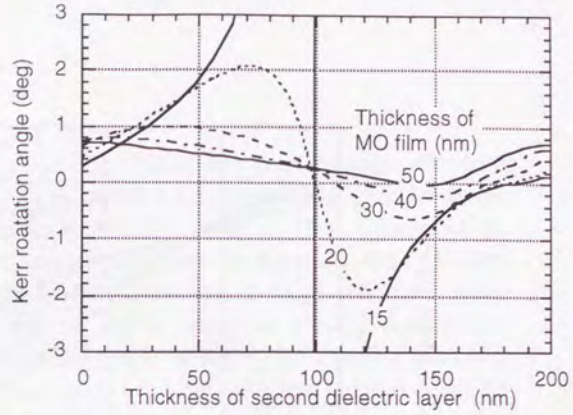

(b) Kerr elipticity

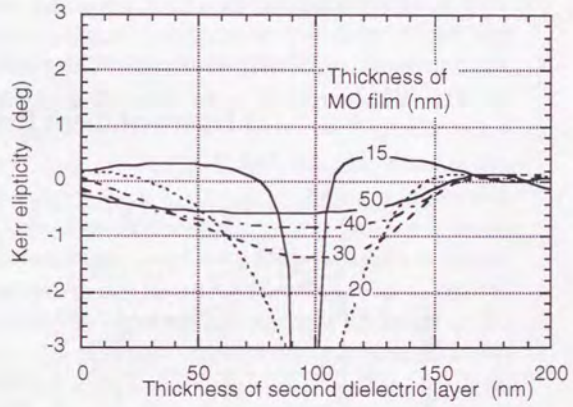

(c) Reflectivity

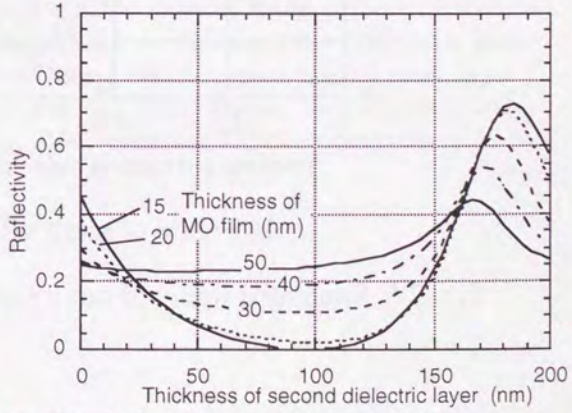

Fig. 2.4 Kerr simulation for quadrilayered disk.

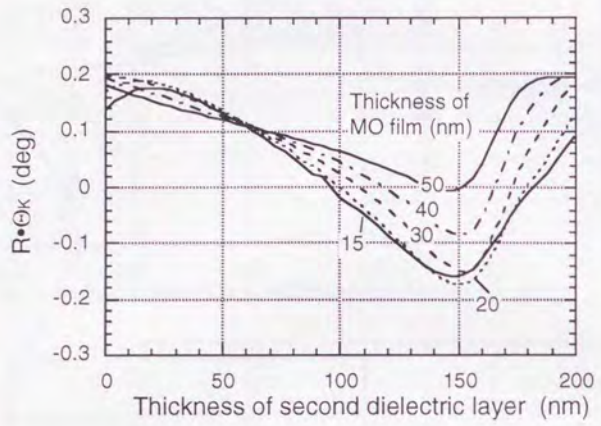

(a) Figure of merit $R \cdot \Theta_K$

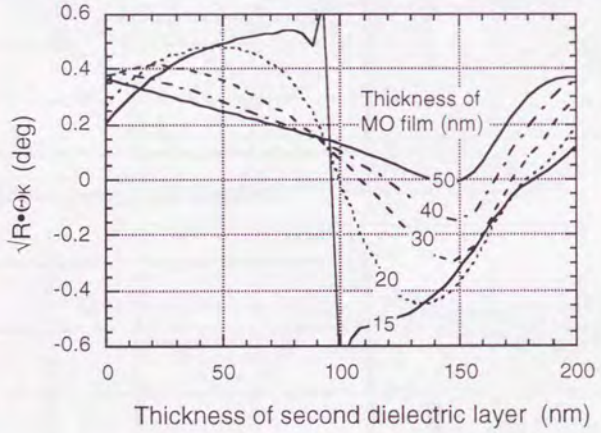

(b) Figure of merit $\sqrt{R} \cdot \Theta_K$

Fig. 2.5 Simulated figure of merit for quadrilayered disk.

For the trilayered disk in Fig 2.2(a), the Kerr rotation, the Kerr ellipticity, the reflectivity and the FOM were calculated. Figure 2.3 shows the results as functions of the first dielectric layer. The thickness of the second dielectric layer shows no effect because the thickness of the MO film is thick enough. The first nitride layer with a large refractive index produces a large Kerr rotation angle, while it greatly reduces the reflectivity. Therefore, the enhancement effect in the FOM is relatively small. In the practical use, maximum available refractive index is about 2.3 since dielectric films with higher refractive index have generally some absorbance. Therefore, the maximum Kerr rotation angle of about 0.76 degree is obtained when the thickness and the refractive index of the first nitride layer are 75 nm and 2.3, respectively. The Kerr ellipticity, the reflectivity, $\sqrt{R} \cdot \theta_K$, and $R \cdot \theta_K$ in this case are -0.26 degree, 18.5 %, 0.326 degree, and 0.141 degree, respectively.

For the quadrilayered disk shown in Fig. 2.2(b), the Kerr rotation, the Kerr ellipticity, and the reflectivity were simulated as shown in Figure 2.4. The Kerr rotation angle and the Kerr ellipticity are greatly dependent on the thickness of the second dielectric layer, especially if the MO film is thinner than 20 nm. The shape of the curve for the Kerr rotation is a kind of dispersion function that has a pole at about 100 nm in a thickness of the second dielectric layer. Near the pole the reflectivity is very little. The two kinds of FOMs ($\sqrt{R} \cdot \theta_K$, $R \cdot \theta_K$) are shown in Fig. 2.5. The FOM $R \cdot \theta_K$ of 0.181 degree is obtained if the thicknesses of the MO film and the second dielectric layer are 20 and 25 nm. The value of $R \cdot \theta_K$ is about 1.3 times larger than that for the trilayered disk. In this case, FOM ($\sqrt{R} \cdot \theta_K$) is also greatly enhanced up to 0.435 degree, which is more than 1.3 times larger than that for the trilayered disk. The Kerr rotation, Kerr ellipticity, and reflectivity are 1.05 degrees, -0.05 degree, and 17.2 %, respectively.

Table 2.2 Disk structure and Optical properties.

	Trilayered disk			Quadrilayered disk		
Structure	d (nm)	n	k	d (nm)	n	k
UV-resin	∞	1.5	0.0	∞	1.5	0.0
Aluminum	--	--	--	30	0.5	7.0
SiN	75	2.3	0	25	2.0	0.0
TbFeCo	100	3.0 ±0.03	3.6 ±0.035	20	3.0 ±0.03	3.6 ±0.035
SiN	75	2.3	0.0	85	2.0	0.0
substrate	∞	1.5	0.0	∞	1.5	0.0
	Simulation	Experiment		Simulation	Experiment	
Kerr rotation (deg.)	0.76	0.8		1.05	1.1	
Kerr ellipticity (deg.)	-0.26	--		-0.05	--	
Reflectivity (%) (with substrate)	18.5 (21.2)	15 (18)		17.2 (20.6)	15 (18)	
$R \cdot \theta_K$ (deg.)	0.141	0.12		0.181	0.17	
$\sqrt{R} \cdot \theta_K$ (deg.)	0.326	0.31		0.435	0.43	

A comparison of the simulation and the experimental results is summarized in Table 2.2. The simulated values of the reflectivity include no effect of the substrate surface. The influence of the substrate surface was considered by the following equation:

$$R_{total} = R_{sub} + T_{sub}{}^2 R_{film}\left(1 + R_{sub}R_{film} + \left(R_{sub}R_{film}\right)^2 + \ldots\right) \ldots\ldots (2.6)$$

where, R_{film}, R_{total}, R_{sub}, and T_{sub} are the reflectivity of multilayered film, the total reflectivity with the substrate reflection, the reflectivity of the substrate surface, and the transmittance of the substrate surface, respectively. The first term in the large parentheses of Eq. (2.6) is direct reflection from the multilayered film. The other terms in the parentheses come from multiple-reflection between the substrate surface and the film surface. Since the reflectivity of the substrate is relatively small compared with unity, those higher order terms are negligible. In the parentheses in Table 2.2, the simulated values in consideration of the substrate reflection are listed. On the other hand, the raw experimental value of the reflectivity (in the parentheses in the table) contains the influence of the substrate reflection; therefore the influence of the substrate reflection is removed by reversely calculating Eq. (2.6).

As in Table 2.2, the experimental result showed good agreement with the simulated values. Furthermore, the quadrilayered disk with a reflection layer showed good optical characteristics such as Kerr rotation angle and FOM compared with the trilayered disk.

2.1.4 Negative Kerr rotation

It is remarkable that Fig. 2.4(a) shows the negative Kerr rotation angles. This phenomenon is not unique characteristics of the quadrilayered disk. For example, a magnetic bilayer discussed in the next subsection shows a kind of negative Kerr rotation. In addition, even a bilayered film shows a negative Kerr rotation as described below.

Figure 2.6 explains the origin of the negative Kerr rotation as follows. A two-interface system as in the left figure was considered. In this system, **A**, the light reflected at the surface of the dielectric layer, and **B**, the light

reflected at the interface between the MO film and the dielectric layer, were considered. If **B** is greater than **A**, which is the slightly enhanced case, the direction of the enhanced Kerr rotation angle θ_K* is always the same as that of the original Kerr rotation angle θ_K while the value of the rotation angle varies. On the other hand, if **A** is greater than **B**, which is the deeply enhanced case, the direction of the enhanced Kerr rotation angle θ_K* is different from that of the original Kerr rotation angle θ_K, and the Kerr rotation angle θ_K* is much larger than the original one θ_K.

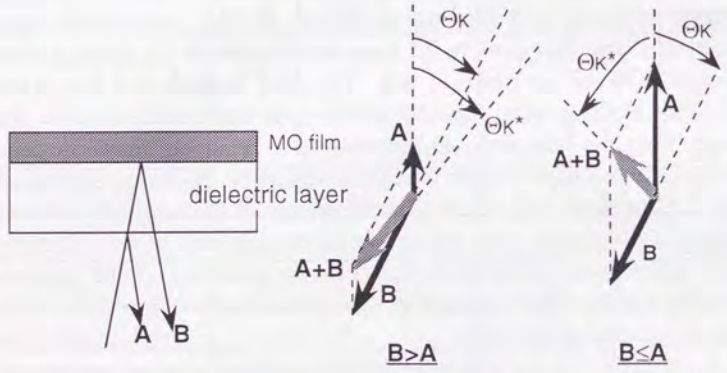

Fig. 2.6 Explanation of inverse Kerr rotation.

Figure 2.7 shows an example of negative Kerr rotation on bilayered disk. On the substrate, a thin MO film (GdTbFeCo) and a dielectric layer (SiN) were formed. The graph shows the Kerr rotation angle as a function of the thickness of GdFeCo layer. The letter **G** and **D** denote the Kerr rotation angles measured from glass substrate side and from dielectric layer side, respectively. The solid and the broken lines show the simulated results. The gray and the white circles show the experimental results from **G** side

and from **D** side, respectively. It is obvious that the experimental results are in good agreement with the simulated result.

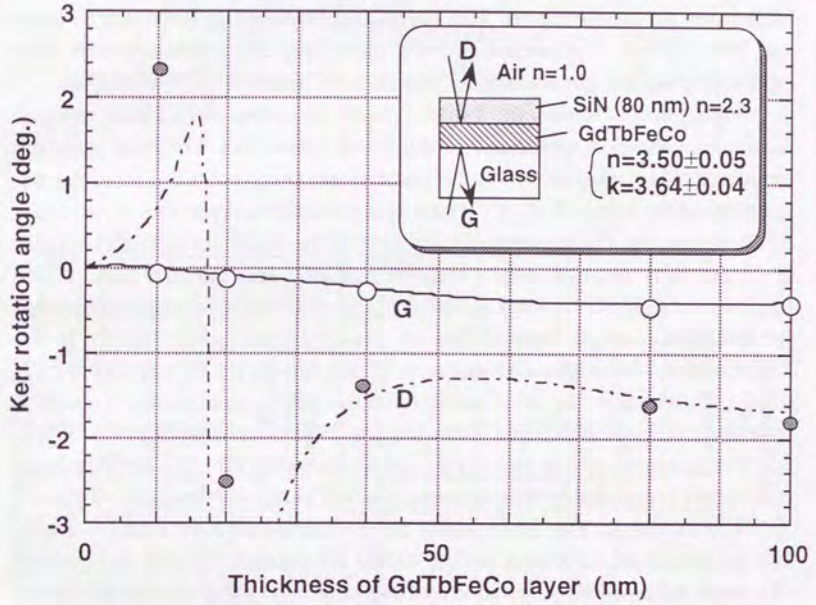

Fig. 2.7 Example of inverse Kerr rotation on bilayered disk.

2.1.5 Kerr enhancement with a magnetic bilayer

Figure of merit of the MO disks with a magnetic multilayer [2.9] is studied in this section. The disk structure used is shown in the Fig. 2.8(a). On a glass substrate, TbFeCo/GdTbFeCo bilayer was formed with SiN dielectric layers on each side. In this case the GdTbFeCo layer is used as a readout layer [2.10] because of lager Kerr rotation angle [2.11, 2.12] than

TbFeCo. Although the Kerr rotation angle of GdTbFeCo is larger than TbFeCo, the coercivity is much smaller than that for TbFeCo; therefore, the magnetic multilayer is used for combining the merits of both materials. In the bilayer film, TbFeCo and GdTbFeCo layers are exchange-coupled with each other. In the multilayer film, the exchange-coupling force acts to align the TM sub-lattice moments of each layer into the same direction. The exchange-coupling phenomenon is discussed in detail in the next chapter.

Figure 2.8(b) shows the simulated and the experimental Kerr rotation angles for various magnetization states in bilayered film. The lines show the simulated Kerr rotation angle for various magnetic states. In the figure, magnetization states (**A**, **B**, **C**, **D**) are schematically shown: the arrow in the figure shows the TM moment of each film. If the thickness of GdFeCo layer is 0, the Kerr rotation angle coincides to that for TbFeCo film. If the thickness of GdFeCo is thick (~100 nm), the Kerr rotation coincides to that for GdTbFeCo single layered film because the light hardly reaches to the TbFeCo layer. When the TM-moments of the two layers are parallel to each other (**A**), which is the most stable condition, Kerr rotation angle shows a little improvement compared with that for TbFeCo and GdTbFeCo. When the TM-moments of the two layers are anti-parallel (**B**), the Kerr rotation curve shows remarkable enhancement at a GdTbFeCo thickness of 45 nm.

The circles in Fig 2.8(b) show the experimental Kerr rotation angle. The white and the dark ones are the values for parallel (**A**) and anti-parallel (**B**) cases, respectively. The Kerr rotation angle and the magnetization state were analyzed by observing the Kerr hysteresis loop from both sides of the disk as shown in Fig. 2.9. In Fig. 2.9, a Kerr loop from film side (F-side) reflects the magnetization direction of the TbFeCo layer only. A Kerr loop from the substrate side (S-side) mainly reflects the magnetization direction of the GdFeCo layer. From two kinds of measurement, the magnetization state (**A**, **B**, **C**, **D**) was determined. Thus Kerr rotation angles were plotted into Fig. 2.8(b). The experimental result is in good agreement with the simulated line.

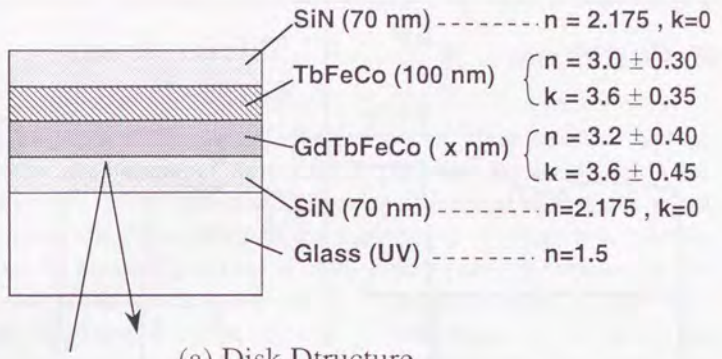

(a) Disk Dtructure

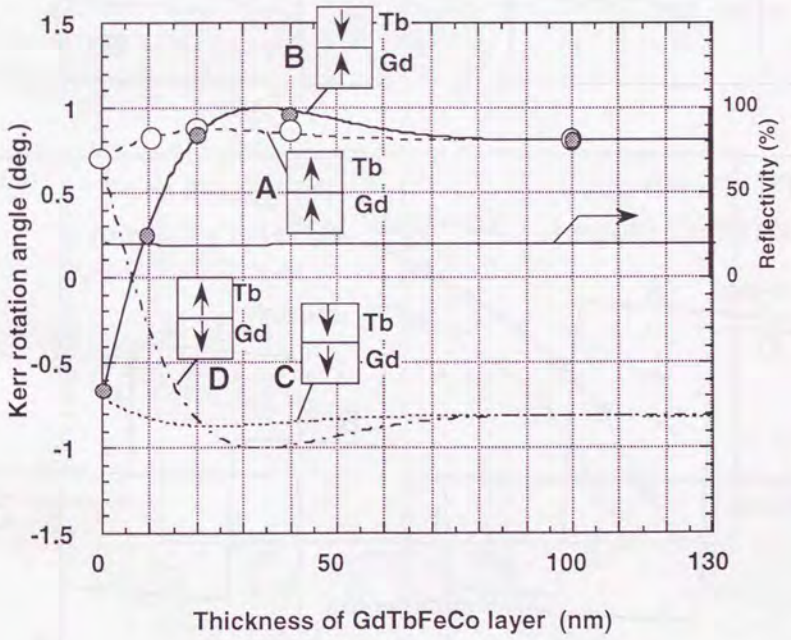

(b) Simulated result

Fig. 2.8 Kerr simulation for magnetic bilayer.

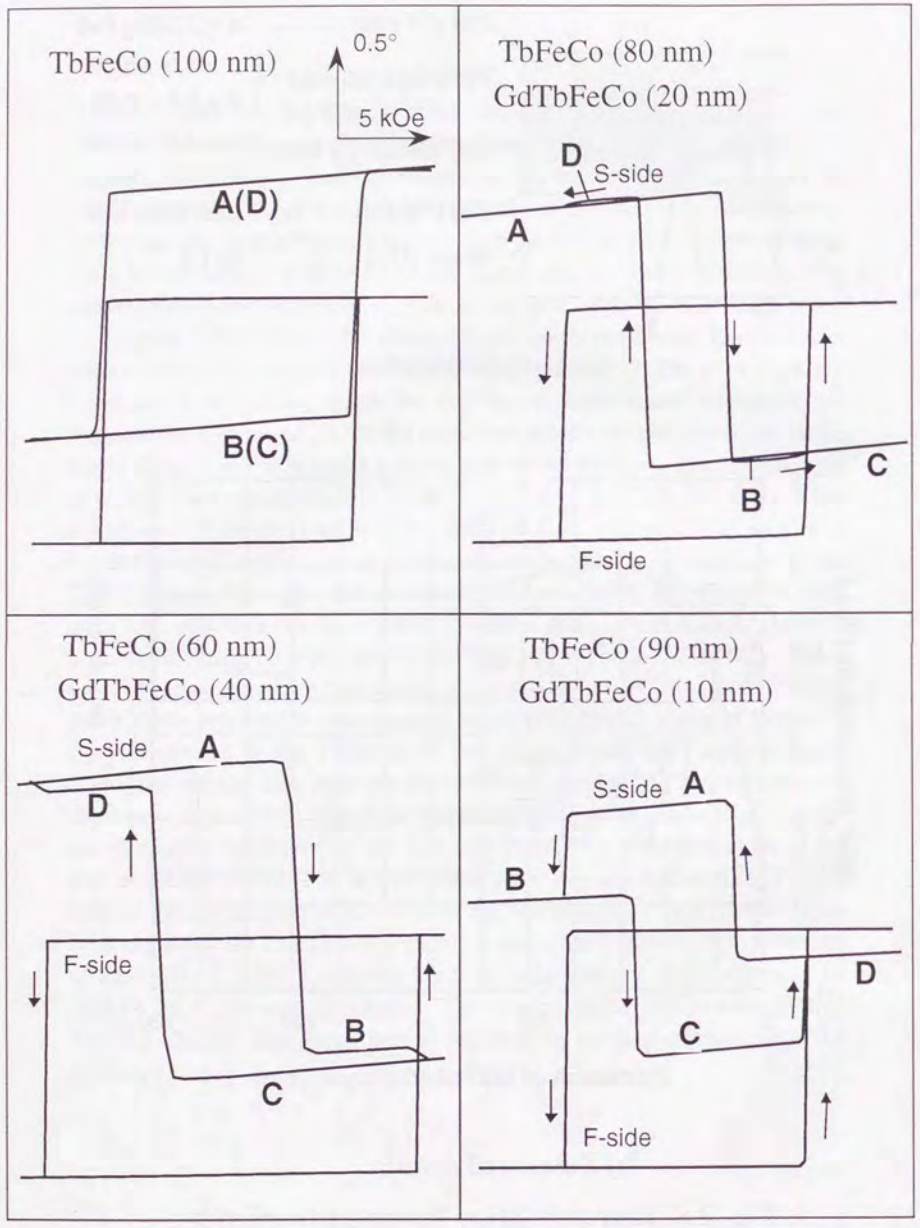

Fig. 2.9 Kerr hysterisis loops for magnetic bilayer.

In addition to the figure of merit at the room temperature, the temperature dependence of Kerr rotation plays an important role. In the readout process, the temperature of the magnetic film is remarkably raised by the laser irradiation although the laser power is lower than that for recording. By irradiating normal level of readout power the temperature on the recording film rises to above 100 °C. Therefore, the Kerr rotation angle at higher temperature must be taken into consideration. Fig. 2.10 shows the temperature dependence of the Kerr rotation angles for the GdTbFeCo and the TbFeCo film. At room temperature, GdTbFeCo has 1.2 times higher Kerr rotation than TbFeCo. At 150 °C, GdTbFeCo has 1.3 times higher Kerr rotation than TbFeCo. Therefore, the good CNR at high readout power is expected.

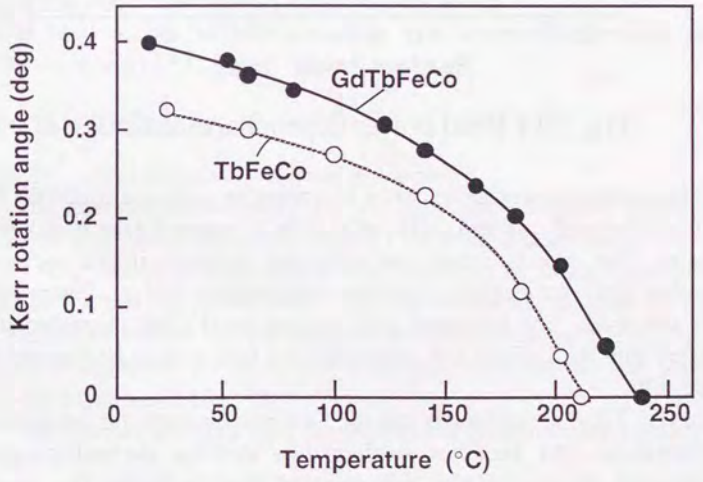

Fig. 2.10 Temperature dependence of Kerr rotation.

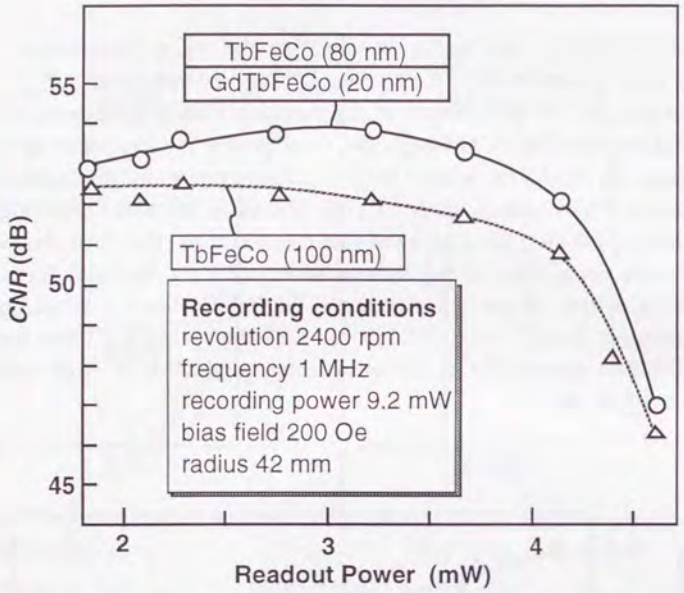

Fig. 2.11 Read power dependence of ***CNR.***

The readout power dependence of carrier to noise ratio (CNR) for TbFeCo (trilayered) disk and GdTbFeCo/TbFeCo magnetic bilayer disk was evaluated. The disk structure was trilayered structure in the previous subsection. Only the magnetic layer was changed into bilayer. Figure 2.11 shows the result. The bilayered disk showed good CNR characteristics compared with the TbFeCo disk, especially at a high readout laser power of about 3 mW.

In Fig. 2.8, it is remarkable that the Kerr rotation angle for the parallel magnetization (**A**) becomes smaller than that for the anti-parallel magnetization (**B**) at a GdTbFeCo thickness of 20 nm to 80 nm. This means that the TbFeCo layer shows a negative Kerr rotation. By another simulation, it was found that the negative Kerr rotation is occurs even if two

layers are made of the same material. This means that, in a thick film, reflection by the material that locates deeper position than 20 nm from the surface shows negative Kerr rotation. This results in the reduction of Kerr rotation, which agrees with the result that an MO layer with a thickness of 20 nm shows a good FOM for the quadrilayered structure.

2.1.6 Suitable optical structure for the MO disk

The quadrilayered disk with a reflection layer showed good optical characteristics (Kerr rotation angle and FOM) compared with the trilayered disk. This is mainly due to the multiple-reflection between the MO layer and the reflection layer. When the reflectivity is low, an inverse Kerr rotation appears. This was explained by the interference between the light reflected at the surface of the dielectric layer and the light reflected at the MO layer.

Study of the optical Kerr enhancement characteristics for magnetic bilayer film showed that the thickness of the readout layer should not be more than 40 nm and that the readout characteristics are improved by using the readout layer, especially at a high readout power.

In addition, the NdTbFeCo readout layer was studied for short-wavelength recording [2.13].

2.2 Thermal design

2.2.1 Measurement of thermal properties

The thermal conductivity for Al-alloy and magnetic layers was estimated from the electrical conductivity by using Wiedemann-Franz's law [2.14]. The electrical conductivity was measured by using four-terminal method. The thermal conductivity of silicon nitride was obtained by fitting the thermal simulation into the experimental temperature profile [2.15]. The thermal conductivity for glass, poly-carbonate, resin and air was obtained from the literature [2.16].

The thermal constants used for the thermal simulation are summarized in Table 2.3.

2.2.2 *Thermal simulation*

Thermal simulation of the temperature distribution on the disk while recording and readout was done as follows. First the following three dimensional thermal diffusion equation was assumed:

$$C\rho\left(\frac{\partial T}{\partial t}\right) = k \cdot \nabla^2 \cdot T + Q, \quad \text{.....(2.7)}$$

where, C is the specific heat, ρ is the density, T is the temperature, t is the time, κ is the thermal conductivity for each film on a disk. Q is the heat given from the irradiation of laser light. The values of thermal constants such as C, ρ, and κ were determined experimentally and theoretically. With the thermal constants in Table 2.3, Eq. (2.7) was numerically calculated. For the calculation, layered films were divided into 2×10^5 elements of 0.1-μm width × 0.1-μm length × 0.01-μm height. Temperature profiles on the disks were, thus, obtained by solving the three dimensional thermal diffusion equation using the finite difference method with a super-computer [2.17, 2.18]. As a result of calculation, the thermal distribution on the magnetic film was obtained as isotherms.

Table 2.3 Thermal constants.

material	thermal conductivity	density	specific heat
	(W/K•cm)	(g/cm3)	(J/K•g)
magnetic layer	0.2	7.6	0.37
nitride layer	0.1	3.0	0.74
UV-resin	0.002	1.2	1.5
Glass	0.01	2.3	0.7
Air	0.0003	0.0013	1.0
Al	2.3	2.7	0.9
Al-alloy	0.5	2.7	0.9

2.2.3 *Model for domain formation*

Simulating the magnetic domain formation process during recording is more complicated than the optical and thermal simulation, mainly because the magnetization process is nonlinear in itself. The various domain formation models for numerical simulation has been reported. Tanaka [2.19] and Kawazoe [2.20] treated a domain formation with a small finite domain reversal unit. Hasegawa numerically solved Landau-Liphshitz-Gilbert's Equation, the equation of the motion of magnetic spin [2.21]. Mansuripur treated the MO film as a union of small patches [2.22, 2.23]. The patches are loosely coupled with the adjacent ones through the exchange-coupling force. The calculation is performed by a large scale parallel computer.

In this study, the magnetic domain formation process was assumed as the following model. The main advantage of the model is that it is easy to abstract the physical essence from the result because of the simplicity.

Figure 2.12 shows domain formation model, which was first introduced by Huth [2.24], and improved by Takahashi [2.25]. As the temperature of the media rises with a laser beam irradiation, the magnetic domain expands as shown in Fig. 2.12(a). The expansion is performed by magnetostatical forces: external magnetic field H_{ext} and demagnetizing field H_d. The coercive force H_c acts as a damping force of the expansion. At every instant of the domain expansion, the domain wall position (domain radius r) is determined by the following equation:

$$H_c(T) = \left| H_{ext} + H_d(T) - \left(\frac{\sigma_w(T)}{2rM_s(T)}\right) - \left(\frac{\partial \sigma_w}{2M_s \partial r}\right) \right| \quad \text{.....(2.8)}$$

where, σ_w, M_s, and T are the domain wall energy, the saturation magnetization, and the temperature at the domain wall position, respectively. Eq. (2.8) shows a equilibrium condition of the forces acting on the domain wall. The right side of the equation is deduced by differentiating the total magnetic energy. The third and the forth terms come from the wall energy, acting as a shrinking force.

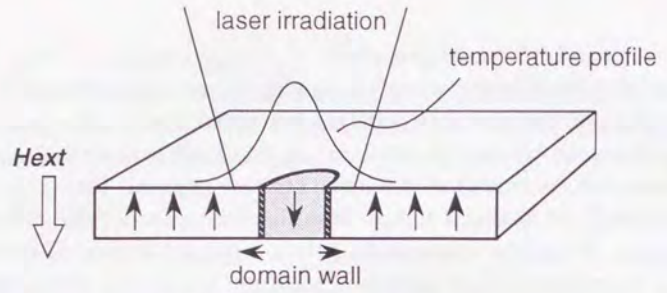

(a) heating process

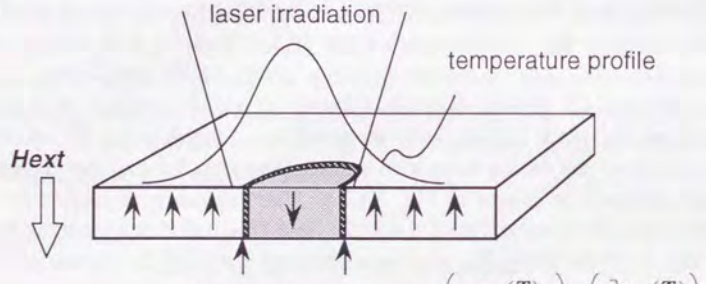

$$H_c(T) = H_{ext} + H_d(T) - \left(\frac{\sigma_w(T)}{2rM_s(T)}\right) - \left(\frac{\partial\sigma_w(T)}{2M_s\partial r}\right)$$

(b) about maximum temperature

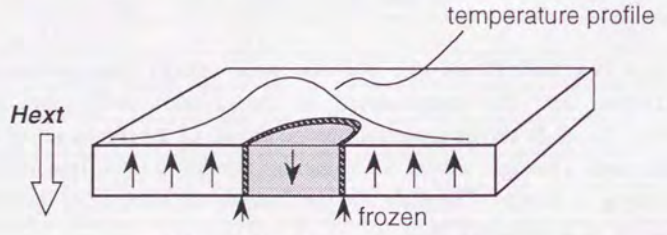

(c) cooling process

Fig. 2.12 Domain formation model.

The demagnetizing field H_d at a point in the domain wall was calculated from the following equation:

$$H_d = \int \frac{2M_s}{h}\left(\frac{1}{(\Delta x^2+\Delta y^2)^{1/2}} - \frac{1}{(\Delta x^2+\Delta y^2+h^2)^{1/2}}\right)dxdy \quad \text{.....(2.9)}$$

where, h is the thickness of the magnetic film; Δx and Δy denotes the distances from the point in the domain wall.

The wall energy $\sigma_w(T)$ at room temperature was estimated to be 1 erg/cm^2 {1×10^{-3} J/m^2}. Since the wall energy at the Curie temperature is zero, it was assumed that the wall energy linearly decreases to zero as the temperature increases to the Curie temperature.

A result of the numerical calculation of Eq. (2.8) is shown in Fig. 2.13, where the forth term of Eq. (2.8) is ignored. At a small domain radius, the coercivity becomes smaller than the right side of Eq. (2.8), which is the expansion force; therefore the domain expands until the Eq. (2.8) is fulfilled. At a large domain radius, the coercivity becomes higher than the expansion force; therefore, the domain is frozen. Consequently, the domain expands to the maximum radius that satisfy the Eq. (2.8) throughout the time evolution of the temperature profile.

If the external field is strong enough in Eq. (2.8), the influence of demagnetizing field and the domain wall energy is negligible; therefore the domain radius is determined by the equilibrium of the external field and the coercivity. That is, the domain wall stops at the position where the external field equals the coercivity.

Since coercivity is a function of the temperature, the equilibrium condition is represented by a certain temperature that is called a recording temperature. In the area where the temperature is higher than the recording temperature, the external field is higher than the coercivity; thereby the domain expands freely. Thus, the domain expands within the area where the temperature is higher than the recording temperature; consequently, the domain shape follows an isotherm of the maximum temperature experienced throughout the recording process.

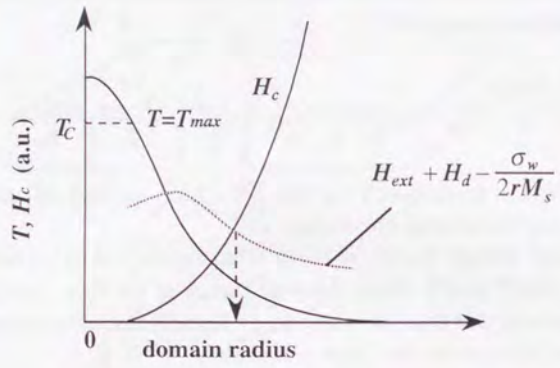

Fig. 2.13 Domain formation for light intensity modulated recording.

In the light intensity modulation recording, which is the most popular recording method, the domain shape was assumed to be an isotherm of the maximum temperature profile though the domain is not simply approximated by the circular (cylindrical) one.

Figure 2.14 shows the domain formation process in the magnetic field modulation overwriting (MMO). First, a circular domain is formed at high temperature (heated) region as shown in Fig. 2.14(a). Second, as the laser spot moves to the right in the figure, the domain is elongated, following trace of the heated region as shown in Fig. 2.14(b). Third, when the external (modulation) field is reversed as shown in Fig. 2.14(c), the direction of the magnetization in the heated area is reversed. In other word, reversely magnetized domain is formed in the heated region. As a result of domain reversal, a chevron-shaped domain is formed as shown in Fig. 2.14(c). Thus, by the repetition of the magnetic field reversal on information to be recorded, the information is recorded in the form of chevron-shaped domains as shown in Fig. 2.14(d)

It is noted that the domain shape (heated area) is not circular in detail, but follows isotherm at every instant. The detailed isotherm is oval as discussed in the next chapter.

It is also noted that the domain wall mobility is not considered in the model. The finite value of domain wall mobility will result in the smaller size of the recorded domain because the domain will be frozen before reaching its maximum size.

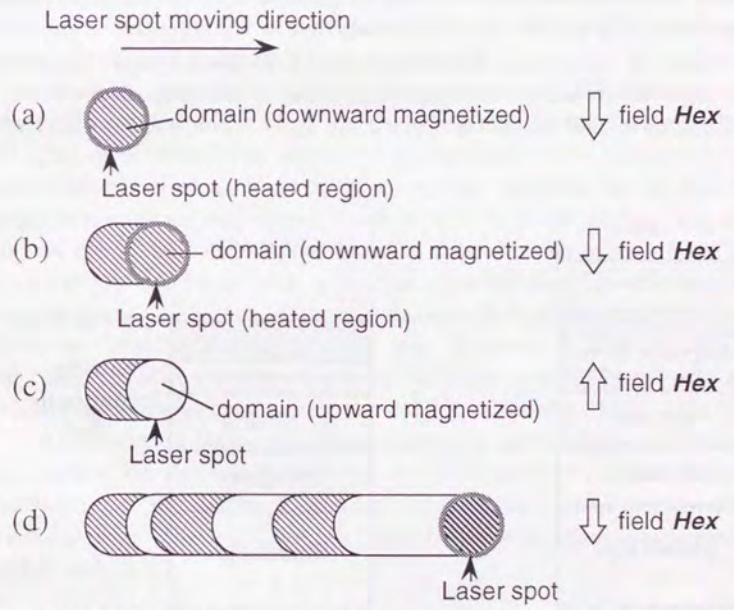

Fig. 2.14 Domain formation for magnetic field modulation.

2.2.4 Trilayered and quadrilayered disk

Domain shape and recording characteristics were investigated for trilayered and quadrilayered structure disks as shown in Fig. 2.15. The substrate is 5.25 inches (130 mm) in diameter and 1.2 mm in thickness. Spiral v-shaped grooves of 1.6-μm pitch are formed on an ultraviolet light curing resin (UV resin) layer on a grass substrate. Figure 2.15(a) shows a trilayered disk in which aluminum film is deposited behind the magnetic film. Both the trilayered and quadrilayered disks were coated with UV resin to protect them from crashing against the flying magnetic head, which is used for MMO. As the magnetic film, $Tb_{27}Fe_{63}Co_{10}$ was used. The Curie temperature T_c is 200 °C. The composition of magnetic film was determined by inductively coupled plasma (ICP) spectroscopy. Dynamic write-read characteristics were measured using a newly developed flying head-type drive [2.26] for MMO.

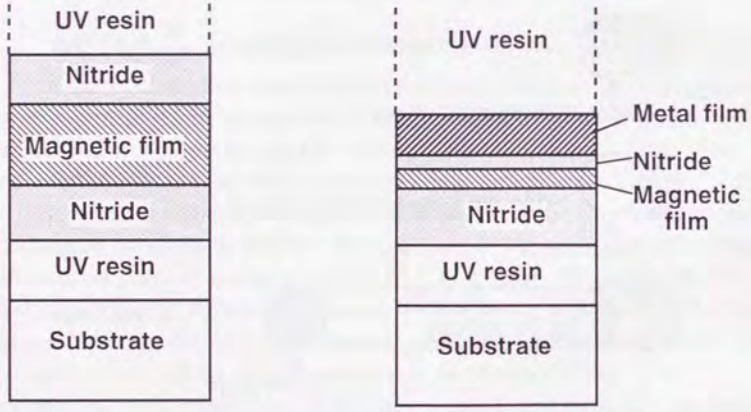

(a) Trilayered disk (b) Qudrilayered disk

Fig. 2.15 Typical thermal structures of MO disk.

2.2.5 Recording characteristics

Figure 2.16(a) shows the dependence of the carrier-to-noise ratio (***CNR***) on write power P_w of trilayered disk. At 1-MHz magnetic field modulation frequency (5.6-μm domain length), the ***CNR*** increases with increasing P_w. On the other hand, the ***CNR*** has a peak value at 8 mW followed by a decrease with increasing ***P***w at the 7.4 MHz (0.75-μm domain length) condition. The maximum ***CNR*** is only 45 dB, which is not sufficient for actual high-density devices.

Figure 2.16(b) shows the dependence of ***CNR*** on P_w for quadrilayered disk. A little dependence of ***CNR*** on ***P***w was observed above 7 mW when 0.75-μm domains were recorded. The maximum ***CNR*** of 48 dB is obtained, which is 3 dB higher than that for trilayered disk.

To make clear the cause of difference in the ***CNR*** character, we observed recorded domains on the trilayered and the quadrilayered disk. Here, for clear observation, domains were recorded on the non grooved flat area of the disk instead of on the grooved area, and from the air side. The magnification of the microscope was 80×2×10. As shown in Fig. 2.17, each domain has a "tail" at its edge, which is formed at the cooling edge of a continuously irradiated laser spot. The recorded domains are separated clearly from each other when the domain is long enough (2.3 μm). However, overlapping of domains was observed at a higher-density recording condition (the domain length 0.75 μm) on trilayered disk. This overlapping seems to cause a decrease in ***CNR*** as shown in Fig. 2.16(a).

As mentioned above, the domain shape is influenced by the thermal distribution on the magnetic film. To understand the situation more precisely, both the shapes of recorded domains and readout characteristics were simulated. The simulation was done by using the method described in §2.2.2. and §2.2.3.

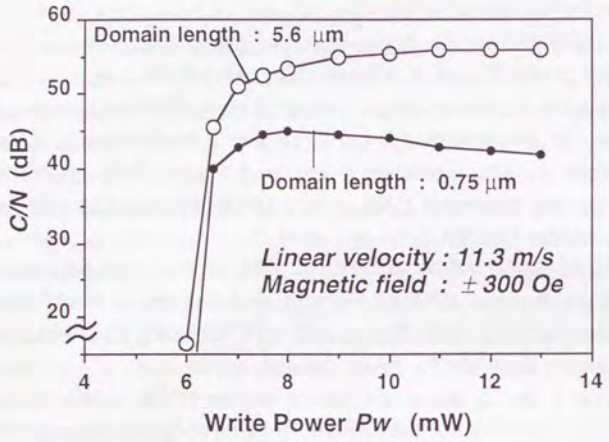

(a) trilayered disk

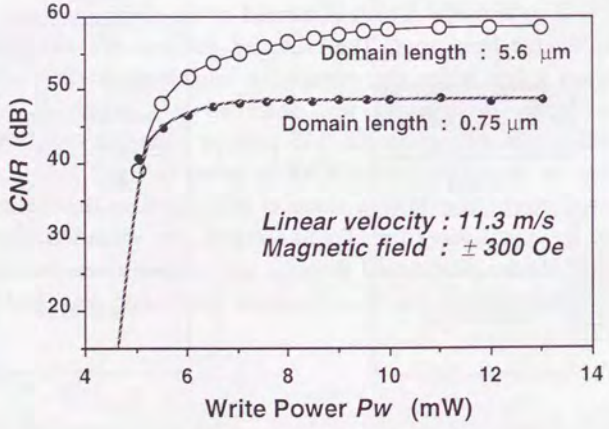

(b)quadrilayered disk

Fig. 2.16 CNR of trilayered disk as a fuction of write power.

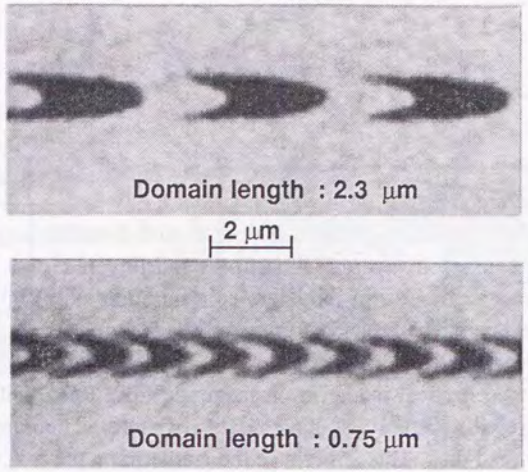

Linear velocity : 11.3 m/s
Magnetic field : ± 300 Oe
Write power Pw : 14 mW

(a) Domains on quadrilayered disk

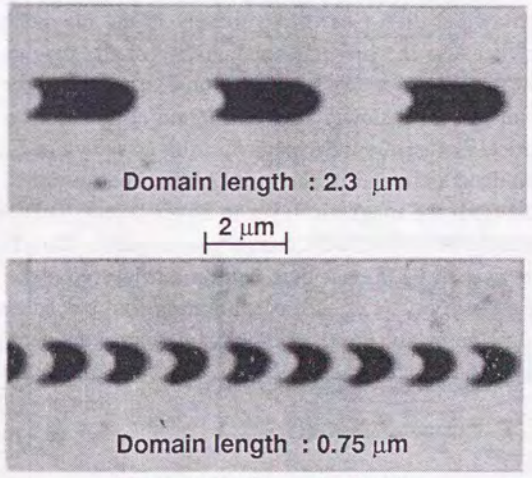

Linear velocity : 11.3 m/s
Magnetic field : ± 300 Oe
Write power Pw : 10 mW

(b) Domains on quadrilayered disk

Fig. 2.17 Domains recorded by MMO.

2.2.6 *Thermal analysis through simulation*

Figure 2.18 shows the simulated isotherms and domain shapes on the magnetic film for (a) trilayered disk, (b) quadrilayered disk, and (c) trilayered disk of the same film thickness configuration as (b) but with no aluminum metal layer. The laser beam runs on the disk from right to left.

Recorded domain on a trilayered disk (a) has the relatively long tails, which reflects the elliptical isotherm on magnetic film. Recorded domains on the quadrilayered structure disk have relatively short tails compared with those on a trilayered disk. This is because the isotherm on the magnetic film is more circular. Moreover, it is proved the aluminum layer acts as a heat sink layer and improves the heat flow so as to reduce the tail length because the recorded domain on disk (c) has longer tail than disk (a)

The difference in the shape of the isotherms is explained as follows. Figure 2.19(a) shows schematic diffusion of the heat given from the laser beam. In the trilayered disk, heat flows mainly in the magnetic film (in-plain direction) because the thermal conductivity of the magnetic film is higher than that of the nitride (SiN_x). Therefore, heat tends to be stored in the magnetic film decreases slowly after irradiation of the laser beam, which causes the elliptical isotherm on the magnetic film as shown in Fig. 2.18(a). In quadrilayered disk, a circular isotherm is obtained because the heat flows quickly outward from the magnetic layer to cover layers. This situation is realized by adding a heat-sink layer behind the magnetic film. In this case the magnetic layer must be thinner than that on a trilayered disk in order to improve writing sensitivity. Furthermore, a nitride film placed between the magnetic film and the metal film (heat sink) can control the heat flow from the magnetic layer to the heat-sink layer.

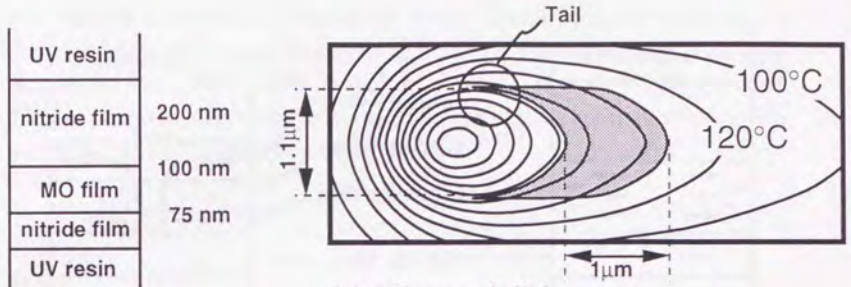

(a) trilayered disk

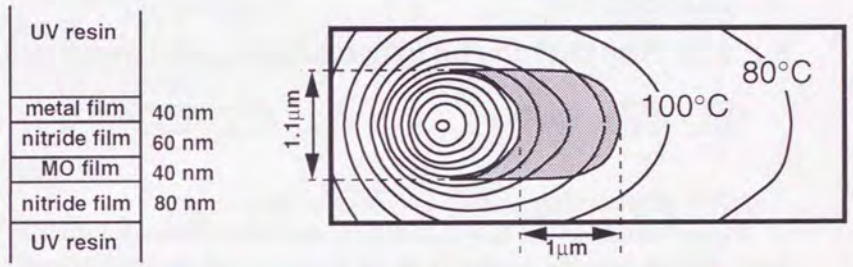

(b) quadrilayered disk

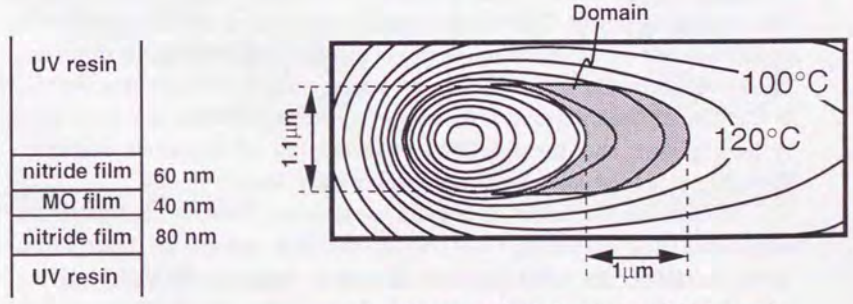

(c) trilayered disk (thin MO layer)

Fig. 2.18 Isotherms and Domain shape obtained from simulation.

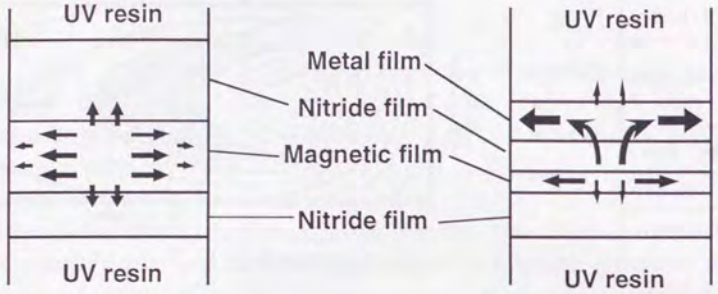

(a) Trilayered disk (b) Quadrilayered disk

Fig. 2.19 Heat diffusion for trilayered and quadrilayered disk.

2.2.7 Domain shape and readout characteristics

Figure 2.20 shows the laser power dependence of the recorded domain shape obtained from the simulation on the trilayered and the quadrilayered disk. In the case of trilayered disk, the domain shape changes with increasing laser power. Both the width and the length of the domain increase with increasing power. The tail of a domain recorded at about 8- or 10-mW power extends to neighboring domain, resulting in overlapped domains. Therefore, a circular laser spot can no longer resolve each domain clearly. In the case of quadrilayered disk, tails of a recorded domain are short even at high power and there is little overlapping of recorded domains. Therefore a circular laser beam can resolve each domain clearly.

To evaluate the effect of domain overlapping, readout characteristics were simulated assuming Gaussian distribution pattern of laser beam intensity. Here, the wavelength of the laser beam is 830 nm and the numerical aperture of the objective lens is 0.6. In the case of trilayered disk (Fig. 2.21(a)), ***CNR*** increases with P_w in the case of long domain length (low frequency recording). However, ***CNR*** shows decrease with increasing

P_w above 8 mW for high-density (0.75-μm domain length) recording. In the case of quadrilayered disk (Fig. 2.21(b)), ***CNR*** keeps increasing with increasing P_w above 8 mW even for recording of short-length domains. These characteristics of the readout simulation coincide with the experimental results shown in Fig. 2.16.

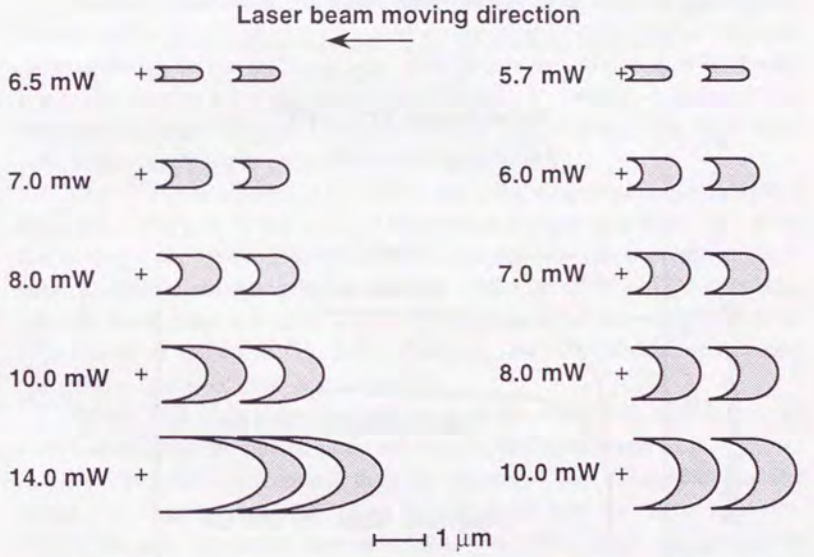

(a) Trilayered disk (b) Quadrilayered disk

Fig. 2.20 Simulated domains on (a) tirlayered disk, and (b) quadrilayered disk.

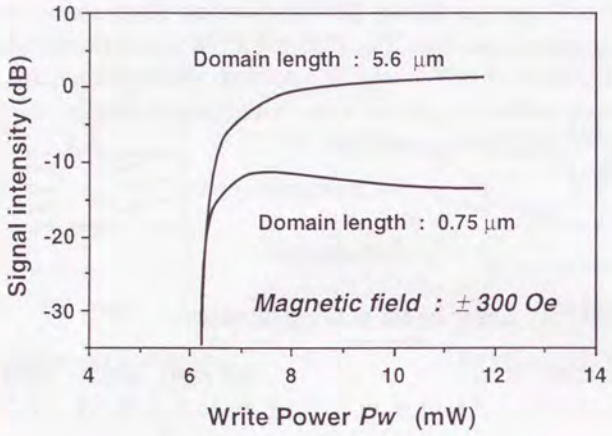

(a) trilayered disk

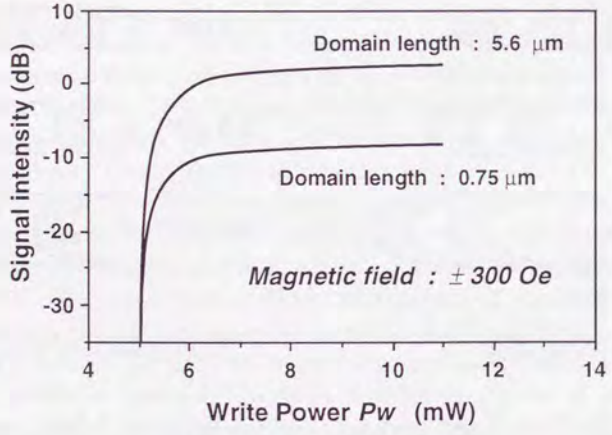

(b)quadrilayered disk

Fig. 2.21 Signal intensity obtained from simulation.

2.2.8 Comparison with light intensity modulation

As mentioned in the previous section, short-tail domains from MMO were observed at both low-(2.5 MHz) and high-(7.4 MHz) frequency recording conditions as shown in Fig. 2.17(b). Here, domain width does not decrease even with decreasing domain length. Also, a domain edge is not influenced by the preceding domain even in high-density recording, because the thermal profile is the same for any recording length. Therefore, MMO is favorable for mark edge recording that can realize higher density than mark position recording.

On the other hand, domains recorded by light intensity modulated recording (LIM), which is conventional recording without overwriting, are oval as shown in Fig. 2.22 are oval. This shows the influence of backward heat flow even in a quadrilayered disk. Moreover, contact of domains was observed as high frequency (domain length : 0.75 μm). The high laser power was necessary to obtain enough domain width.

The CNR characteristics for MMO and LIM method on a quadrilayered disk at 7.4 MHz (0.75-μm domain length) are compared in Fig. 2.23. With increasing write power Pw, the ***CNR*** of MMO remains constant above 7 mW as mentioned in the previous section, while the ***CNR*** of LIM decreases after the peak value at 6 mW. This decrease of the ***CNR*** is caused by contact of domains as shown in Fig. 2.22. Therefore, the allowable power margin for LIM is narrower than that for MMO.

Figure 2.24 shows the time variation of the maximum temperature of the medium with the pulsed laser irradiation. The quadrilayered disk shows a more rapid thermal response than the trilayered disk. This is due to the small heat capacity of thin MO-layer and the quick heat flow in the heat-sink layer. Because of quick thermal response a clear shape of domain is expected although the domain by LIM in the previous section is unacceptable. This is proved by Maeda et al. by a precise domain technique with multiple laser pulse [2.27].

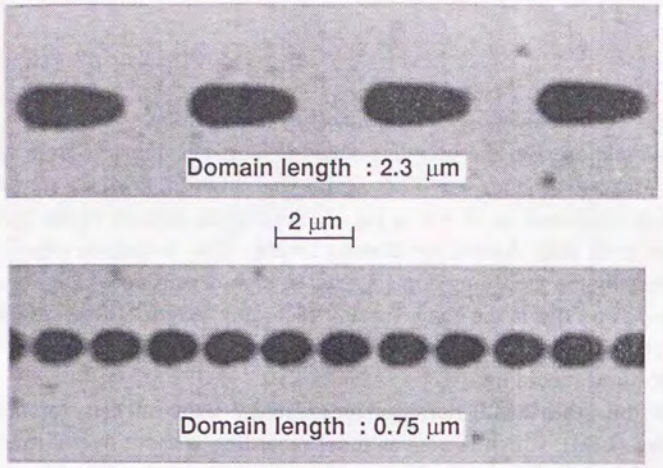

Linear velocity : 11.3 m/s
Magnetic field : + 300 Oe
Write power Pw : 12 mW

Fig. 2.22 Domains recorded with LIM on quadrilayered disk.

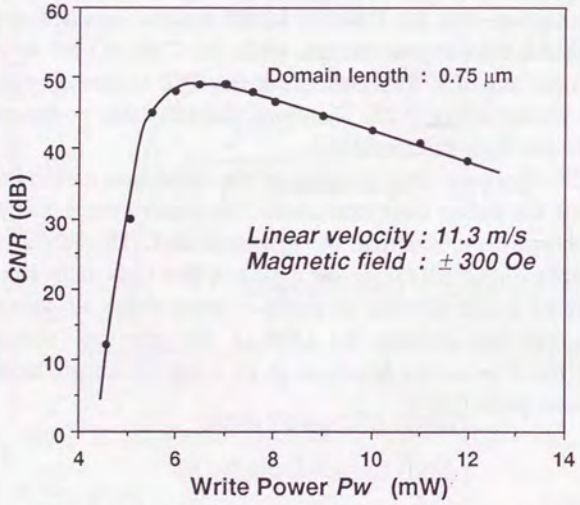

Fig. 2.23 *CNR* for LIM on quadrilayered disk.

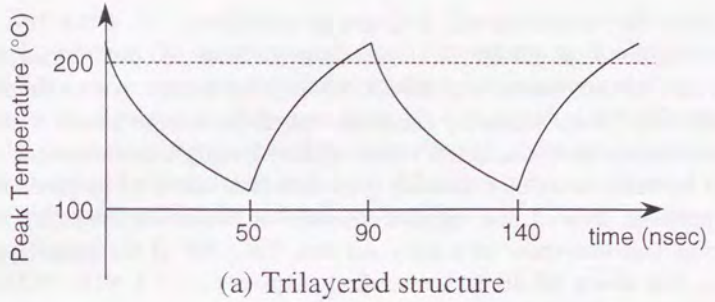

(a) Trilayered structure

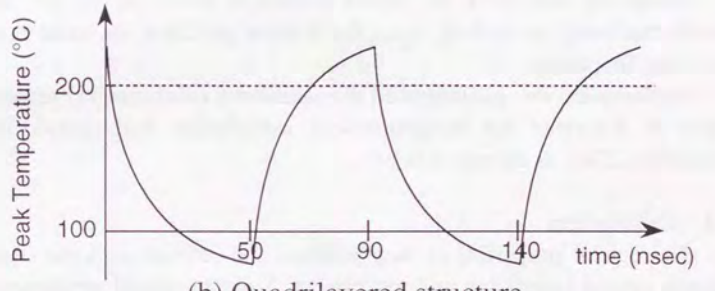

(b) Quadrilayered structure

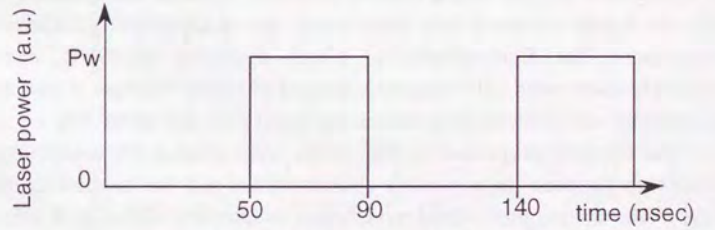

(c) Recording laser waveform

Fig. 2.24 Thermal responses for trilayered and quadrilayered disks.

2.2.9 *Suitable thermal structure for MO disk*

Evaluation of the domain shape and of the write/read characteristics for a trilayered disk showed that the tails of recorded domains reduce the ***CNR*** under high-power recording conditions when the domain length is short. Good write/read characteristics were achieved using a quadrilayered disk that has aluminum film to provide quick heat flow out of the magnetic film. Experiment showed that recorded domains on a quadrilayered disk have shorter tails than those on a trilayered disk. The ***CNR*** of the quadrilayered disk was about 50 dB at a recording frequency of 7.4 MHz (0.75-μm domain length) and at a linear velocity of 11.3 m/s.

Compared with LIM, the MMO method is more suitable for high-density mark-edge recording, since the thermal profile is the same at any recording frequency.

Furthermore, the quadrilayered disk showed a quick thermal response, which is desirable for magnetic-field modulation with pulsed-laser irradiation [2.28], as discussed in §4.2.

2.3 Conclusion

The optical properties of Kerr rotation and reflectivity were studied through optical simulation and experiment. Suitable optical structures for MO media are a quadrilayered structure with an aluminum reflective layer, and a magnetic bilayer with a readout magnetic layer. In the quadrilayered disk, the figure of merit and reflectivity are independently controlled. Furthermore, the Kerr ellipticity, which degrades the SNR, can be completely eliminated. The magnetic bilayer is useful because it can use a magnetically soft readout layer, which has good MO characteristics.

The thermal properties of MO disks were studied by analyzing the relationship between the recording characteristics and the thermal structure of the media for magnetic-field modulation overwriting (MMO). A suitable thermal structure for the MO media is the quadrilayered structure with a thermal-diffusive metal layer. The quadrilayered disk reduces the length of the "tail" in the domain recorded by MMO, eliminating the overlap between domains and increasing the signal intensity and quality.

Fortunately, the quadrilayered structure has both good optical and thermal properties. To maintain consistency between the optical properties and the thermal properties, the optical properties should be controlled by changing the thicknesses of the two dielectric layers and of the MO-film, and the thermal properties should be controlled by changing the thermal conductivity of the heat-sink (metal) layer. Changing the composition of the metal film greatly affects the thermal conductivity.

References

[2.1] F. Kirino, N. Ogihara, M. Takahashi, and N. Ohta, Material Trans., JIM, **34**, 604 (1993).

[2.2] K. Egashira, T. Yamada, J. Appl. Phys., **45**, 3643 (1974).

[2.3] M. Takahashi, H. Sukeda, M. Ojima, and N. Ohta, J. Appl. Phys. **63**, 3838 (1988).

[2.4] T. Niihara, M. Takahashi, H. Miyamoto, F. Kirino, N. Ogihara, an N. Ohta, J. Magn. Magn. Materials, **88**, 177 (1990)

[2.5] H. Miyamoto, T. Niihara, H. Sukeda, M. Takahashi, T. Nakao, M. Ojima, and N. Ohta, J. Appl. Phys. **66**, 6138 (1989).

[2.6] K. Egashira, T. Yamada, J. Appl. Phys., **45**, 3643 (1974).

[2.7] T. Niihara, N. Ohta, K. Kaneko, Y. Sugita, and, S. Horigome, IEEE Trans. on Magn., **22**, 1215 (1986).

[2.8] S. Grove and W. Challener, Jpn. J. Appl. Phys., **28**, Suppl. **28-3**, 51 (1989).

[2.9] T. Kobayashi, T. Tsuji, S. Tsunashima, and S. Uchiyama, Jpn. J. Appl. Phys., **20**, 2089 (1981)

[2.10] S. Tsunashima, S. Masui, T. Kobayashi, and S. Uchiyama, J. Appl. Phys., **53**, 8175 (1982)

[2.11] M. Nakamura, T. Ishida, S. Tsunashima, and S. Uchiyama, J. Magn. Soc. Jpn., **11**, 201 (1987).

[2.12] S. Tsunashima, K. Tsuji, T. Kobayashi, S. Uchiyama, J. Magn. Soc. Jpn., **5**, 73 (1981).

[2.13] T. Niihara, H. Miyamoto, and R. Suzuki, Digest of the 14th Annual Conf. on Magn. in Jpn., 364 (1990).

[2.14] C. Kittel, Introduction to Solid State Physics, 5th edition, John Wiley & Sons., Inc., New York (1976).

[2.15] H. Nakagawa, S. Nakamura, M. Takahashi, and A. Arimoto, Appl. Opt., **31**, 4562 (1992).

[2.16] AMERICAN INSTITUTE OF PHISICS HANDBOOK, 2nd edition, McGraw-Hill Book Company, Inc. (1963)

[2.17] M. Takahashi, T. Niihara, and N. Ohta, J. Appl. Phys. **64**, 262 (1988).

[2.18] H. Miyamoto, T. Niihara, H. Sukeda, M. Takahashi, T. Nakao, M. Ojima and N. Ohta, J. Appl. Phys. **66**, 6138 (1989).

[2.19] F. Tanaka, S. Tanaka, Y. Sasano, K. Ono, S. Suzuki, H. Sukeda, T. Kaku, T. Niihara, T. Nakao, M. Kasai, H. Miyamoto, K. Akagi, Y. Miyamura, N. Ohta, and M. Ojima, SPIE **1316**, Optical Data Storage ' 90, 245 (1990)

[2.20] Y. Kawazoe, X. Hu, T. Yorozu, T. Imazu, and N. Ohta, J. Magn. Soc. Jpn., **17**, Suppl. **S1**, 188 (1993)

[2.21] M. Hasegawa, K. Moroga, M. Okada, O. Okada, and Y. Hidaka, J. Magn, Soc. Jpn. **15**, Suppl **S1**, 307, (1991)

[2.22] M. Mansuripur, J. Appl. Phys. **61**, 1580 (1987)

[2.23] M. Mansuripur, J. Appl. Phys. **63**, 5809 (1988)

[2.24] B. G. Huth, IBM J. Res. Dev. **18**, 100 (1974)

[2.25] M. Takahashi, H. Sukeda, M. Ojima, and N. Ohta, J. Appl. Phys. **63**, 3838 (1988).

[2.26] H. Sukeda, M. Ojima, M. Takahashi, And T. Maeda, Jpn. J. Appl. Phys. **26** (1987), p. 2437

[2.27] T. Maeda, T. Toda, H. Ide, F. Kirino, S. Mita, and K. Shigematsu, IEEE Trans. on Magn., **29**, 3788 (1993).

[2.28] S. Yonezawa and H. Miyamoto, Digest of Symp. on Opt. Memory 1994, 65 (1994)

3 Magnetic Multilayer for Overwriting

Magneto-optical multilayers have been investigated for overwriting, magnetic super-resolution, and so on. In these media, the exchange-coupling force between layers plays a very important role and has been studied from various point of view [3.1], [3.2], [3.3]. Therefore, as mentioned above, analyzing the mechanism of domain formation is needed to obtain a functional medium with magnetic multilayers. In this chapter, the properties of magnetic multilayers for light-intensity modulation overwriting [3.4] (LMO) are studied.

To achieve practical LMO, many problems must be solved. Some of these problems, such as the power margin (§3.1) and the thermal crosstalk (§3.2), are based on the fact that LMO needs three levels of laser power: recording power, erasing power, and readout power. Others, such as the initialization noise (§3.3) and the degradation after overwrite repetition (§3.4), originate from the exchange-coupling force between the magnetic layers.

3.1 Overwriting and readout power margin

3.1.1 Readout stabilization by using magnetic transfer

In LMO, two levels of laser power is required for overwriting, which makes it difficult to control the laser power levels. Therefore, it is necessary to obtain a wide power margin for two levels of recording power and readout power.[3.5]

In this section, an application of domain transfer (magnetic printing) is studied to obtain a good overwrite power margin. This is performed by improving the readout stability or by preventing the erase process.

As shown in §1.2.3, depending on the power level (P_H and P_L), the direction of the magnetization in the heated area is controlled under a constant bias field H_{bias}. In other words, P_H forms the recorded domains and P_L erases the domains. Therefore, overwriting is performed by modulating the laser power between P_H and P_L.

In order to obtain a sufficient overwriting power margin, T_L must be set low as shown in Fig. 3.1. However, if P_L is set low, a high read power induces L-process and destroys the recorded domains. This information damage is a major problem for obtaining a good overwriting margin. Therefore, the following method for improving the read power margin without any information damage was proposed. A large read power margin is achieved by applying a transfer magnetic field H_{tr} before readout. The principle is explained as follows.

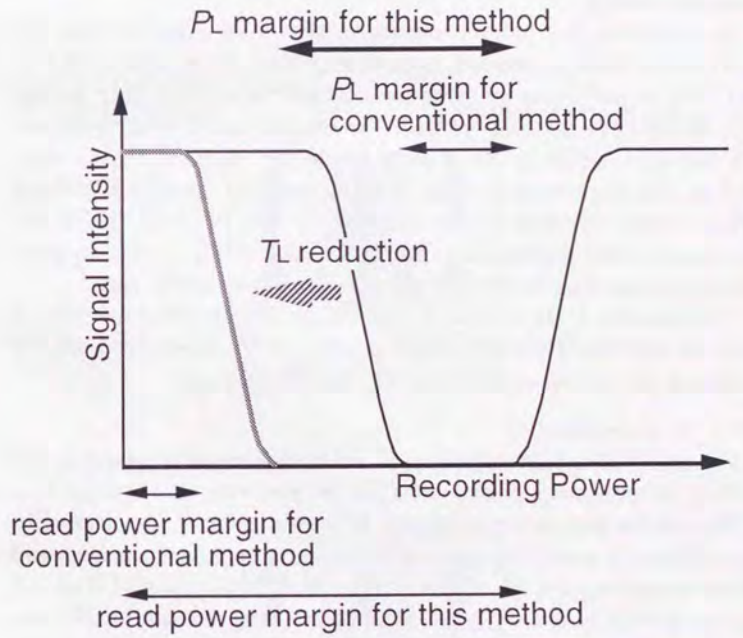

Fig. 3.1 Extension of read power margin.
(Stabilization against readout laser)

Figure 3.2(a) shows the magnetization state after overwriting. The two magnetic layers are magnetized in the same direction both inside and outside of the recorded domains. This magnetization state is stable because no interface wall exists between the two layers.

Figure 3.2(b) shows the magnetization state after the initialization. The initialization produces the interface domain walls between the memory layer (M-layer) and the writing layer (W-layer). This domain wall energy induces the L-process during overwriting . In other words, no information damage occurs in the absence of domain walls. Therefore, returning the magnetization state from Fig. 3.2(b) to Fig. 3.2(c) is a key to avoiding the information damage.

By applying $\boldsymbol{H}_{tr}$ before readout as shown in Figure 3.2(c), the magnetization state is returned from that in Fig. 3.2(b) to that in Fig. 3.2(a). This is performed by using the magnetic transfer process. In Fig. 3.2(b), the effective coercivity of the W-layer inside the recorded domain is lower than that outside of the domain due to the interface domain wall. Therefore, the magnetization of the W-layer inside the domain is reversed by $\boldsymbol{H}_{tr}$, whose direction is the opposite to that of $\boldsymbol{H}_{ini}$. Thus, the magnetization state is returned to the stable state in Fig. 3.2(a). In other words, the domains on the M-layer are transferred onto the W-layer.

Consequently, if $\boldsymbol{H}_{tr}$ is applied, L-process is eliminated and information damage is suppressed during readout process. If $\boldsymbol{H}_{tr}$ is switched off, the information can be overwritten through L- and H-processes.

3.1.2 Experiment

Figure 3.3 shows an experimental set up for magnetic transfer. For recording, an initializing magnet and a bias magnet were used to apply $\boldsymbol{H}_{ini}$ and $\boldsymbol{H}_{bias}$ to the medium, respectively, as shown in Fig. 3.3(a). During or before readout, a transfer magnet set between the initializing magnet and the bias magnet applies $\boldsymbol{H}_{tr}$ to the media. The field intensity of $\boldsymbol{H}_{ini}$ and $\boldsymbol{H}_{bias}$ are 400 kA/m and 40 kA/m, respectively. The intensity of $\boldsymbol{H}_{tr}$ was varied from 160 kA/m to 320 kA/m. In the actual drive $\boldsymbol{H}_{tr}$ is applied by the bias magnet because the field must be switched for recording and reading.

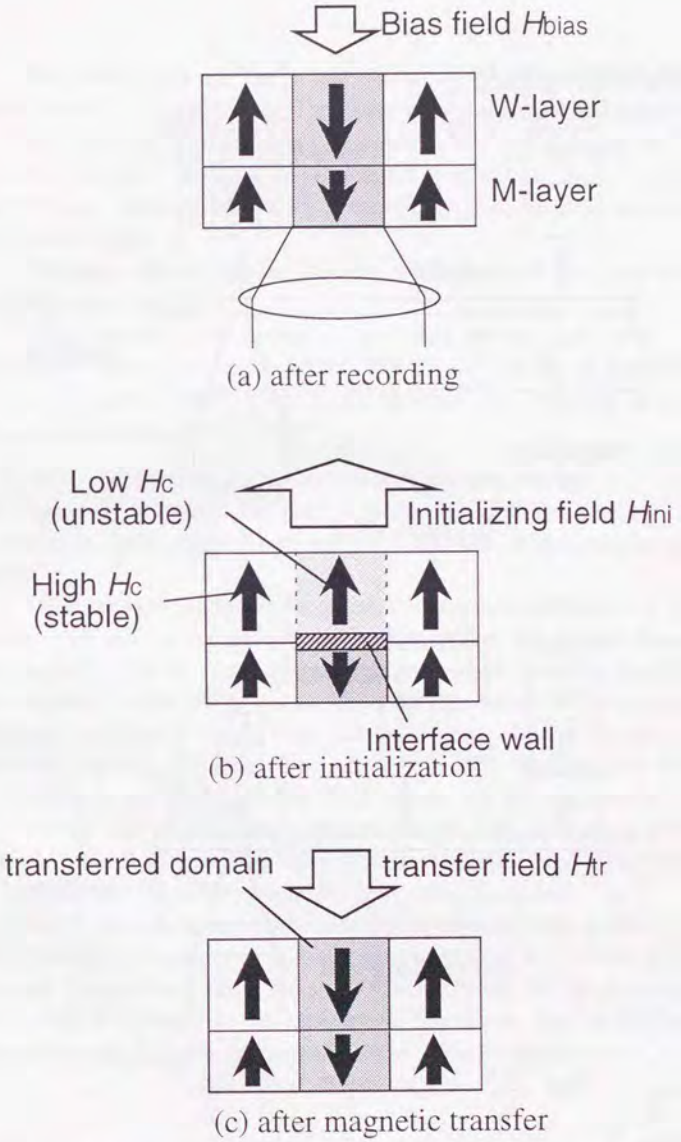

Fig. 3.2 Magnetic domain transfer process.

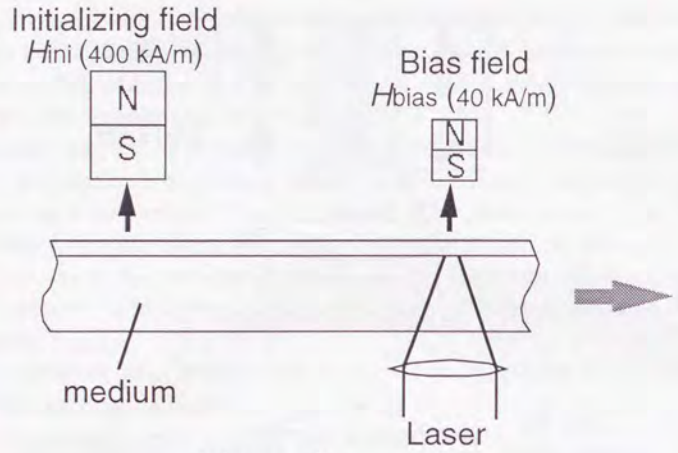

(a) recording

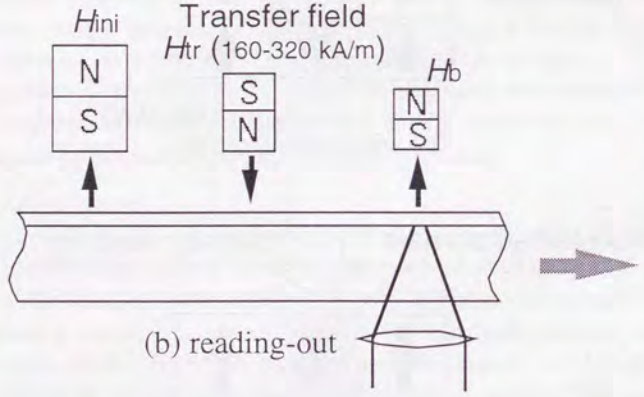

(b) reading-out

Fig. 3.3 Experimental set up.

The wavelength and the numerical aperture of the optical head were 830 nm and 0.55, respectively. The linear velocity was set at 4.2 m/s.

The structure of the medium is shown in Fig. 3.4(a). As shown in Fig. 3.4(b) the M-layer and the W-layer are TM-dominant and RE-dominant, respectively. These layers were prepared by rf-magnetron sputtering of composite targets.

The disk substrate is glass/2p (photo polymerization) replica with 1.6-μm-pitch spiral grooves.

For domain observation, a polarized microscope with an oil-immersion-type objective lens (x100, NA 1.1) was used. In order to avoid optical disturbance from grooves, the domains are observed on a mirror area without groove.

3.1.3 Magnetic characteristics and duplication process

Figure 3.5(a) shows the Kerr hysteresis loop of the medium at room temperature. Small minor loops and magnetic states of the medium are also shown.

After the information is recorded, the magnetic moments of the two layers undergo exchange-coupling each other. Since the layers are ferrimagnetic, the exchange-coupling is performed in such a way that the TM moments of the two layers are aligned in the same direction. As a result the magnetizations of the M-layer and the W-layer align in the anti-parallel direction. In Fig. 3.5, the directions of the TM moment and the total magnetization are shown as the solid arrows and the transparent arrows, respectively. The magnetization state after recording is shown as B or D in Fig 3.5. State B differs from state D in the magnetization direction of the M-layer, due to the difference in the recorded information.

When an upward magnetic field of 300 kA/m to 1000 kA/m is applied on the medium in state B or D, the magnetization of the W-layer in state B reverses but that in state D does not. That is, state B changes to state A while state D remains in the same state. Therefore, $\boldsymbol{H}_{\mathrm{ini}}$ of 300 kA/m to 1000 kA/m can initialize the magnetization of the W-layer.

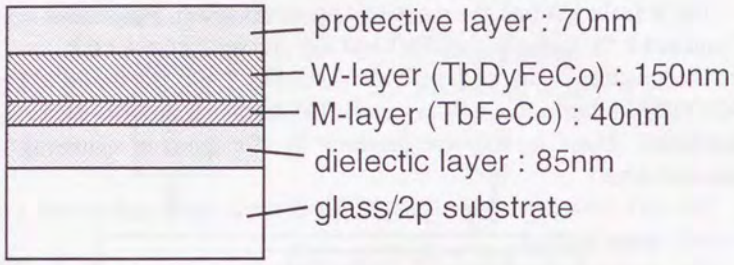

(a) structure of the medium

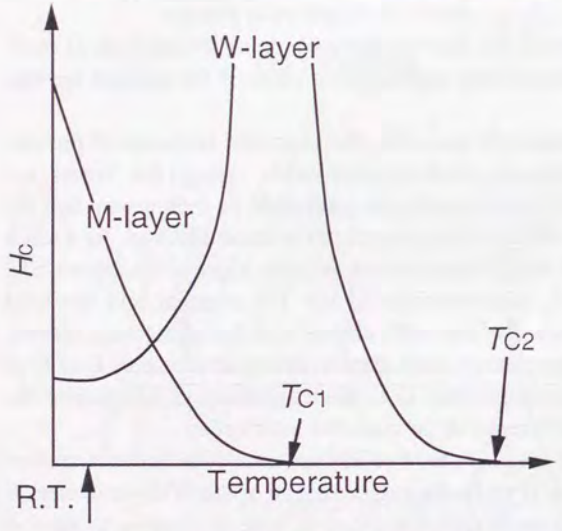

(b) temperature dependance of the coercive forces

Fig. 3.4 Configurations of the medium.

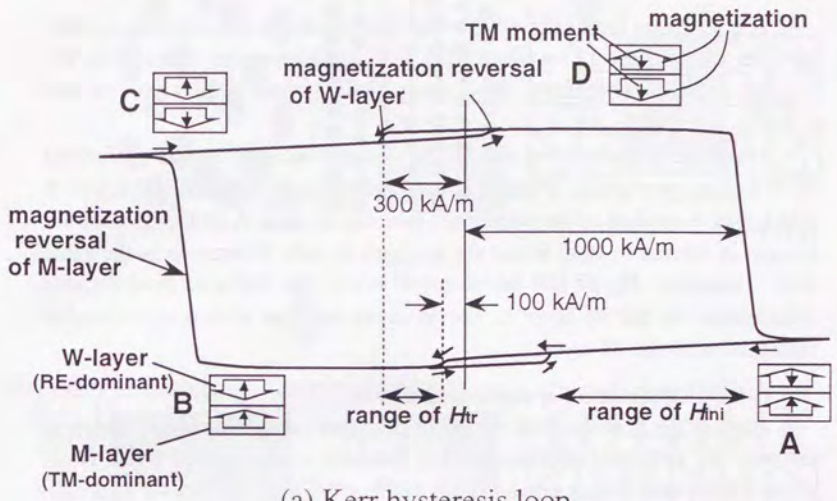

(a) Kerr hysteresis loop

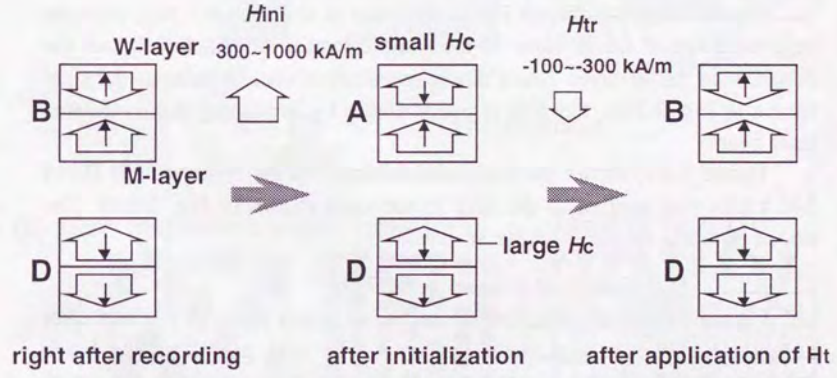

(b) initialization and transfer process

Fig. 3.5 Characteristics of magnetic transfer medium.

If a magnetic field over 1000 kA/m is applied, the magnetization of the M-layer in the state D reverses. This lead to information damage by the magnetic field. Therefore, H_{ini} must be less than 1000 kA/m in this medium.

Magnetic transfer from the M-layer to the W-layer can be performed by following procedure. When a downward magnetic field of 100 kA/m to 300 kA/m is applied to the initialized medium in state A or D, the medium in state A returns to state B and the medium in state D remains in the same state. Therefore, H_{tr} of 100 kA/m to 300 kA/m can duplicate (transfer) the information in the M-layer to the W-layer without disturbing recorded information in the M-layer.

3.1.4 Observation of duplicated domains

Figure 3.6(a) shows the recorded domains on the W-layer, which is observed by polarized microscope. The domains were recorded under H_{bias} of 3.2 kA/m with a laser power of 12.7 mW at a linear velocity of 11.3 m/s. The recording frequencies were 7.5 MHz and 2 MHz, which corresponded to the domain lengths of 0.75 μm and 2.8 μm, respectively.

Figure 3.6(b) shows the initialized state of the W-layer. H_{ini} puts the magnetization of the W-layer in the same direction of H_{ini} and erases the domains on the W-layer. Since this magnetization state is same as the state shown in Fig. 3.2(b), the disk is overwritable by irradiating the modulated laser beam.

Figure 3.6(c) shows the duplicated domains on the W-layer after H_{tr} of 240 kA/m was applied to the disk in the state shown in Fig. 3.5(b). The erased domains reappear on the W-layer.

3.1.5 Stabilization of domains in readout

Figure 3.7 shows the readout carrier (C) and noise (N) levels after various DC laser powers were irradiated. The dark gray line, the black solid line and the dotted line indicate the readout intensities with H_{ini}, with both H_{ini} and H_{tr} of 240 kA/m, and without H_{ini}, respectively.

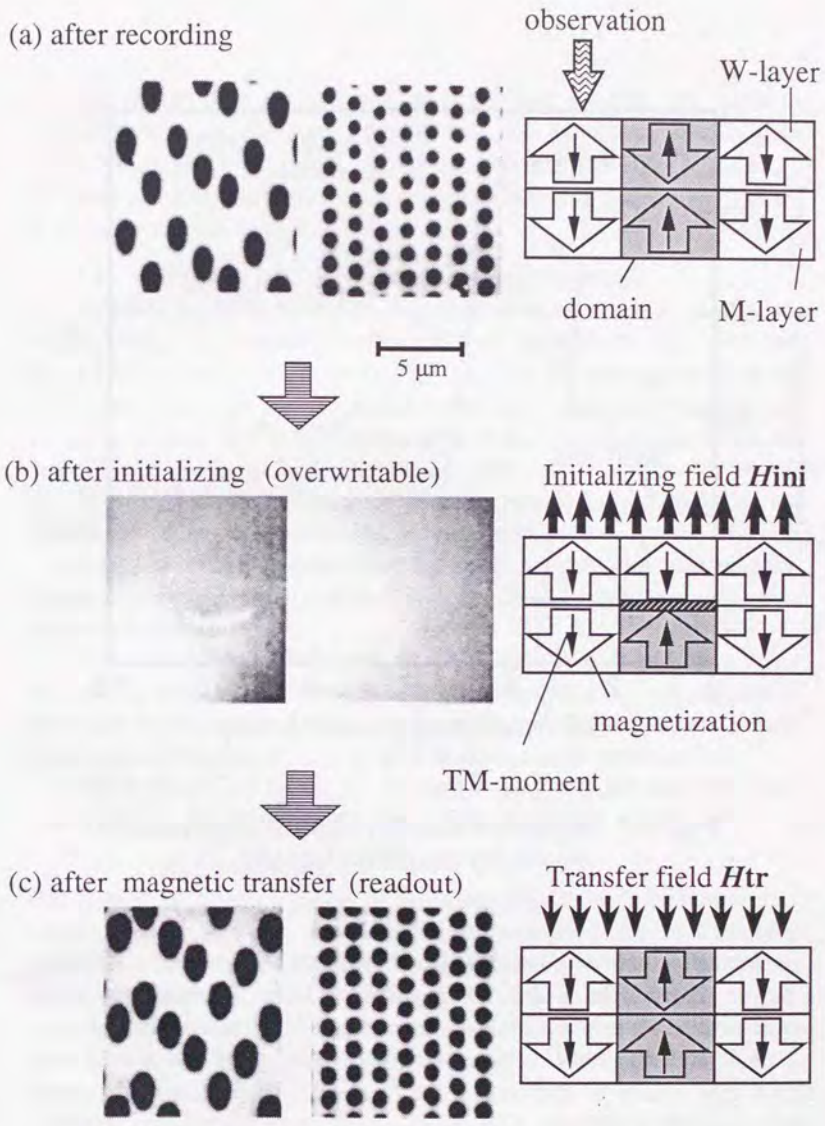

Fig. 3.6 Duplicated domains.

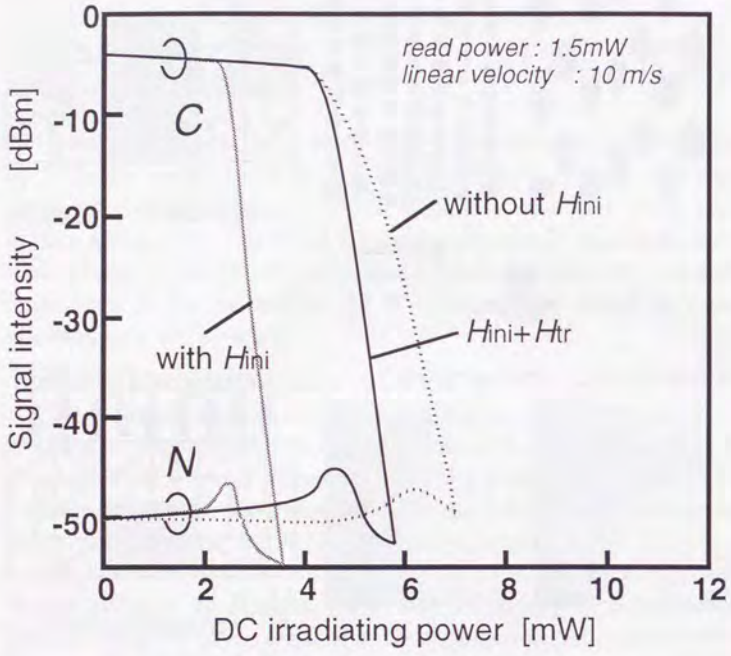

Fig. 3.7 Improved stability against high readout power by magnetic transfer.

With H_{ini} (dark gray lines), which is the normal overwriting condition, a DC irradiated light of 2.5 mW degrades C level. Therefore the read power must be set below 2.5 mW in order to avoid information damage.

With both H_{ini} and H_{tr} (black solid lines), a DC irradiated light of less than 4 mW causes no decrease in the C level. Therefore, a read power above 2.5 mW is allowed. This shows extension of information stability against high DC power irradiation.

Assuming that the domain transfer was perfect, the readout characteristics with H_{tr} must coincide with that without initializing field (dotted line). However, this is not the case. Furthermore, the N level at a DC power of 2 to 4 mW slightly increased. Therefore, the domain transfer is not perfect in this case.

3.1.6 Magnetic field dependence of printed domains

To study the incompleteness of the domain transfer, the domain shapes on the W-layer were observed after a H_{tr} of 160 kA/m to 320 kA/m was applied. The results are shown in Fig. 3.8. The left photographs and the right photographs are the domains recorded at frequencies of 2 MHz and 7.5 MHz, respectively. It was confirmed that the domain shapes on the M-layer showed no change under the transfer field.

When H_{tr} is 160 kA/m, some domains recorded at 7.5 MHz are not transferred. This is because H_{tr} is too small to transfer the domains completely. Although some domains are not transferred, the other domains are completely transferred without irregular shape. Large domains are also completely transferred.

When H_{tr} is 240 kA/m, the domains are copied almost uniformly. H_{tr} is the same as that of the readout experiment discussed in §3.1.5. Therefore, the result is inconsistent with the noise increase and the incomplete transfer in the previous section. This problem is discussed in the next section.

When H_{tr} is 320 kA/m, the domains expand into the entire W-layer. This is because H_{tr} is so large that the initializing process occurs.

3.1.7 Nucleation model

Figure 3.9 shows a model of the domain nucleation. Assuming that domain transfer always occurs from a nucleation point and the nucleation points are scattered almost uniformly, large domains have many nucleation points but small ones have few. Therefore, some small domains are not duplicated. Since this is a statistical problem, some large domains are not duplicated either. Furthermore some domains are not transferred even at H_{tr} of 240 kA/m.

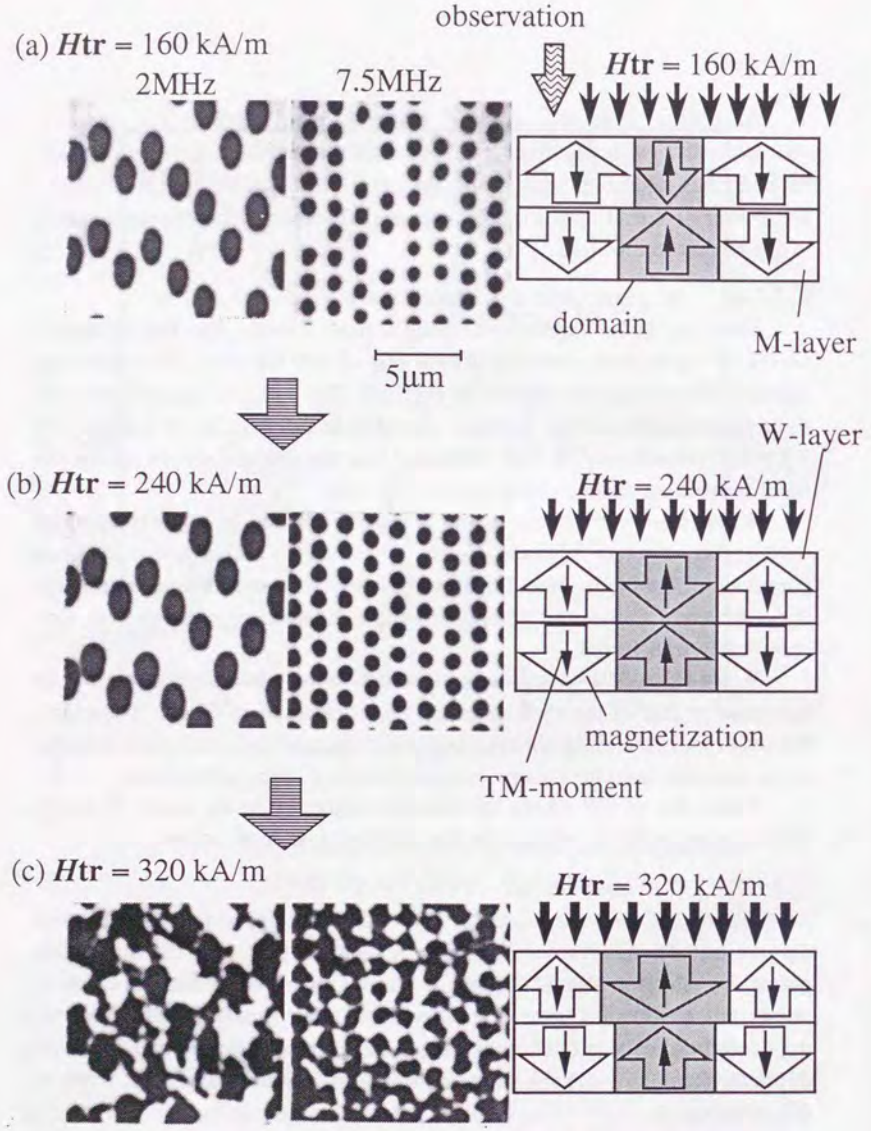

Fig. 3.8 Domains duplicated with various ***Htr***.

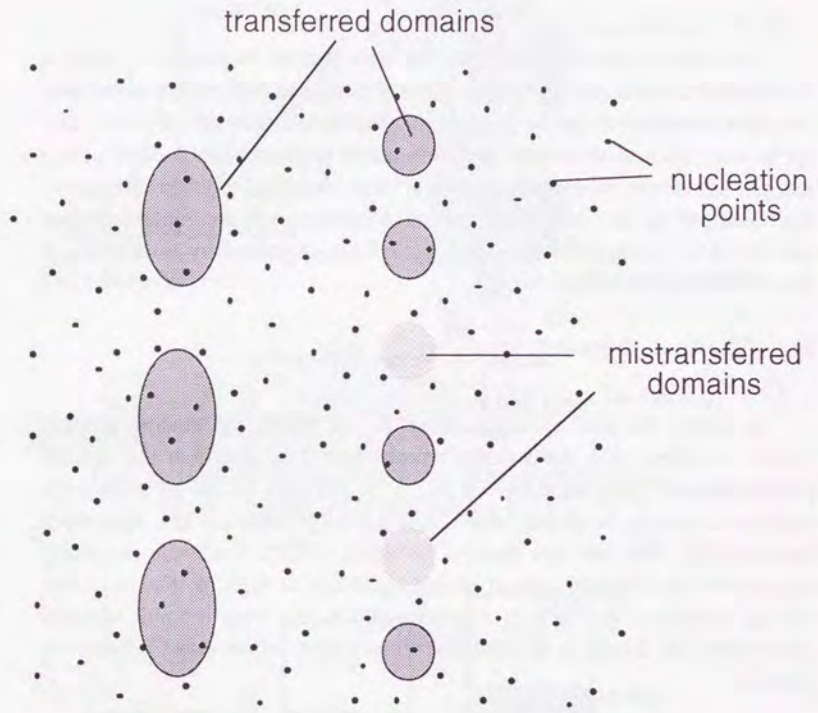

Fig. 3.9 Model on the incomplete transfer.

This deduction from the model is consistent with the readout experiment. According to the model, the incomplete domain transfer is avoidable because this is the statistical problem. The higher the H_{tr}, the more the number of nucleation points. Therefore, obtaining a wider magnetic field margin and applying an adequate H_{tr} can reduce the incomplete transfer.

3.1.8 Summary

The domain transfer phenomenon was applied to LMO to obtain a good power margin. By applying a suitable magnetic field to the multilayer, recorded domains on the M-layer were transferred onto the W-layer. The application of domain transfer before readout improved the readout power margin. However, an increase in noise was observed after irradiation of high read power. The reason for the noise increase was incomplete domain transfer. The incompleteness was successfully explained by introducing a domain nucleation model.

3.2 Thermal cross-talk

3.2.1 Thermal cross-talk

In LMO, the erasing temperature T_e, at which the erasing process occurs, is lower than the writing temperature T_w, at which the writing process occurs. Here, as shown in Fig. 3.10, the data on the adjacent track might accidentally be erased when information is recorded at a high track density [3.6]. We call this thermal crosstalk (TCT). Since the recording temperature in magneto-optical recording is not as high as that in phase-change recording, the TCT in magneto-optical recording is more strongly affected by the change in the ambient temperature, which make it harder to control.

3.2.2 Thermal structure of recording medium

Figure 3.11 shows three typical disks with different thermal structures. On glass-2/p (photo-polymerization) substrates, exchange coupled multilayers(memory and writing layer) are deposited between SiN films (a protective layer and a dielectric layer). Here, the memory and the writing layers are made of TbFeCo and TbDyFeCo, respectively. An interface nitride layer is inserted between the memory and the writing layers in order to control exchange-coupling force [3.7]. To study the relationship between thermal structure of the disks and TCT, three typical disks were evaluated. Disk A, Disk B and Disk C are of normal, UV-resin coated and metal layer coated structures, respectively.

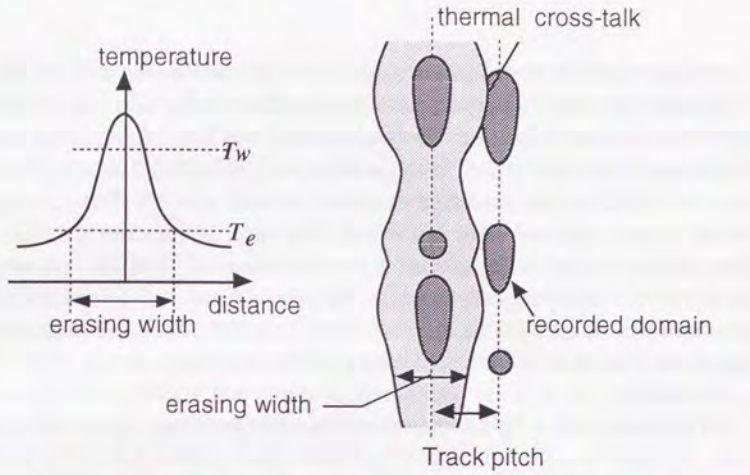

Fig. 3.10 Temerature profile while recording and Thermal Cross-Talk (TCT).

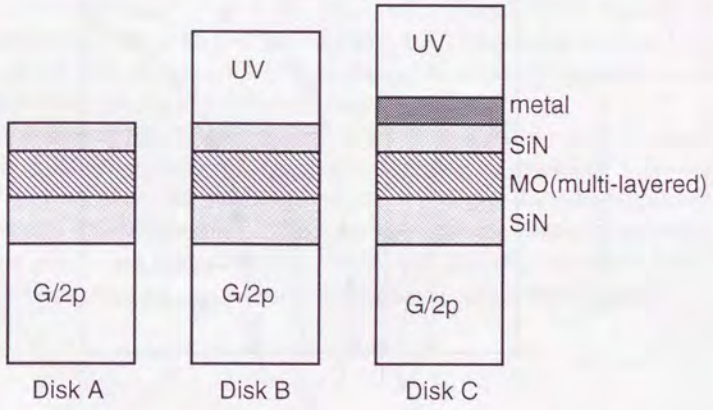

Fig. 3.11 Disk structures; Disk A: normal, DiskB: UV-resin coated, Disk C: UV-resin coated with metal layer.

Figure 3.12 shows typical overwrite characteristics on the disks in Fig. 3.11. First, the relationship between recording laser power and output MO-signal voltage was measured. The laser power was not modulated so that stripe shaped domain should be formed on the disks. Next, erasing laser beam was irradiated on the stripe domains recorded with 0.6 μm-width and the relationship between laser power and MO-signal voltage was measured. These are the severest conditions for overwriting in pit-edge recording method. Relative erase power margins $(P_{ws}-P_{ec})/(P_{ws}+P_{ec})$ for these disks are almost the same (~28%) because three disks have the same magneto-optical multilayers with the same erasing and writing temperatures.

TCT was evaluated as shown in Fig. 3.13(a). First, domains with

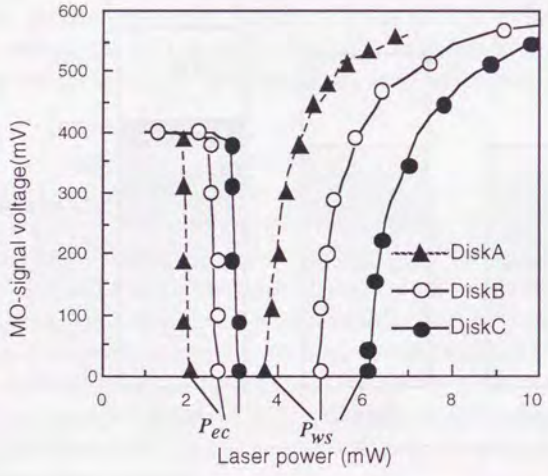

Fig. 3.12 Overwrite characteristics.

different widths were recorded on a track. Here, we call these domains pre-recorded domains. Next, the DC(non-modulated) laser light was irradiated on the adjacent track. Then, the minimum laser power P at which a part of the pre-recorded domains on the adjacent track can be erased was measured. In other words, P is also the maximum laser power without TCT.

The results are shown in Fig. 3.13(b). The horizontal axis is the distance of thermal interference, which is defined to be the distance between the domain wall of the pre-recorded domains and the center of the track where the DC laser light is irradiated. Here, the power P is normalized with the power P_{ec} at which the domains on 0.6μm-width on its own track can be erased completely. The power is normalized in order to compensate for the difference in sensitivity among the disks. Since P is the maximum laser power without TCT and P_{ec} is the minimum erasing power without erase residue, the writing and erasing power level should be set between P and P_{ec}. Therefore, the ratio P/P_{ec} should be large in order to ensure a good power margin. The smallest track pitch without TCT can be evaluated from the case when P equals the power for recording a 0.6-μm-width domain, which we call P_{wc}.

For example, in the Disk A, P_{wc}/P_{ec} is 2.2. Therefore, the distance of the thermal interference is 0.82 μm and track pitch must be wider than 1.12 μm to avoid TCT. As shown later, the change in ambient temperature and off track make this track pitch even larger.

As shown in Fig. 3.13(b), the curve for Disk B has the steepest slope and the smallest distance of thermal interference at the same value of P_{wc}/P_{ec}. Disk C has the smallest slope and the largest distance of thermal interference. This means that TCT is very strong on the thermally diffusive structure with metal layer. Therefore, on disk C, P_{wc}/P_{ec} cannot be made large and, consequently, the erasing power margin cannot be expanded.

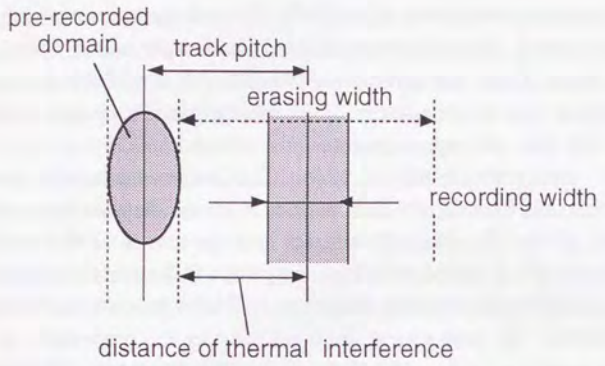

(a)how to evaluate thermal interference

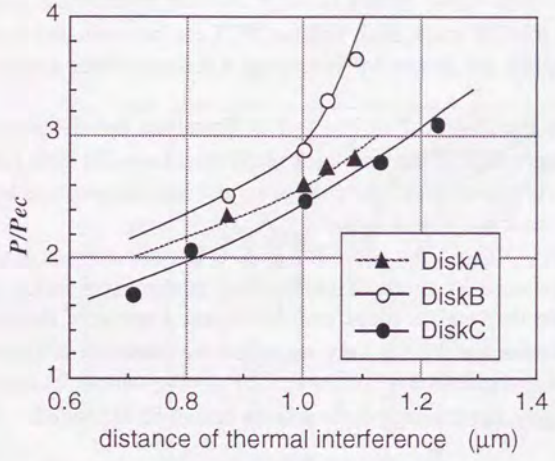

(b)thermal interference

Fig. 3.13 Thermal interference on various disk structures.

These results can be explained from the heat flow in the disks as shown in Fig. 3.14. In disk A, the heat flows horizontally within the magnetic layer which has the highest thermal conductivity in this structure. Therefore, the temperature rises much on the adjacent track. On the other hand, Disk B has UV resin on the top which has higher thermal conductivity than the air. Hence, in disk B, the heat can flow up into the UV resin, and heat flow within the magnetic layer is relatively small. Disk C has metal layer with very high thermal conductivity. Thus the heat flow within the metal layer is dominant.

We may conclude that, a structure which has thick layer with a right level of thermal conductivity on the top is the most effective in reducing TCT.

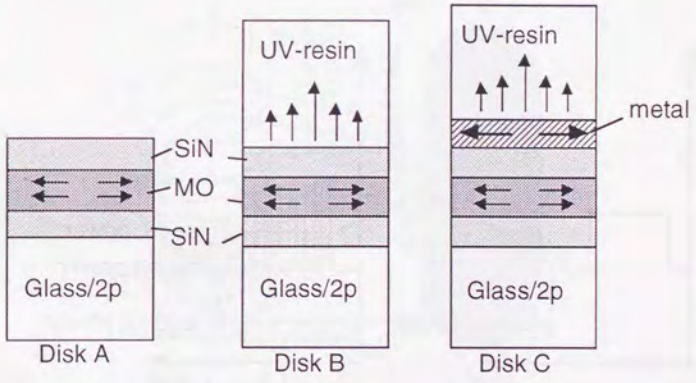

Fig. 3.14 Thermal flow on various disk structures.

3.2.3 *Control of recording pulse shape*

As mentioned above, it is necessary to reduce the temperature rise on the adjacent track while recording. This means the temperature profile must be changed. It had been shown that the pulse train write compensation method is effective in reducing thermal interaction and intersymbol interference in the mark length recording method [3.8]. Pulse shape control like this method seems to be also effective in reducing TCT. Here, the effect of the pulse shape control was studied.

Figure 3.15 shows two pulse shapes, (a) rectangular and (b) comb-shaped pulses. In the comb-shaped pulses, the width of each pulse corresponds to a shift of 0.2 μm in the optical spot position on the disk, which is short enough to ensure a continuous written domains.

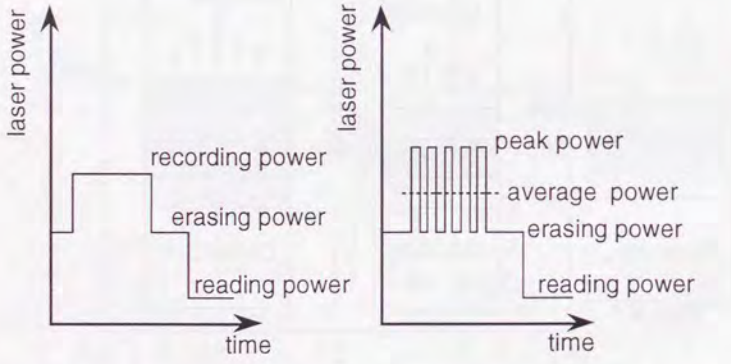

(a) conventional pulse (b) comb-shaped pulse

Fig. 3.15 Pulse shape controle.

Figure 3.16 shows the reduction mechanism of TCT using comb-shaped pulses. When the domains are recorded on the track A using comb-shaped light pulses, the average power required in recording a domain with a certain width (~0.6 μm) becomes smaller than when rectangular pulse is used because the temperature at the domain edge (area D) can be raised before the heat diffuses away. Therefore, only the peak power of the light defines the domain size. On the other hand, the temperature rise on the adjacent track B (area C) depends on the accumulation of heat which has flowed within the magnetic layer. Therefore, the temperature rise on the adjacent track B (area C) does not respond to peak power but rather average power of comb-shaped pulses. Consequently, comb-shaped pulses are expected to reduce the thermal diffusion and TCT.

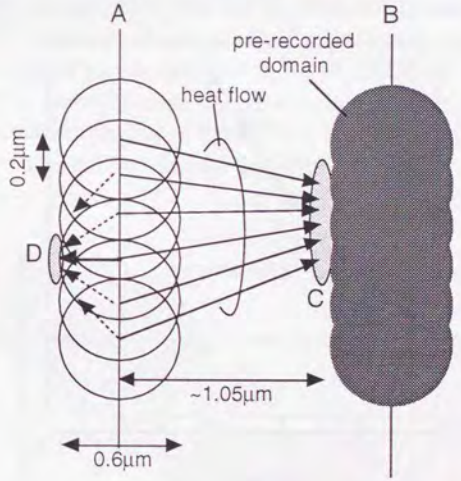

Fig. 3.16 Reduction of themal cross-talk by comb-shaped pulse

Figure 3.17 shows the relationship between the recording width and the distance of thermal interference when conventional DC light and comb-shaped pulse light were irradiated on disk B. The distances of thermal interference are measured by the same method as in Fig. 3.12(a). Smaller erasing width was obtained by using comb-shaped pulses, which means that this pulse shape is effective in reducing TCT. When the recording width is 0.6 μm, the distance of thermal interference can be reduced from 0.82 μm to 0.75 μm using comb-shaped pulses. Consequently, the track pitch can be reduced down to 0.95 μm.

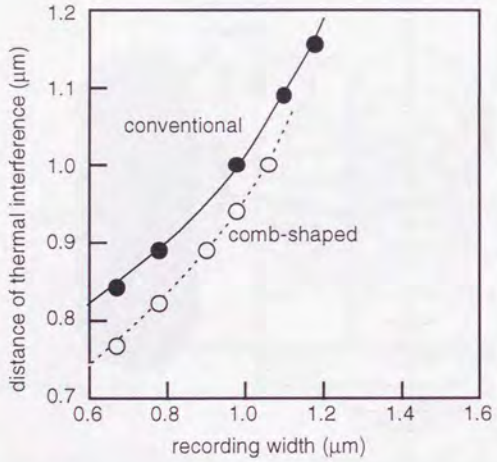

Fig. 3.17 Themal cross-talk with comb-shaped pulse.

3.2.4 Ambient temperature and off track

To prove the feasibility of high track density recording, the effect of the ambient temperature and the off track on to erasing width should be evaluated.

Figure 3.18 shows how the rise in the ambient temperature T_a makes the erasing width larger. Figure 3.18 shows the temperature profiles for (a) high ambient temperature and (b) low ambient temperature. Here, the writing temperature T_w and the erasing temperature T_e are fixed because the temperature dependence of the magnetic characteristics does not change. The power P_{ec} and P_{wc} are adjusted to be proportional to temperature rise T_e-T_a and T_w-T_a, respectively. Therefore the ratio $(T_w\text{-}T_a)/(T_e\text{-}T_a)$ and P_{wc}/P_{ec} is made larger when the ambient temperature T_a is high.

If T_w and T_e are 245°C and 125°C, respectively and T_a changes from 25°C to 50°C, the ratio $(T_w\text{-}T_a)/(T_e\text{-}T_a)$ increases from 2.2 to 2.6. In other words, P_{wc}/P_{ec} increases from 2.2 to 2.6. Then, as shown in Fig. 3.12(b), the distance of thermal interference increases to 1.0 μm in the case of disk B. Therefore, the rise in the ambient temperature T_a by 25°C makes the distance of thermal interference larger by 0.18 μm.

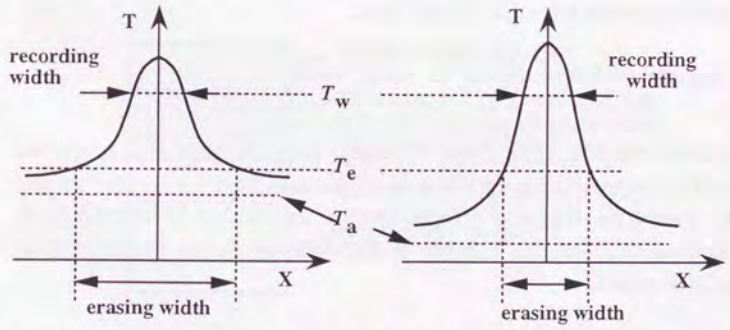

(a) High temperature(50°C) (b) Low temperature(0°C)

Fig. 3.18 Ambient temperature Ta and erasing width.

The effect of the off track is evaluated as follows. In Fig. 3.16, if the light spot shifts to the right on the track B at which the pre-recorded domain is formed and the light spot shifts to the left on the track A, the effective track pitch will be reduced by twice the distance of the track offset. Therefore, track pitch must be designed to be larger by that amount. For example, when the off track is 0.1 μm, the track pitch should be designed 0.2 μm larger for that.

From the analysis discussed above, the minimum track pitch without TCT is found to be 1.33 μm, which is 0.95 μm for the nominal condition plus 0.18 μm and 0.2 μm for the consideration of the ambient temperature change and the off track, respectively. This result proves the possibility of recording 1 GB information on each side of an 130-mm disk with 1.35 μm track pitch.

3.2.5 Summary

Thermal crosstalk (TCT) of LMO, which is erasure of the domains recorded on the adjacent track, was analyzed. The comb-shaped laser pulses and use of the disk with a thick layer having moderate thermal conductivity on the top, were found to be quite effective in reducing the TCT. If the ambient temperature rise and track offset are taken in to account, 1.35 μm track pitch is the minimum. This proves the possibility of recording 1GB information on each side of a 130-mm disk.

3.3 Improvement of signal to noise ratio

3.3.1 Noise increase after initialization

In LMO method, large (200-500 kA/m) magnetic field $\boldsymbol{H}_{\mathrm{ini}}$ is applied to align the magnetization of W-layer in one direction before the writing process. Therefore, $\boldsymbol{H}_{\mathrm{ini}}$ may affects domains recorded in M-layer [3.9]. In the following sections, the stability of the domains during the initializing process is analyzed.

Figure 3.19 shows the disk structure. On the glass/2p (photo-polymerization) substrate, M- and W-layer are sandwiched between protective layer and dielectric layer. Here, M- and W-layer are made of Tb-Fe-Co and Tb-Dy-Fe-Co, respectively. An interface nitride layer is inserted between M- and W-layer to control exchange-coupling force [3.7]. The write-read characteristics with and without initializing process was evaluated on this disk.

Figure 3.20 shows relationship between reproduced signal intensity and recording laser power. In Fig. 3.20, laser power was modulated between read and write power level. Recording signal frequency, duty, linear velocity and initializing field $\boldsymbol{H}_{\mathrm{ini}}$ were 1 MHz, 50 %, 8.5 m/s and 480 kA/m {6 kOe} respectively. The solid line (a) shows the signal intensity reproduced with initializing field $\boldsymbol{H}_{\mathrm{ini}}$ (after initialization), and the dotted line (b) the signal intensity without initializing field Hini (before initialization). Noise level after initialization is 5-8 dB higher than that before. The readout power was chosen low enough not to erase the recorded domains. Therefore, the noise increase ΔN indicates that recorded domains are affected by Hini in the initializing process.

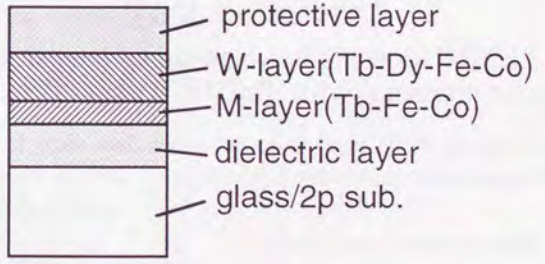

Fig. 3.19 Disk structure.

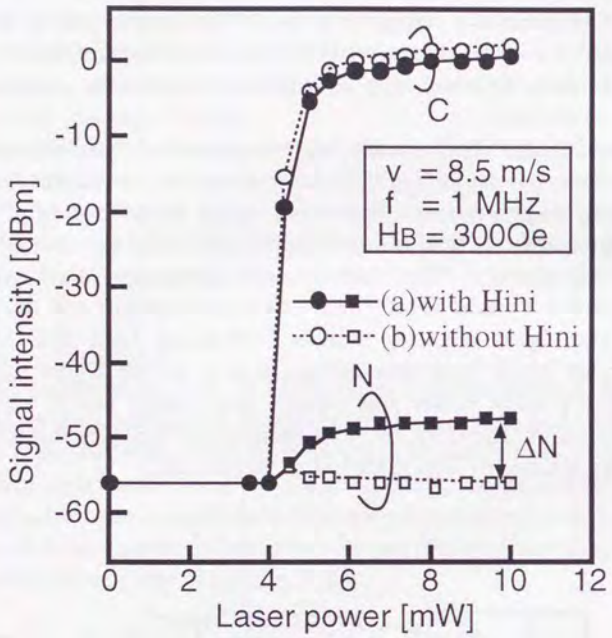

Fig. 3.20 Relationship between signal intensity and laser power (a) with Hini, (b) without Hini.

3.3.2 Analysis of domain stability

To improve the stability of recorded domains against H_{ini}, the magnetic properties of memory layer are evaluated. First, effective external field H_{eff}^{M}, which is effectively applied to M-layer when the initializing field $+H_{ini}$ or $-H_{ini}$ is applied to the magnetic films, is considered. H_{eff}^{M} is

described as follows when the demagnetizing field on the domain wall is negligibly small.

$$H_{eff}^{M} = H_{ext} + H_{exc}^{M} \quad \text{.....(3.1)}$$

where, H_{ext} and H_{exc}^{M} are external and exchange fields acting on M-layer, respectively. The sign of H_{eff}^{M} is defined as positive if H_{eff}^{M} tends to reverse the direction of magnetization of M-layer, and is defined as negative if H_{eff}^{M} tends to keep the direction of magnetization of M-layer. Sign (+) of H_{exc}^{M} term depends on the direction of magnetization of RE-dominant W-layer. The variation of H_{eff}^{M} against H_{ext} is shown in Fig. 3.21. Figure 3.21(a) and(b) show the case of RE-dominant M-layer and TM-dominant M-layer, respectively.

In the case of RE-dominant M-layer in Fig. 3.21(a), a large H_{ext} is applied enough to align the magnetization of M-layer in downward direction as shown in the figure (point A). Next, H_{ext} is removed (point B). Then, H_{exc} acts in (-) direction because TM-moment of each layer stays in the same direction and this state is very stable. When H_{ext} becomes equal to the effective coercivity of W-layer ($H_c^{W}+H_{exc}^{W}$), the magnetic state changes from C to D since W-layer has smaller coercivity than M-layer. Consequently, direction of H_{exc}^{M} changes to positive and H_{eff}^{M} increase by $2H_{exc}^{M}$. As shown in Fig. 3.21(a), when H_{ext} is equal to H_{ini} (point E), H_{eff}^{M} has the following maximum value.

$$H_{eff}^{M} = H_{ini} + H_{exc}^{M} \quad \text{.....(3.2)}$$

Since domain wall coercivity of M-layer H_w^{M} needs to be larger than the maximum H_{eff}^{M}, the stability condition for domains recorded on M-layer is the following.

$$H_w^{M} > H_{ini} + H_{exc}^{M} \quad \text{.....(3.3)}$$

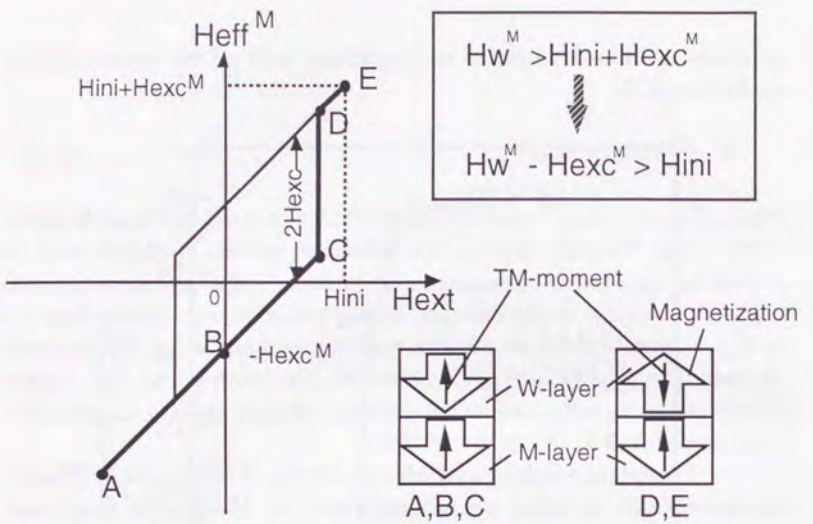

(a) RE-dominant M-layer

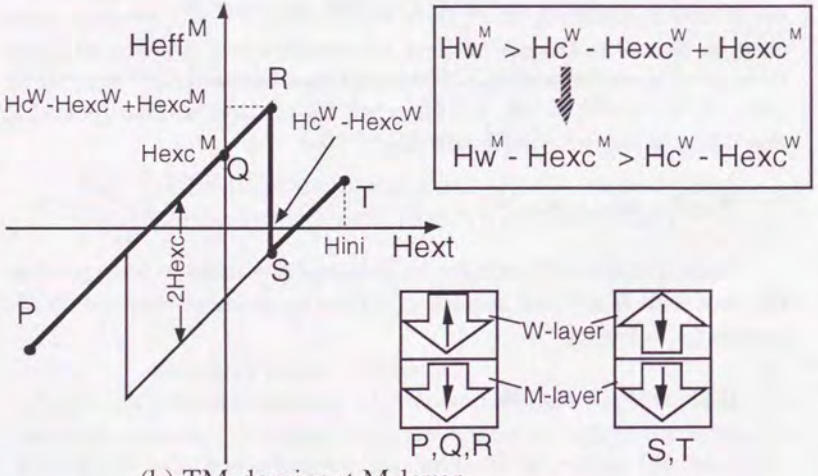

(b) TM-dominant M-layer

Fig. 3.21 Effective field applied on M-layer.

In the case of TM-dominant memory layer as shown in Fig. 3.21(b), a large H_{ext} is applied enough to align the magnetization of M-layer in downward direction (point P). Next, H_{ext} is removed (point Q). Then, H_{exc} acts in (+) direction because TM-moment of each layer stays in the opposite direction and this state is unstable. When H_{ext} becomes equal to the effective coercivity of W-layer ($H_c{}^W$-$H_{exc}{}^W$), the magnetic state changes from R to S since W-layer has smaller coercivity than M-layer. Consequently, direction of $H_{exc}{}^M$ changes to negative and $H_{eff}{}^M$ decreases by $2H_{exc}{}^M$. Since $H_{eff}{}^M$ at point R is usually greater than that at point T, $H_{eff}{}^M$ reaches the maximum value as follows when H_{ext} is equal to the effective coercivity of W-layer (at point R).

$$H_{eff}{}^M = H_c{}^W - H_{exc}{}^W + H_{exc}{}^M \quad \text{.....(3.4)}$$

Therefore, in this case, the condition of the stability becomes

$$H_w{}^M > H_c{}^W - H_{exc}{}^W + H_{exc}{}^M \quad \text{.....(3.5)}$$

In some case with TM-dominant M-layer, $H_{eff}{}^W$ reaches the maximum value when H_{ext} is equal to H_{ini} (point T). This situation can occur when the exchange force is somewhat smaller. In this case, the stability condition becomes as follows.

$$H_w{}^M > H_{ini} - H_{exc}{}^M \quad \text{.....(3.6)}$$

Since H_{ini}=480 kA/m {6 kOe} and $H_c{}^W$-$H_{exc}{}^W$= 80 kA/m{1 kOe} in our case, stability conditions (3.3), (3.5) and (3.6) become as follows.

$$H_w{}^M - H_{exc}{}^M > 480 \text{ kA/m } \{6 \text{ kOe}\} \quad \text{(RE-dominant)} \quad \text{.....(3.7)}$$

$$H_w{}^M - H_{exc}{}^M > 80 \text{ kA/m } \{1 \text{ kOe}\} \quad \text{.....(3.8)}$$

$$H_w{}^M + H_{exc}{}^M > 480 \text{ kA/m } \{6 \text{ kOe}\} \quad \text{(TM-dominant)} \quad \text{.....(3.9)}$$

These conditions indicate that TM-dominant M-layer is more suitable than RE-dominant M-layer in terms of domain stability.

3.3.3 Result and discussion

Figure 3.22 shows the relationship between noise increase ΔN after initialization and $H_w{}^M$-$H_{exc}{}^M$ in the various disks of different exchange field and coercivity. Here, the compositions of M- and W-layer were varied

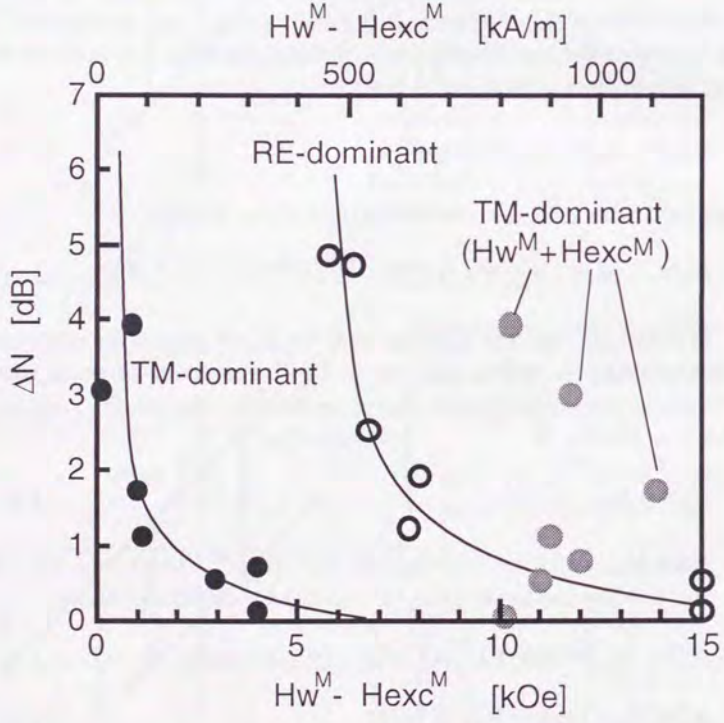

Fig. 3.22 Relationship between domain wall coercivity of memory layer and noise increase after initialization.

in order to change the coercivity. The exchange field was changed by varying the thicknesses of M-layer (20-40 nm), W-layer (80-200 nm) and interface nitride layer (0-2 nm), respectively.

In the case of RE-dominant M-layer, $H_w{}^M$-$H_{exc}{}^M$ is directly measured from the virgin curve of the M-layer as shown in Fig. 3.23(a). But in the case of TM-dominant M-layer, only $H_w{}^M$+$H_{exc}{}^M$ can be measured from the virgin curve as shown in Fig. 3.23(b). Therefore, $H_{exc}{}^M$ is derived using relationship as follows [3.10].

$$H_{exc}{}^M = H_{exc}{}^W \bullet M_s{}^W \bullet h^W / (M_s{}^M \bullet h^M) \quad \text{..... (3.10)}$$

where, $M_s{}^M$, $M_s{}^W$, h^M and h^W are magnetization of the M-layer, magnetization of W-layer, thicknesses of M-layer and W-layer, respectively. $M_s{}^M \bullet h^W$ and $M_s{}^W \bullet h^W$ were measured with a magnetometer.

In Fig. 3.22, ΔN increases at around 80 kA/m {1 kOe} (TM-dominant) and 480 kA/m {6 kOe} (RE-dominant) of $H_w{}^M$-$H_{exc}{}^M$, which corresponds to the conditions (3.7) and (3.8), respectively. In the case of TM-dominant M-layer, $H_w{}^M$+$H_{exc}{}^M$ are also plotted, but no clear relationship corresponding to the conditions (3.9) was observed.

Taking these results into consideration, the disk was constructed with TM-dominant M-layer having 640 kA/m {8 kOe} of $H_w{}^M$-$H_{exc}{}^M$. No noise increase after initializing process was detected with the disk.

In the case of TM-dominant M-layer, the magnetization stays as shown in Fig. 3.24(a) just after recording. After initialization, it stays as shown in Fig. 3.24(b) . So, magnetization state Q or R shown in Fig. 3.21(b) does not appear in actual recording condition. This can be explained if a model of recorded domains as shown in Fig. 3.24(d) is used. Supposing domains recorded on the W-layer are larger than those on the M-layer [3.11], state Q in Fig. 3.21(b) can appear at the outer margin of domains on M-layer.

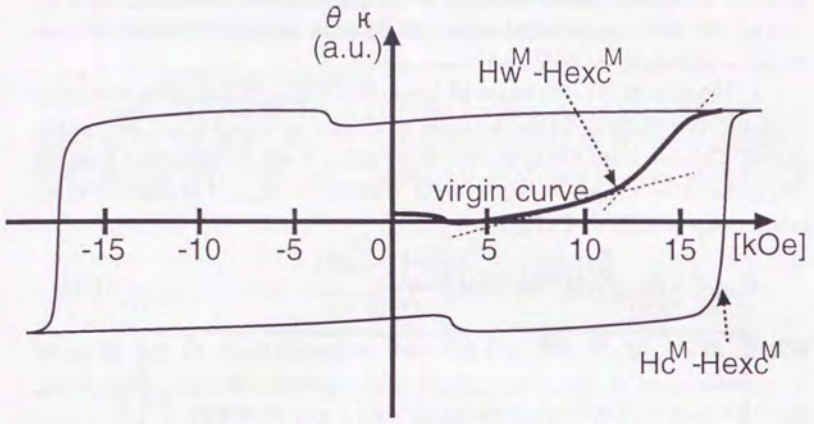

(a) in the case of RE-dominant Memory layer

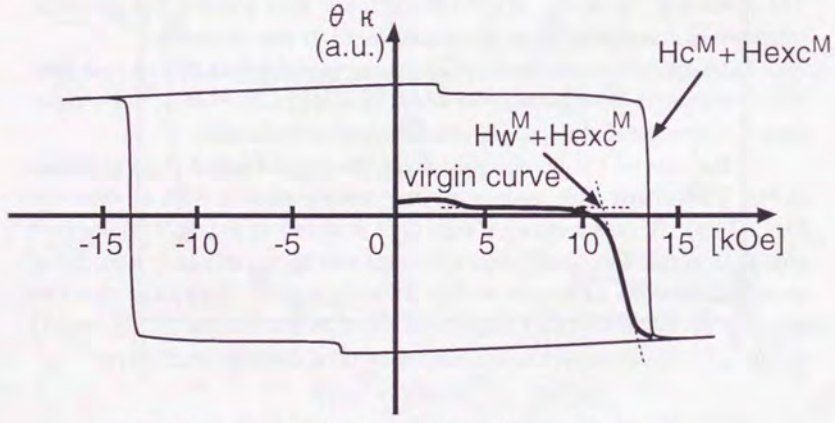

(b) in the case of TM-dominant Memory layer

Fig. 3.23 Examples of Kerr hysteresis loop with virgin curve.

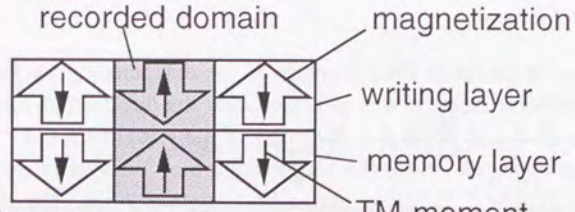

(a) just after recording

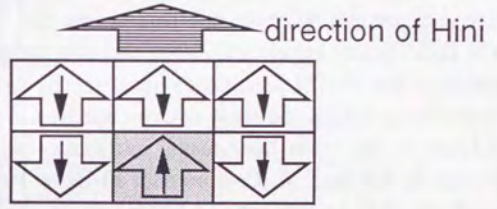

(b) after initialization

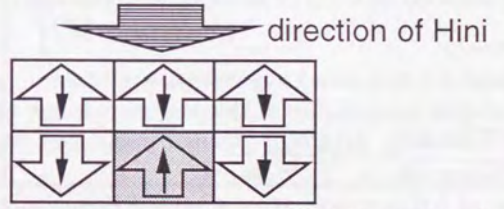

(c) when the direction of Hini is reversed
(before magnetization of W-layer is reversed)

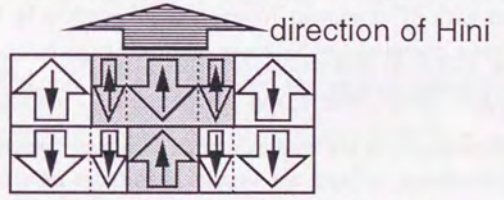

(d) an image of real domain structure

Fig. 3.24 Initializing process in the case of TM-dominant memory layer.

In order to verify the existence of the magnetization state described above, the noise increase was measured after the direction of the initializing field was changed. When the direction of the initializing field is changed, state Q is appeared before the magnetization of W-layer is reversed (Fig. 3.24(c)). Figure 3.25 shows the noise increase when the direction of initializing field $\boldsymbol{H}_{\mathrm{ini}}$ is reversed. Relationship similar to Fig. 3.22 can be observed with the TM-dominant M-layer. However, with the RE-dominant M-layer, less noise increase can be observed. This proves that the analysis mentioned above is right. In this experiment, noise increase in RE-dominant M-layer is smaller than that in TM-dominant one. It means that changing the direction of initializing field is the most severe condition in the case of TM-dominant M-layer, on the other hand, usual initializing process is the most severe condition in the case of RE-dominant M-layer. However, for the reversibility of the disk, conditions (3.6) and (3.7) are necessary. Therefore, in the case of TM-dominant M-layer, the stability of the domains must be checked when the direction of the initializing field is reversed.

3.3.4 Summary

Noise increase ΔN after initializing process was detected on the LMO with exchange-coupled magnetic films. Domains recorded on M-layer are affected by the initializing field $\boldsymbol{H}_{\mathrm{ini}}$ through initializing process, and consequently ΔN appeared.

In the case of RE-dominant M-layer with RE-dominant W-layer, domain wall coercivity of M-layer $\boldsymbol{H}_{\mathrm{w}}{}^{\mathrm{M}}$ needs to be larger than the sum of initializing field and exchange force for domain stability. In the case of TM-dominant M-layer with RE-dominant W-layer, $\boldsymbol{H}_{\mathrm{w}}{}^{\mathrm{M}}$ needs to be larger than the sum of effective coercivity of W-layer and exchange force. No noise increase after initializing process was observed with TM-dominant M-layer having large $\boldsymbol{H}_{\mathrm{w}}{}^{\mathrm{M}}$.

Results mentioned above are well explained assuming sizes of domains recorded on TM-dominant M-layer are smaller than those recorded on RE-dominant W-layer.

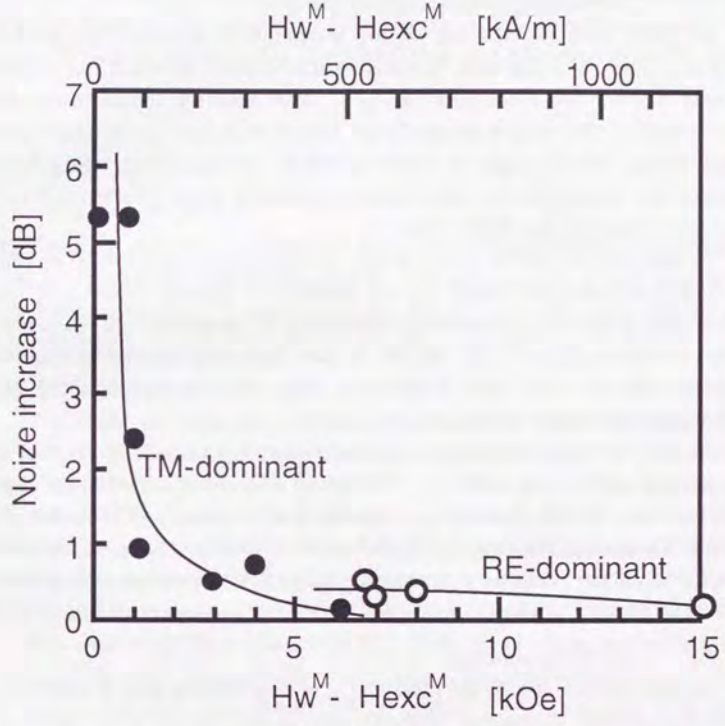

Fig. 3.25 Relationship between domain wall coercivity of memory layer and noise increase when the direction of initializing field is reversed.

3.4 Overwrite repeatability

3.4.1 Thermal degradation of MO media

In LMO with ECML, the writing temperature, at which the writing process occurs, is higher than the erasing temperature at which the erasing process occurs as discussed in §3.2. The writing temperature for overwritable (OW) disk is normally set higher than for conventional non-overwritable (NOW) disks in order to obtain enough power margin for overwriting. Therefore, the maximum temperature while overwriting may rise higher than that for NOW disks.

In the case of NOW disks, it has been reported that the write/read characteristic becomes worse after a number of erasing cycles and this degradation is caused by thermal relaxation of the perpendicular anisotropy in the magnetic film [3.12], [3.13]. In the first- and second-generation magneto-optical disks, this relaxation was avoided by reducing the maximum temperature during erasing.

In the following subsections, the degradation process after number of overwriting cycles on LMO is studied [3.14]. First, the temperature distributions on OW disks were compared with that on NOW disk by thermal simulation. Second, a degradation mode characteristic of OW disk with ECML were studied by comparing the activation energy obtained by Arrhenius method.

3.4.2 Arrhenius analysis

In order to investigate the mechanism of degradation after a number of overwrite cycles, Arrhenius analysis was used. This is also useful to accelerate the repetition experiments.

The main cause of the degradation in rare-earth transition metal alloy magneto-optical disk is said to be the thermal relaxation of the amorphous structure of the magnetic film during the laser irradiation [3.12]. The relaxation speed v obeys the Arrhenius' expression.

$$v \propto \exp\left(-\frac{E_a}{K_B T}\right) \quad \text{(3.11)}$$

where, E_a, K_B and T are the activation energy, Boltzmann's constant and the absolute temperature, respectively. If the cause of the degradation is the thermal relaxation, the number of overwriting cycles when the degradation begins (N) should be inversely proportional to the relaxation speed v. That is,

$$N \propto \exp\left(\frac{E_a}{K_B T}\right) \quad \text{(3.12)}$$

Therefore, Ea can be evaluated by measuring the number of overwriting cycles N for various overwriting power. The temperature T was evaluated from the overwriting laser power by using the computer simulation described below.

3.4.3 Experiment

Overwrite and write/read characteristics such as carrier to noise ratio (CNR) were evaluated by using a magneto-optical disk drive (Nakamichi Co., OMS-1000) with an 830 nm wavelength laser and a 0.55 numerical aperture lens. The readout laser power, the bias magnetic field and the initializing magnetic field were 1.0 mW, 32 kA/m {400 Oe} and 410 kA/m {5.1 kOe}, respectively. CNR values were evaluated under the conditions of 0.5 MHz carrier frequency with 50 % duty writing pulses.

The overwrite repeatabilities for OW disks were evaluated by measuring the W/R characteristics with and without initializing field after repetitive irradiation of overwriting laser power. The initializing field was applied to the disk after the repetitive irradiation.

Both NOW and OW disks had 1.4 μm pitch v-shaped grooves which were made by photo-polymerization (2P). The magnetic and dielectric layers were formed by rf-magnetron sputtering. Each OW disk has a TbFeCo memory layer and a TbDyFeCo writing layer. In order to control the exchange force between memory and writing layers, a TbFeCo-N intermediate layer was introduced. This was formed by rf-sputtering with Ar-N_2 mixed gas instead of pure Ar gas [3.7].

Temperature profiles on the disks were obtained by solving the three dimensional thermal diffusion equation using the finite difference method with a super-computer [3.15].

Figure 3.26 shows typical disk structures for OW and conventional NOW disks. This figure does not show the detailed structures of the magnetic layers because only the thermal properties are considered in this section. Two types of OW disks were studied to evaluate the effect of the thermal diffusive layer.

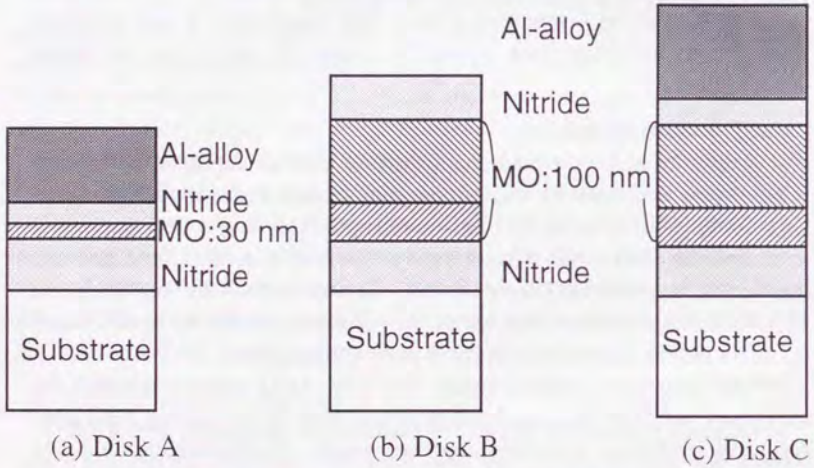

Fig. 3.26 Cross-sectional structures of the disks. (a)Disk A: conventional NOW disk with Al-alloy thermal diffusion layer. (b)Disk B: typical OW disk with ECMLs. (c)Disk C: OW disk with Al-alloy thermal diffusion layer on the top.

3.4.4 Temperature profiles

The temperature profiles for the three types of disks shown in Fig. 3.26 were obtained by computer simulation. We assumed that domains were formed in the region where the temperature in the magnetic film exceeds the constant writing temperature.

In the case of OW disks, width of the recorded domain was fixed at 0.6 μm, which is the maximum width to avoid thermal cross-talk between tracks discussed as before. In the case of the NOW disk, the erasing width was fixed at 1.1 μm in order to completely erase the pre-recorded domains. The erasing process caused the most damage in the NOW disk because the temperature on the magnetic films was the highest.

Calculated temperature profiles are shown in Fig. 3.27. This result shows small differences among these disks. This can be explained as follows.

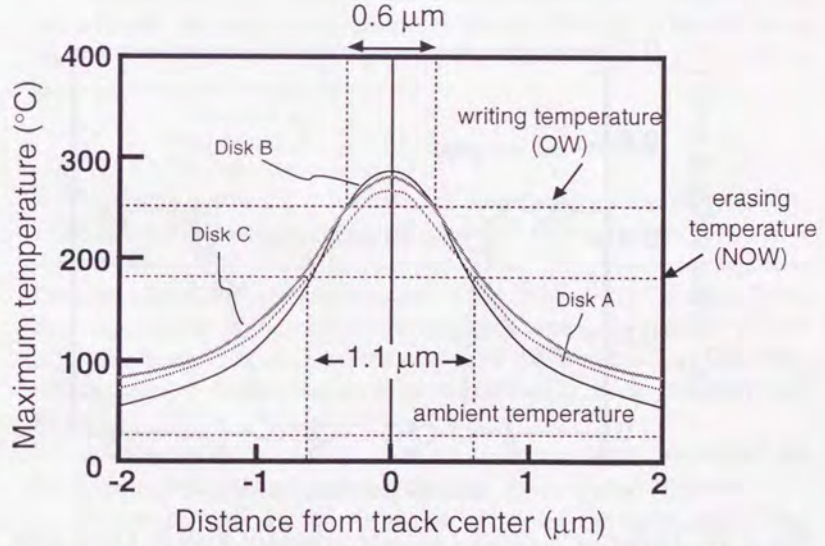

Fig. 3.27 Calculated temperature profiles for the disks in Fig. 3.26.

Although the writing temperature in the OW disks is higher than that in the NOW disk, the domain width for the OW disks is narrower than the erasing width for NOW disk. Therefore, the maximum temperatures for these disks are similar. In addition, since the differences between writing and maximum temperatures of OW disks are small because of the narrow domain width, the effect of the Al-alloy thermal diffusive layer was small.

From these results, overwrite (erase/write) repeatabilities are expected to be almost the same for these three disks. Since the repeatability for the NOW disk is over 10^6 times, repeatability of more than 10^6 times is also expected for OW disks.

To check the result of the calculation, experimental and calculated results were compared on OW disk B as shown in Fig. 3.28. This shows the output signal voltage after an unmodulated laser beam was irradiated on the

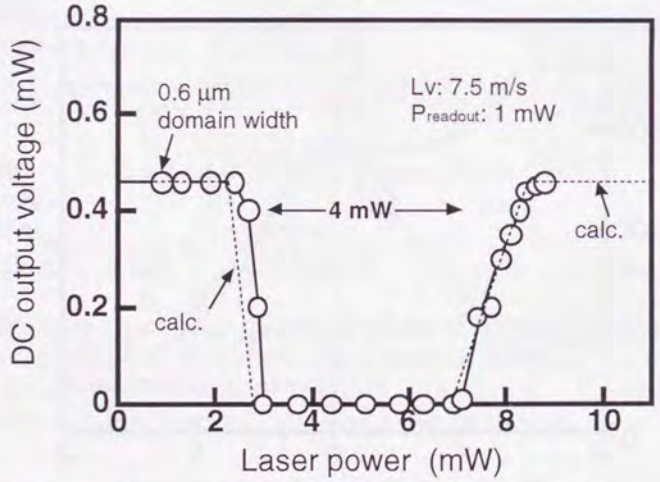

Fig. 3.28 Typical overwrite characteristics for disk B. Open dots are the experimental data, broken line is the numerical estimation.

spinning disk. The irradiation was performed so that a stripe domain should be formed on a track of the disk. The writing and erasing temperatures for calculation were determined from the temperature dependence of static magnetic properties.

First, a 0.6-μm-wide stripe domain is formed on the disk by irradiating with 8.3 mW unmodulated laser power. Next, laser power shown on the horizontal axis was irradiated, and after the irradiation, the output signal was evaluated using 1.0 mW readout power. When the laser power increases to 2.0 mW, the output signal begins to decrease because the erasing process occurs. When the laser power is 3.0 mW, the signal becomes zero, which shows that the stripe domain formed on the disk was completely erased. When the laser power reaches 7.0 mW, the output signal begins to increase again, which shows that the width of the stripe domain is increasing.

Because the output signal is zero when the laser power is between 3.0 and 7.0 mW, the erase power margin of the disk is 4 mW. The disk needs laser power of 8.3 mW to form a 0.6-μm-wide domain and 3.0 mW to erase a 0.6-μm-wide stripe domain.

3.4.5 Overwrite repeatability

Overwrite repeatability for OW disk B was evaluated as shown in Fig. 3.29. The vertical axis indicates the relative carrier and noise levels after various numbers of overwrite repetition cycles. The noise level begins to increase around 10^4 overwrite cycles. This number, 10^4, is much lower than expected from the calculated maximum temperature shown in Fig. 3.27. The noise increase occurred only after the initialization. Therefore, this degradation process seems to be characteristic to the OW disk with ECML.

In order to analyze the degradation process in detail, we carried out acceleration experiments based on Arrhenius' theory discussed above.

Figure 3.30 shows the Arrhenius' plots for the three disks. This acceleration experiment was performed by varying the overwriting power, resulting in a change in maximum temperature during overwriting. The

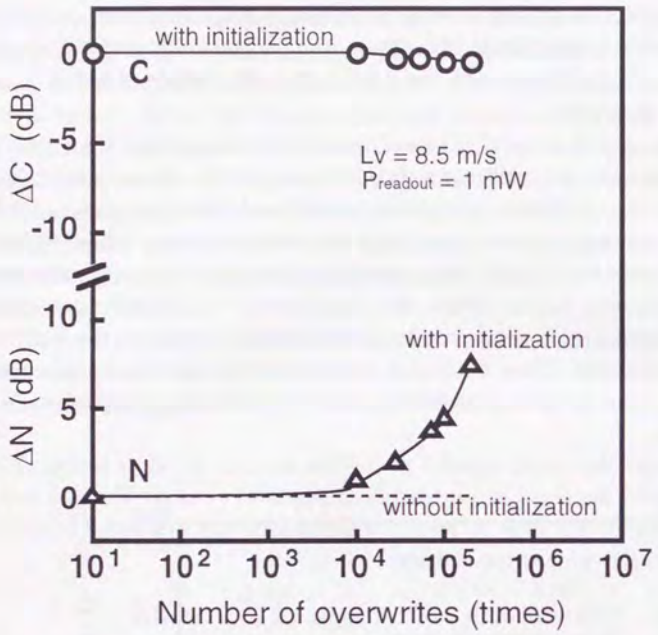

Fig. 3.29 Carrier and noise levels after various numbers of repetitive overwrites.

inverse of the maximum absolute temperature is plotted on the horizontal axis. This is because the degradation mainly occurs at the maximum temperature since the relaxation speed is maximum as shown by Eq. (3.11). Repeatability is defined as the number of repetition cycles when the noise level of the readout signal begins to increase. Overwrite repeatabilities for the OW disks were evaluated under initializing field, which was applied to align the direction of magnetization in the writing layer.

First, the lines in Fig. 3.30 for OW disks B and C with the initialization have smaller gradient than that for the NOW disk A. Also the

numbers of repetition for OW disks are smaller than that for NOW disk. In addition, the lines for disks B and C with initialization are similar. This shows that the thermal diffusive layer is ineffective in suppressing the degradation process. This is consistent with the simulation.

Next, the line for disks B and C without initialization is steeper and similar to that for disk A. Therefore, the degradation of ECML disks is the same as that of NOW disk if the disks are used as non-overwrite disks, which do not need the initialization. In other words, the repeatability was restricted by the noise increase after initialization.

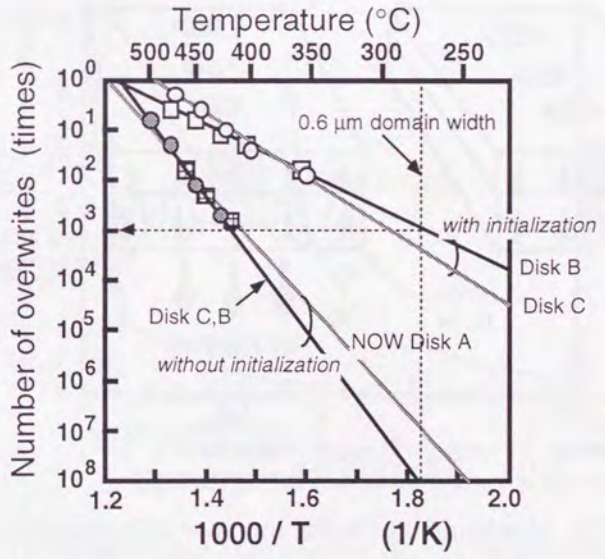

Fig. 3.30 Arrhenius plots for the disks shown in Fig. 3.26 using higher laser power for acceleration.

3.4.6 *Initialization noise*

In §3.3, noise increase after initialization was discussed. As shown in Fig. 3.31, the origin of initialization noise was found to be the fluctuation of the domain wall on the memory layer which occurs when the effective magnetic field exceeds the domain wall coercivity. Furthermore, this initialization noise was reduced by using a transition-metal dominant memory layer having high domain wall coercivity as shown in Fig. 3.32.

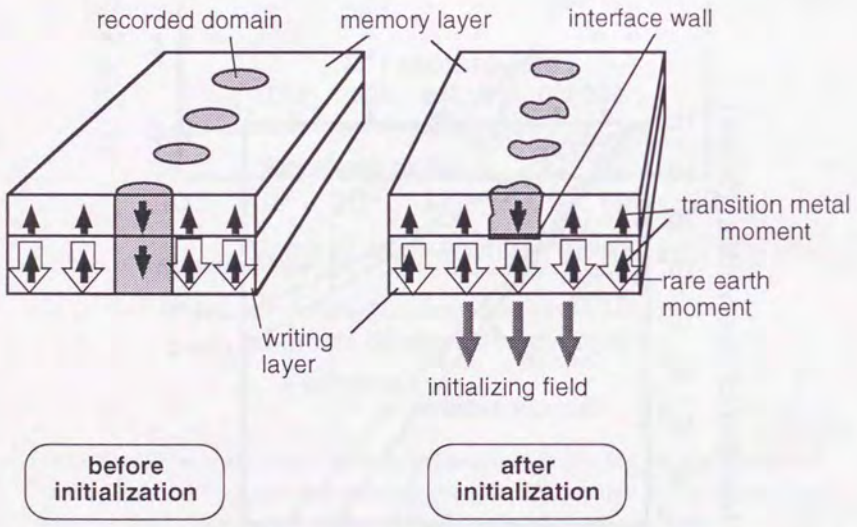

Fig. 3.31 Mechanism of noise increase after initialization.

In the case of the present study, it is thought that the domain wall coercivity decreases due to degradation of the perpendicular anisotropy, which is the result of thermal relaxation of the amorphous structure. Based on this idea, the noise increase is the result of the coercivity reduction after repeated thermal cycles and can be suppressed by using the transition metal dominant memory layer with high domain wall coercivity.

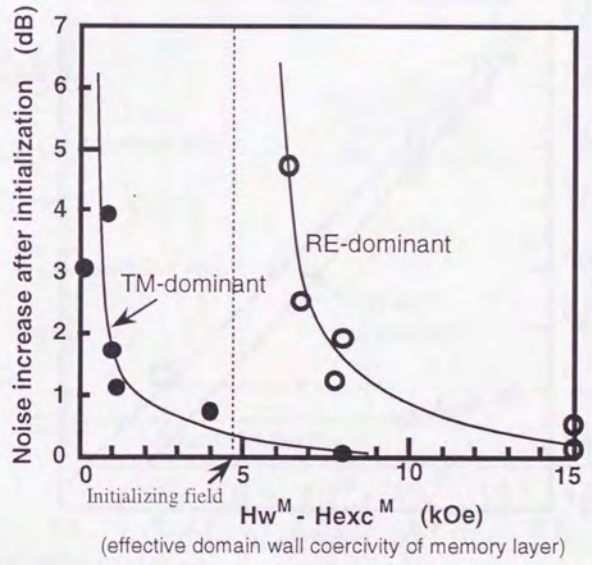

Fig. 3.32 Relationship between the domain wall coercivity of the memory layer and initialization noise.

Figure 3.33 shows the results of the Arrhenius analysis for OW disk D that has a transition metal dominant memory layer with high domain wall coercivity. It shows a steep slope similar to the NOW disk and the difference between the slopes with and without the initialization is greatly reduced.

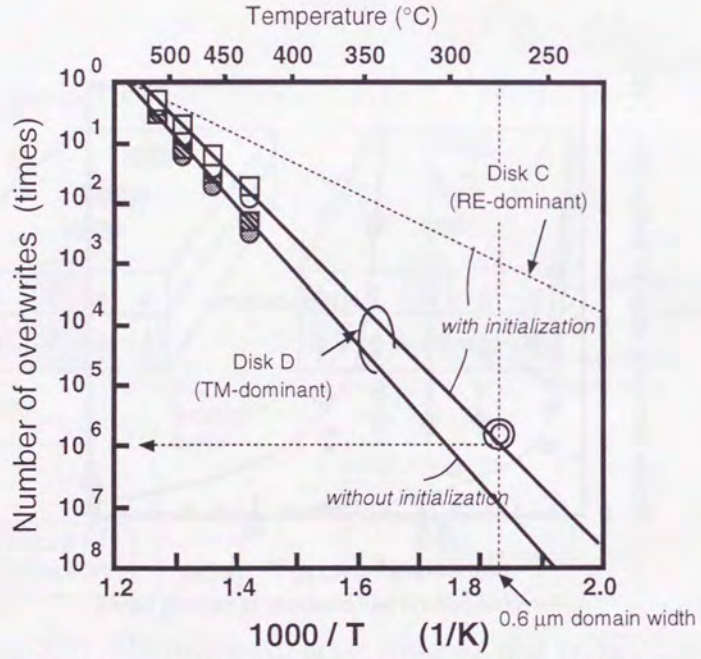

Fig. 3.33 Arrhenius plots for the modified disk D.

From these results, over 10^6 repeatability without CNR degradation is expected. This is confirmed in Fig. 3.34, which shows the write/read characteristics versus the number of overwrite repetition cycles. The measurement was performed without any acceleration. The repeatability of 106 enables practical use of this OW disk.

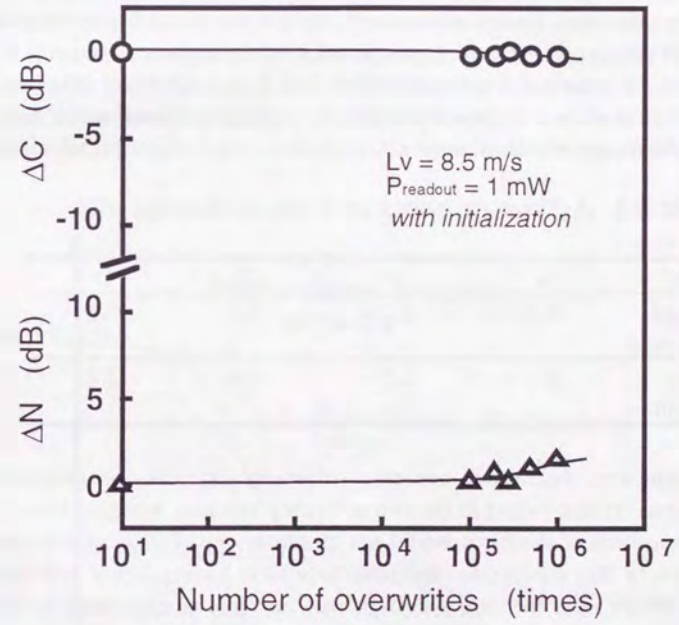

Fig. 3.34 Carrier and noise levels after various numbers of repetitive overwrites for modified OW disk D.

3.4.7 Activation energy

In the previous section, OW disks B and C showed smaller gradients than NOW disk A in the Arrhenius plot shown in Fig. 3.30. From Eq. (3.11), the gradient in the Arrhenius plot coincides with activation energy Ea. The activation energies obtained from the experiments are shown in Table 3.1. As shown in the table, OW disks have two kinds of activation energy, one for the case with initialization and the other for the case without initialization. These activation energies can be explained by the following model.

The activation energy shown in Table 3.1 are much higher than the magnetic energy, which is of the order of the Bohr magneton, and which is 5.5×10^{-5} eV even if the external field is 800 kA/m {10 kOe}. Therefore, the phenomenon is a chemical reaction or a physical movement of atoms and not be a magnetic phenomenon.

Table 3.1 Activation energies from Arrhenius plot.

disk	A	B	C	D
without initialization	3.1	3.5	3.5	3.1
with initialization	3.1	1.3	1.9	2.8

Supposing that there are two different physical (or chemical) phenomena corresponding to the two activation energies, a slight change in the composition of the films would not eliminate one of those phenomena. However, in this study, one degradation process having lower activation energy, which is for the case with initialization, could be eliminated by only modifying the magnetic properties of the memory layer. Therefore, the two activation energies obtained by the Arrhenius plot do not correspond to different physical (or chemical) phenomena but to only one physical (or chemical) phenomenon which is thermal relaxation (or reaction) of the amorphous structure.

If the activation energy is a chemical one, it does not explain the result well because activation energy for chemical reaction is unique. On the other hand, in the structural relaxation of amorphous films the activation energy for movement of atoms is different for each atom in the film because each atom has different surroundings. Therefore, the phenomena is physical one.

Figure 3.35 shows a typical relaxation process of the magnetic anisotropy. For low values of time, the reduction in anisotropy represents the atoms which have higher relaxation speeds. From Eq. (3.11), the atom which has high relaxation speed has small activation energy. Therefore, the reduction in anisotropy represents the atoms with small activation energies. For large values of time, the reduction in anisotropy represents the atoms with lower relaxation speeds and larger activation energies.

During the initialization, the disk needs high coercivity in order to reduce initialization noise, which results from the domain wall fluctuation

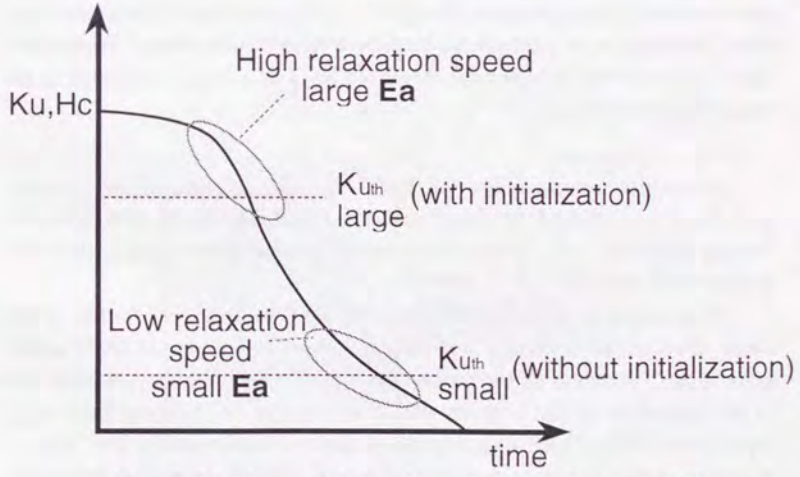

Fig. 3.35 A model for the origin of the two different activation energies.

by the large applied field. After a large number of overwrite repetitions, the coercivity of the memory layer decreases gradually due to the reduction in anisotropy. Therefore, the noise increase after initialization normally occurs earlier than that without initialization. The noise increase after initialization corresponds to the low values of time in Fig. 3.35.

In other words, there are threshold levels Ku_{th} for the anisotropy at which the noise increase occurs. In Fig. 3.35, a high threshold level Ku_{th} limits the gradually decreasing anisotropy at the low values of time. At that time region, the decrease in the anisotropy represents atoms with small activation energies, which is for the case of OW disk. On the other hand, a low threshold level limits the anisotropy at the high values of time. At the region, the decrease in the anisotropy represents atoms with high activation energies, which is for the case of NOW disk. Therefore, the threshold level for the OW disk with initialization is higher than those for the NOW disk or OW disk without the initialization.

Further, an apparent change in the activation energy occurs whenever an observation such as noise increase is performed with a threshold level using these kinds of amorphous media. In other words, every degradation can be reduced by changing the threshold level as a result of change in the magnetic characteristics.

3.4.8 Summary

Overwrite repeatability of LMO media with exchange coupled multilayer was studied by using Arrhenius analysis. In the OW disk, the thermal diffusion layer is less effective for extending the repeatability than that in NOW disk.

A degradation mode characteristic of the OW disks was found. In this mode, the activation energy was lower than for conventional NOW single layer disk. The origin of the mode was found to be initialization noise due to the reduction of the domain wall coercivity in the memory layer after repetition cycles. The degradation mode was suppressed by using a transition-metal dominant memory layer with high domain wall coercivity. Thus, overwrite repeatability of more than 10^6 times was achieved.

3.5 High density mark-edge recording

3.5.1 High capacity overwritable disk

Larger capacity and higher data transfer rate than the present magneto-optical (MO) disks have been pursued for next-generation MO disks. Exchange-coupled direct-overwrite (DOW) MO disks can double the data transfer rate during writing. Mark-edge recording can attain near twofold linear recording density than conventional mark-position recording. Some of the present authors attempted to combine the above two technologies, however, mark-edge jitter was not sufficiently small [3.16].

In this section, the reliable performance of mark-edge recording on exchange-coupled DOW disks [3.17], which yields 2 GB capacity on a 130-mm-diameter disk, is described.

3.5.2 Experiment

A direct-overwrite (DOW) magneto-optical (MO) disk has exchange-coupled quadrilayer including a readout layer of GdFeCo with large Kerr rotation, as shown in Fig. 3.36 [3.18]. This quadrilayered structure was proven to be effective for obtaining high readout signal intensity. The

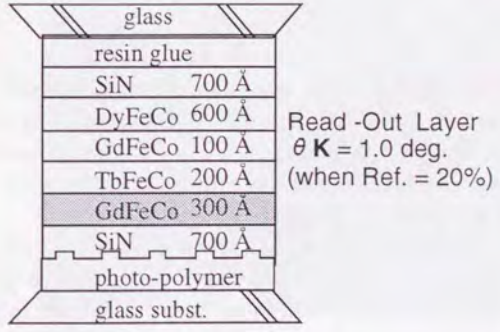

Fig. 3.36 Cross section of exchange-coupled DOW MO disk.

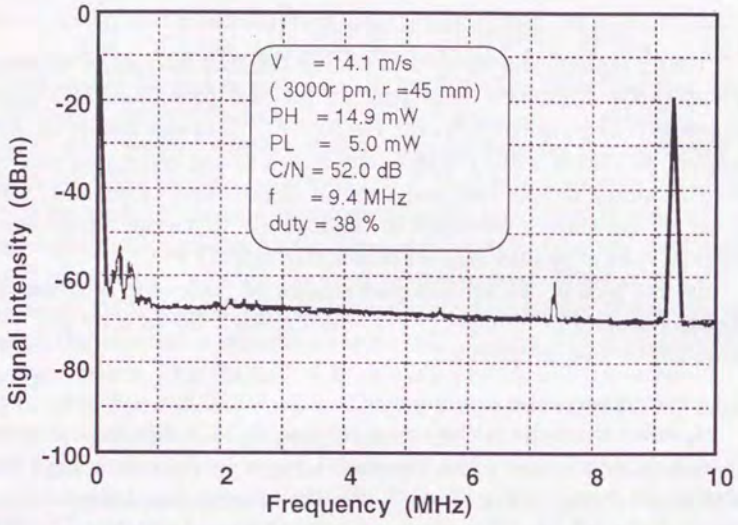

Fig. 3.37 Readout signal spectrum of DOW MO disk.

carrier-to-noise ratio (C/N) for the maximum recording density of 0.75 μm domain length and 1.5 μm mark pitch was 52 dB using a 780 nm laser and 0.55 numerical aperture (NA) lens, as shown in Fig. 3.37. This C/N value is about 3 dB higher than that for the conventional non-overwrite disk with a reflective layer.

Figure 3.38(a) shows a write laser waveform for mark-edge recording, which has been successfully demonstrated to be applicable to non-overwrite MO disks [3.19]. The preheating power level in Fig. 3.38(a) for the non-overwrite MO disk corresponds to the erasing power level for the DOW MO disk.

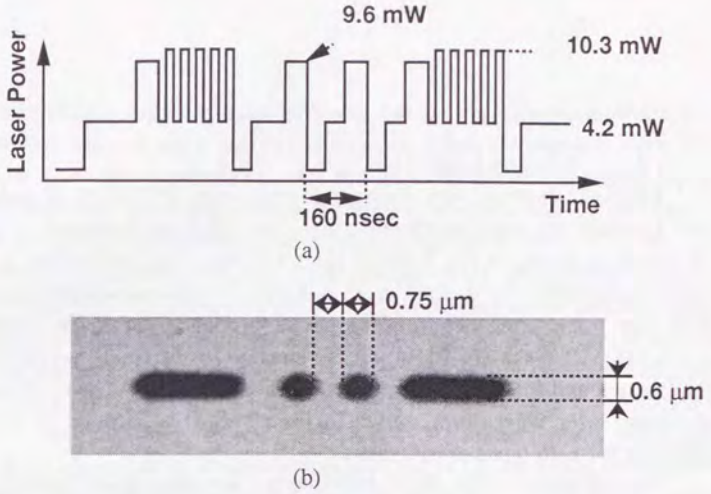

Fig. 3.38 (a) Write laser waveform, (b)Magnetic domain observed by polarization microscope

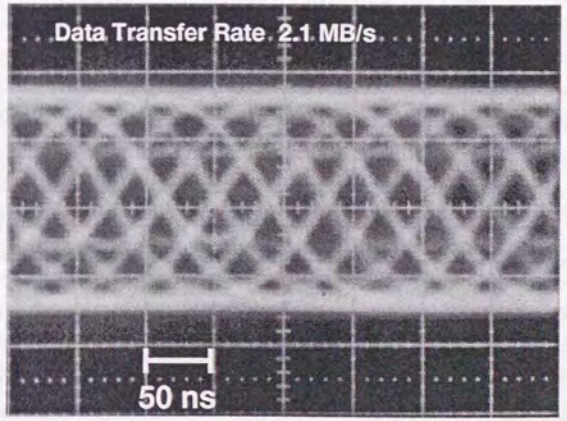

Fig. 3.39 Readout waveform.

3.5.3 *Result and discussion*

Magnetic domains with constant domain width of 0.6 μm are recorded, and nominal thermal interference between adjacent domains is hardly observed, as shown in Fig. 3.38(b). Here, 0.6 μm is the target domain width when considering the thermal cross-talk (§3.2) between adjacent tracks of 1.34 μm track pitch. Thermal response properties of DOW and non-overwrite MO disks are slightly different due to different magnetic layer thicknesses and the presence or absence of a reflective Al layer. However, the write laser wave form shown in Fig. 3.38(a) was found to be quite effective for both types of MO disks.

Specifications of the DOW MO disk are summarized in Table 3.2. All values, except overwritability, are the same as those for the non-overwrite 130 mm next-generation MO disk with 2 GB capacity, which has been discussed at the International Standard Committee for optical disks.

Table 3.2 Specifications of the 130 mm DOW MO disk.

Capacity/both sides	2 GB/130 mm
Track pitch	1.34 μm
Bit pitch	0.56 μm
Minimum mark	0.75 μm
Laser wavelength	780 nm
Modulation code	(1-7)RLL
Disk rotation	3000 rpm

The readout wave form for the (1-7) RLL random code with 1.5 mW read power is shown in Fig. 3.39. A clear eye pattern was observed and the resolution was about 30 %. Here, the detection window width was 40 ns because this measurement was performed at the 30 mm radial position with 3000 rpm. The C/N value for the 2T marks (0.75 μm domains) was about 52 dB, which is identical to that for conventional rectangular write pulses.

Jitter distribution was measured after the analog wave form was sliced with a DC level. Figure 3.40(a) shows the jitter distribution with 105 samples. The edge intervals indicate the intervals between leading edges. Almost the same result was observed for trailing edges. Here, the intervals between leading and trailing edges were not evaluated, because the double edge detection method with two phase-locked loops (PLLs) was assumed [3.20]. Figure 3.40(b) shows the edge intervals relative to the corresponding detection windows. A window margin of over 55 % of the detection window was obtained with the (1-7) RLL modulation code. No thermal interference between symbols was observed.

Here, the measurement was performed with a linear velocity of 9.4 m/s at 30 mm radius. S/N at 60 mm radius was about 1.5 dB lower than that at 30 mm radius. This resulted in the reduction of jitter margin down to 45 %.

The above results are almost the same as those obtained for the non-overwrite MO disk [3.21]. In other words, the same write compensation method can be used for both non-overwrite and DOW disks. This can be justified as follows.

Separated short laser pulses were used in this mark-edge recording. In such a short time region as for these pulses, the high temperature portion always concentrates in the recording films and each pulse forms a corresponding domain. Here, the film thickness is much thinner than the laser spot diameter. Therefore, the temperature gradient across the film dominates the thermal gradient through the film, and the vertical thermal diffusion across the films is greater than the thermal diffusion through the films because the heat flow is proportional to the temperature gradient. The vertical thermal diffusion produces no thermal interference. Consequently, this write wave form forms uniform domains for any mark length.

Since uniform domains are formed, the temperature at the end of every domain is the same. Therefore, the heat flow from the end of the previous domain to the next domain can be equalized at any distance by introducing a dormant period. This means that the thermal interference between marks can be effectively reduced for either non-overwrite or overwrite media. Consequently, this write wave form was proven to be applicable to most media with or without a reflective layer.

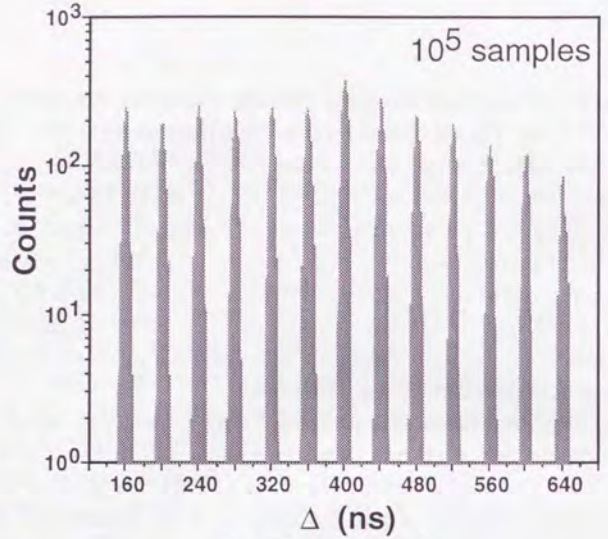

(a) edge intervals

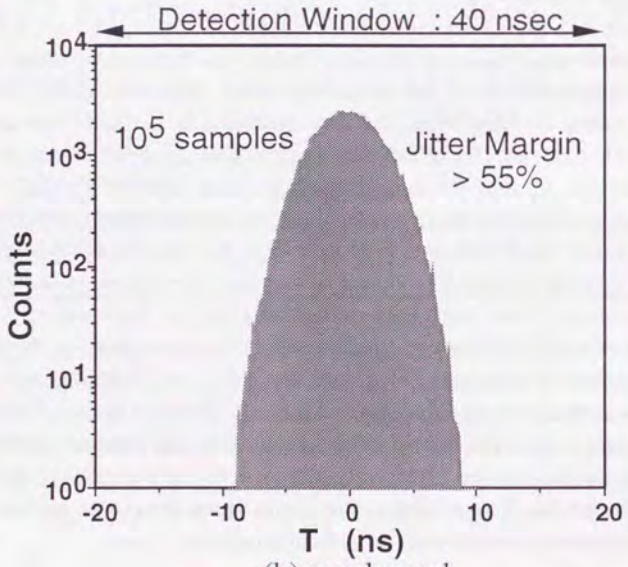

(b) overlapped

Fig. 3.40 Jitter distribution obtained by TIA.

In summary, an exchange-coupled direct-overwrite (DOW) magneto-optical (MO) disk with 2-GB capacity on a 130-mm-diameter disk was obtained with a sufficient jitter margin by precise mark-edge recording. The write laser wave form is common for both non-overwrite and DOW MO disks.

3.6 Conclusion

In light intensity modulation overwriting (LMO), many problems must be solved. Basically, these problems originate because LMO requires two levels of laser power for overwriting and because it uses magnetic exchange coupling between layers.

In §3.1, an application of domain transfer (magnetic printing) was described. The domain transfer process, in which the domain on the M-layer is printed into the W-layer before readout, expands the readout power margin. This doubles the readout power margin of LMO. However, after the domain transfer, the high-level readout power increases the noise level a bit due to the incomplete domain transfer. The incomplete transfer is well explained by the domain nucleation model.

In §3.2, the thermal crosstalk (TCT) of LMO due to erasure of domains recorded on adjacent tracks, was analyzed. Using comb-shaped laser pulses and a disk with a thick layer having moderate thermal conductivity on the top were found to be quite effective in reducing the TCT. If the ambient temperature rise and track offset are taken into account, 1.35 μm is the minimum track pitch. It is thus the possible to record 1 GB of information on each side of a 130-mm disk.

In §3.3, noise increase ΔN after initialization was detected for LMO with exchange-coupled magnetic films. Domains recorded on the M-layer were affected by initializing field H_{ini} during the initialization process, causing ΔN to appear. Fo an RE-dominant M-layer with an RE-dominant W-layer, the domain wall coercivity of the M-layer, $H_w{}^M$, needs to be larger than the sum of the initializing field and the exchange force to achieve domain stability. Fo a TM-dominant M-layer with an RE-dominant W-layer, $H_w{}^M$ needs to be larger than the sum of the effective coercivity of the W-layer and the exchange force. A noise increase after initialization was

not observed with a TM-dominant M-layer having a large $H_w{}^M$. These results are well explained by supposing that the sizes of the domains recorded on a TM-dominant M-layer are smaller than those recorded on an RE-dominant W-layer.

In §3.4, the overwriting repeatability for LMO media with an exchange-coupled multilayer was studied by using Arrhenius analysis. In an overwrite (OW) disk, the thermal-diffusion layer is less effective for extending the repeatability than that in a non-overwrite (NOW) disk. A degradation mode characteristic of the OW disks was found. In this mode, the activation energy was lower than that for a conventional NOW single-layer disk. The origin of the mode was found to be initialization noise due to reducing the domain wall coercivity in the memory layer after overwrite repetition . The degradation mode was suppressed by using a transition-metal dominant memory layer with high domain wall coercivity. An overwrite repeatability of more than 10^6 was achieved.

In §3.5, the mark edge recording technique, another high-density technique, was applied to an LMO disk. A direct overwrite (DOW) MO disk with 2-GB capacity on a 130-mm-diameter disk was obtained with a sufficient jitter margin. The write laser waveform is common to both NOW and DOW MO disks.

In summary, to achieve of high-performance LMO, high-coercive-force, RE-dominant M-layer should be used to reduce the noise level before and after repetitive overwriting and a multipulsed laser waveform should be used to eliminate the thermal crosstalk, thus enabling precise mark formation.

References

[3.1] M. Miyamoto, H. Miyamoto, T. Niihara, K. Andoo and M. Ojima, J. Magn. Soc. Jpn., Vol. **17**, Suppl. No. **S1** (1993) p. 339

[3.2] R. Malmhäll, M. Ojima, H. Awano, T. Niihara, H. Miyamoto, and M. Miyamoto, SPIE, **1663**, 204 (1992)

[3.3] R. Malmhäll, T. Niihara, H. Miyamoto, and M. Ojima, Jpn. J. Appl. Phys, **31**, 1050 (1992)

[3.4] T. Fukami, Y. Nakaki, T. Tokunaga, M. Taguchi, and K. Tsutsumi, Jpn. J. Appl. Phys., **67**, 4415 (1990)

[3.5] H. Miyamoto, K. Andoo, T. Niihara, T. Toda, T. Maeda, and M. Ojima, Jpn. J. Appl. Phys. **35**, 5326 (1996)

[3.6] H. Miyamoto, T. Toda, H. Ide, A. Saito, K. Andoo, T. Niihara, and M. Ojima, J. Magn. Soc. Jpn. **17**, Suppl. **S1**, 179 (1993)

[3.7] M. Miyamoto, H. Miyamoto, T. Niihara, K. Andoo, and M. Ojima, J. Magn. Soc. Jpn. **15**, Suppl. **S1**, 339 (1991)

[3.8] T. Iwanaga and H. Inada, Proc. of Int. Symp. on Optical Memory (1991), p. 215

[3.9] H. Miyamoto, M. Miyamoto, K. Andoo, T. Niihara, and M. Ojima, J. Magn. Soc. Jpn. **15**, Suppl. **S1**, 343 (1991)

[3.10] T. Kobayashi, T. Tsuji, S. Tsunashima, and S. Uchiyama, Jpn. J. Appl. Phys., **20**, 2089 (1981)

[3.11] Y. Yoneyama, T. Sato, Y. Takatsuka, S. Hayashi, and M. Yorozu, Digest of the 14th annual conference on magnetics in Japan 365 (1990)

[3.12] N. Ogihara, K. Shimazaki, Y. Yamada, M. Yoshihiro, A. Gotoh, H. Fujiwara, F. Kirino, and N. Ohta, Jpn. J. Appl. Phys. **28**, Suppl. **28-3**, 61 (1989)

[3.13] Y. Suzuki, J. Appl. Phys. **73**, 4705 (1993)

[3.14] H. Miyamoto, K. Andoo, T. Niihara, and M. Ojima, J. Appl. Phys., **77**, 265 (1995)

[3.15] H. Miyamoto, T. Niihara, H. Sukeda, M. Takahashi, T. Nakao, M. Ojima and N. Ohta, J. Appl. Phys. **66** 6138 (1989)

[3.16] J. Saito H. Akasaka, H. Birecki and C. Perlov, Proc. Int. Magn. Conf. '92, p. 2512.
[3.17] H. Miyamoto, M. Ojima, T. Toda, T. Niihara, T. Maeda, J. Saito, H. Matsumoto, T. Hosokawa, and H. Akasaka, Jpn. J. Appl. Phys., **32**, 5457 (1993)
[3.18] T. Hosokawa, J. Saito, H. Matsumoto, H. Iida, A. Okamuro, S. Kokai and H. Akasaka: Proc. Int. Symp. Optical Memory, 1991, p. 55.
[3.19] T. Maeda, F. Kirino, T. Toda, H. Ide, S. Mita and K. Shigematsu, Dig. Int. Magn. Conf. '93, DD-06.
[3.20] H. Sugiyama, T. Maeda, A. Saito, T. Nishida, S. Horigome, S. Arai, K. Shigematsu, H. Watanabe, and A. Gotoh, Jpn. J. Appl. Phys. **31**, 584 (1992)
[3.21] T. Maeda, T. Toda, H. Ide, F. Kirino, S. Mita, and K. Shigematsu, IEEE Trans. Magn., **29**, 3787 (1993)

4 High-density Recording

To achieve high-density recording, small-domain recording and small-domain readout are important. To record and to read small domains, it is important to reduce the laser spot size by using a short wavelength laser, such as, a blue or green laser. However, the development of blue and green laser diodes is a bit behind the demand for high-density recording. Therefore, other techniques for small-domain recording and reading are needed.

Magnetic-field modulation with pulsed-laser irradiation was studied as a small-domain recording technique. Magnetically induced super-resolution, which is an application of the magnetic multilayer, was studied as a small-domain readout technique.

4.1 High-density recording and readout technique

In MO recording, as described earlier, domains are formed by heating up a particular area to a temperature higher than the recording temperature by using a recording laser spot. The size of the recorded domain can thus be controlled by changing the laser power. Figure 4.1 shows the relationship between the recorded-domain diameter and the recording laser power for light-intensity modulation (LIM) recording. The irradiation from a 4-mW laser beam forms a 0.2-μm-diameter domain. However, forming such a small domain requires strict laser power control, which is very unstable against various fluctuations, such as media sensitivity variance and optical spot aberrations.

Magnetic-filed modulation overwriting (MMO), discussed in chapter 2, is also a good technique for small-domain formation because the length of the domain is determined by the field modulation rate, which is independent of the optical spot size. However, small-domain formation by MMO requires fast modulation of the magnetic field in order to avoid the noise increase caused by edge transition [4.1]. In the next section, a combination of light-intensity modulation and MMO, i.e., pulsed-laser irradiated MMO, is discussed.

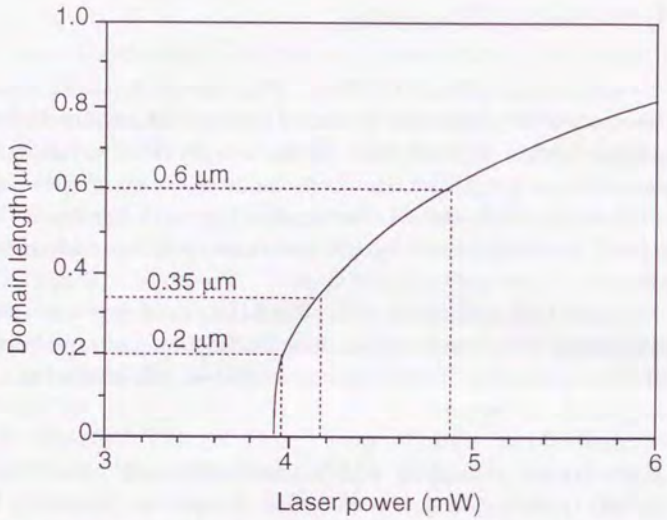

Fig. 4.1 Laser power margin for light-intensity modulation (LIM) recording.

For small-domain readout, it is important to eliminate the optical interference between adjacent marks. This can be done optically, electrically, or magnetically. Two optical cancellation techniques are optical super-resolution [4.2], and land-groove recording technique [4.3]., Two dimensional recording with a three-laser spot [4.4] is an electrical cancellation technique. Magnetically induced super-resolution (MSR) [4.5], [4.6], [4.7], another application of the magnetic multilayer, has been investigated as a technique to improve the resolution.

In §4.3, a new small-domain readout technique is proposed based on analysis of the domain dynamics in MSR.

4.2 Magnetic-field modulation with pulsed-laser irradiation

Direct overwriting using both pulsed-laser irradiation and magnetic field modulation was studied [4.8]. The pulsed laser was irradiated on the media while a constant DC laser beam was irradiated to perform MMO, as discussed in chapter 2. The pulsed irradiation forms a smaller-size high-temperature region in which the magnetization of the MO medium is aligned in the direction of the applied magnetic field. This enables stable formation of small domains.

An outline of this method is shown in Fig. 4.2. A laser-pulse train with a constant duration is irradiated on the MO medium, and a modulated

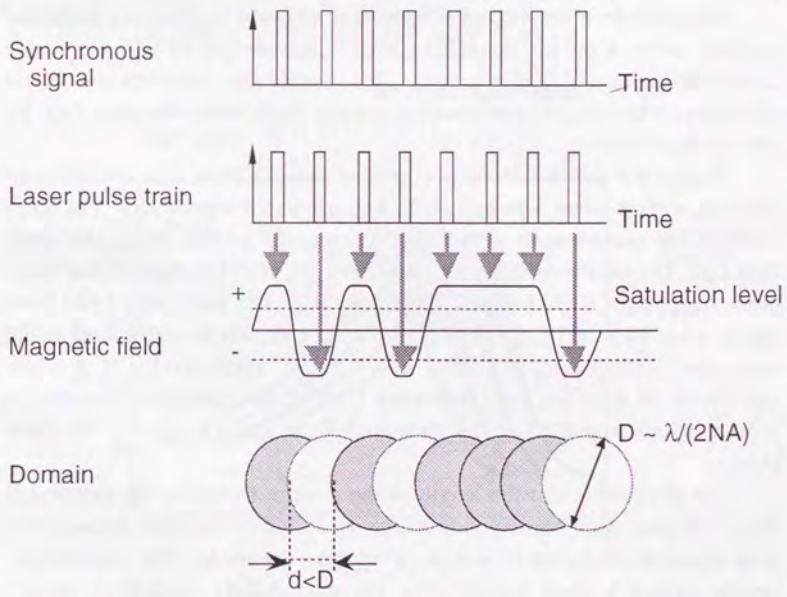

Fig. 4.2 Pulsed-laser irradiated magnetic-field modulation.

magnetic field, which reflects the recording information, is applied to the media in synchronization with the pulsed laser light. The synchronization is performed in such a way that magnetic field direction is only changed between light pulses. This enables the stable formation of small magnetic domains within the limited area where the pulsed laser is irradiated because a sufficient magnetic field is always applied when the media temperature rises with the laser pulse irradiation. In the developed system, the laser irradiates in pulses according to a channel clock generated from pre-recorded pits. Since the laser-spot moving distance in each channel clock period is shorter than the light-spot diameter, the magnetic domains corresponding to adjacent pulses overlap and the recorded magnetic domains become smaller than the size of the optical diffraction. Therefore, high-track-density, high-bit-density recording is achieved.

For example, a bit pitch of 0.3 μm was achieved without any particular problem when a pulsed laser light with a wavelength of 680 nm and a numerical aperture of 0.55 was used. This method also improves the optical efficiency, which is the inverse of the average laser power for recording, by two or three times.

Figures 4.3 and 4.4 show examples of the simulated time evolution of the temperature when a pulsed laser was irradiated repetitively. The lines indicate the temperature profile on the recording film along the track direction. The profile at every moment after the trailing edges of the laser-pulse irradiation is shown with 2-ns intervals. The intervals of the laser pulses were 40 ns (Fig. 4.3) and 20 ns (Fig. 4.4), which correspond to the minimum domain lengths of 0.4 and 0.2 μm, respectively, at a linear velocity of 10 m/s. The lines indicating 0 ns are the maximum temperature profile, which appeared at the moment of the trailing edge of the laser pulse.

The lines show that the length of the domain formed at the moment is about 0.6 μm. This corresponds to the width of the domain because the high-temperature region is almost circular on the media. The temperature profile within a short period after the pulsed-light irradiation greatly depends on the laser-spot profile because the effect of heat diffusion does not appear quickly.

A short time (~5 ns) after the trailing edges of the laser pulses, the temperature on the recording layer rapidly fell below the recording temperature (~210 °C). This shows that a change in the magnetic field direction after 5 ns does not affect the recording domain shape. Therefore, magnetic-field transition speeds of 15 and 5 ns, corresponding to intervals between pulses of 20 ns (Fig 4.3) and 10 ns (Fig 4.4), respectively, are sufficient for the stable formation of recorded domains.

The channel-clock periods were 40 and 20 ns, resulting in 0.4- and 0.2-μm position differences in the domains formed by a series of pulses. This results in the overlapping of adjacent domains because the recorded domain corresponding to each laser pulse had a diameter of about 0.6 μm. Because of this overlapping, rough control of the laser power to form 0.6-μm-diameter domains allows the stable formation of 0.2-μm domains.

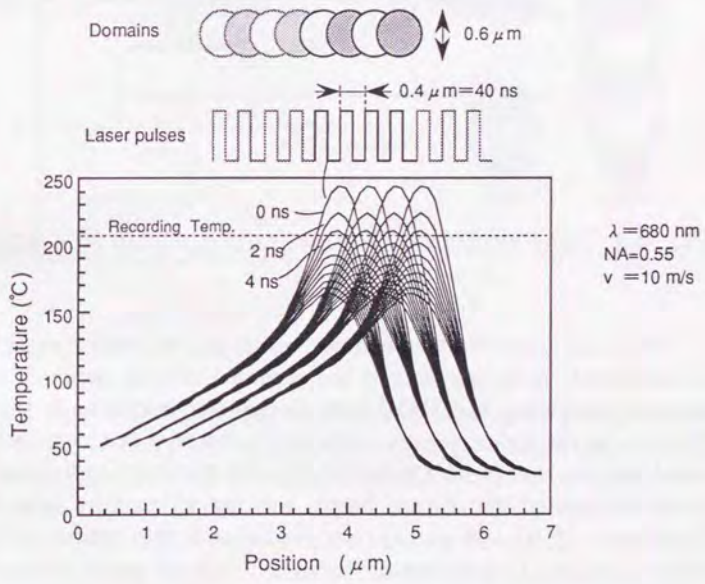

Fig. 4.3 Time evolution of temperature profile (0.4 μm pitch).

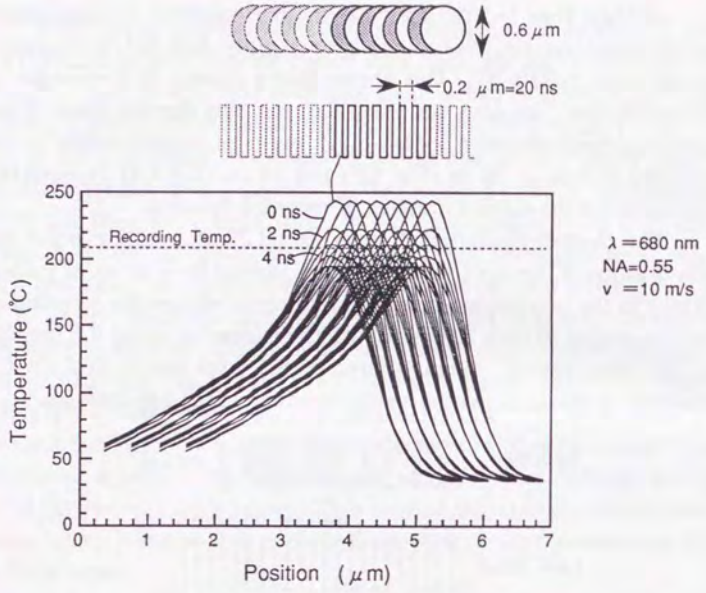

Fig. 4.4 Time evolution of temperature profile (0.2 μm pitch).

From the simulated temperature profile, the recorded domain shape was obtained. A comparison of the recorded domain shape for light-intensity modulation and MMO with pulsed-laser irradiation is shown in Fig. 4.5. In the light-intensity modulation, the recorded domain length varied with the laser power fluctuation, while in the MMO with pulsed-laser power irradiation, the domain length was not affected by laser power fluctuations. MMO with pulsed-laser irradiation is thus promising for the stable formation of small domains because it does not require strict control of the recording laser power.

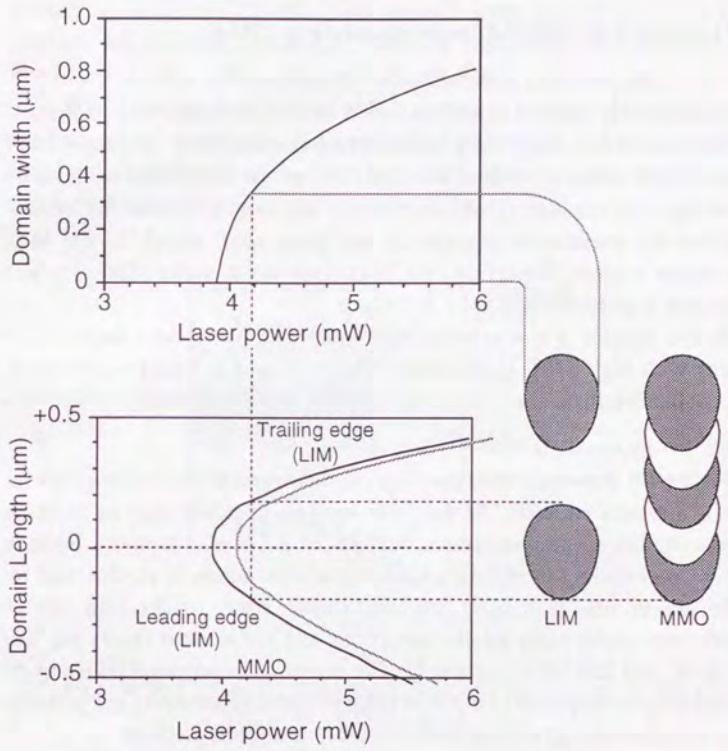

Fig. 4.5 Comparison of recorded domain length stability for light-intensity modulation (LIM), and magnetic-field modulation overwriting (MMO).

4.3 Magnetically induced super-resolution (MSR)

4.3.1 Magnetically induced super-resolution

Magnetically induced super-resolution (MSR) methods using exchange-coupled multilayers have been investigated because they are capable of detecting small domains without blue laser. However, these MSR methods do not enlarge the readout signal amplitude, but only improve the optical resolution by masking a portion of the laser spot, which is the high temperature region. Therefore, the signal to noise ratio (SNR) is not sufficiently high for high-density recording.

In this section, a new readout technique [4.9], which can detect small domains with high SNR, is proposed. The technique is based on the MSR methods, but it utilizes the readout signal characteristics skillfully.

4.3.2 Experiment

Figure 4.6 shows the disk structure used throughout the present section, which is a typical structure for the front aperture detection type of MSR. A magneto-optical multilayer, which consists of a TbFeCo memory layer, a TbDyFeCo switching layer and a GdFeCo readout layer, is sandwiched by nitride layers for protecting the multilayer from oxidization. Curie temperatures of the memory, the switching and the readout layers are 250 °C, 150 °C and 350 °C, respectively. The layers were prepared by using rf-magnetron sputtering with composite targets. The disk substrate is a glass/2p (photo-polymerization) replica with 1.4-μm-pitch spiral grooves.

The write and read characteristics of the disk such as SNR were evaluated by a magneto-optical disk drive with an 830-nm-wavelength laser and a 0.55-numerical-aperture lens, which forms an optical spot of 1.5 μm in diameter, at a liner velocity of 4.2 m/s. The intensity of the bias field H_B during writing is 32 kA/m {400 Oe} and the intensity of H_B during reading was varied from -32 kA/m {-400 Oe} to +32 kA/m {+400 Oe}. In order to cause MSR, the readout power was set at 2.5 mW, which is about a two times higher power than non-MSR readout power of 1.0 mW.

Detection jitters were measured by another magneto-optical disk drive with a 680-nm-wavelength laser and 0.55-numerical-aperture optical lens at

a liner velocity of 7.5 m/s. The readout laser power is 1.7 mW. The domains are recorded by the light intensity modulation with an assist power level for reducing a thermal interference [4.10].

The diameters of the recorded domains were estimated from the readout signal amplitude. The estimation was calibrated with the domain observation, which obtained by a polarized optical microscope with an oil immersion type objective lens (x100, NA1.1).

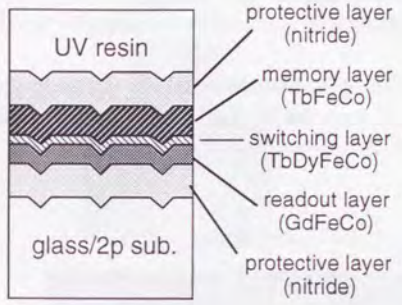

Fig. 4.6 The disk structure, which is a typical structure for MSR detection.

4.3.3 Readout signal characteristics of MSR

Figure 4.7 compares readout signals of the 0.5-μm-diameter domains by non-MSR detection (H_B = 0 ~ 16 kA/m {0 ~ 200 Oe}) and MSR detection (H_B = -24 kA/m {-300 Oe}). The signal by non-MSR detection shows a 2.0-μm-width signal response, which coincides the sum of the domain diameter of 0.5 μm and the optical spot size of 1.5 μm. The readout signal by MSR detection shows a rapid change (decrease) compared with the conventional

readout signal. The decrease time is 70 nsec, which coincides 0.3-μm movement of the laser spot during the signal decrease.

The rapidity is not understandable from the stable mask shape model since domain diameter (0.5 μm) is lager than the movement. Supposing the shape and size of the mask were the same during the readout, the decrease time would be 120 nsec which coincides 0.5-μm movement of the laser spot.

Further, a measurement of H_B dependence revealed that the readout signal profile changes discontinuously from the non-MSR state to the MSR state, and no intermediate state exists. In the other words, there exists a critical field strength which is a border field between MSR and non-MSR detection.

The discontinuity against the bias field is not understandable also if the mask always spreads into the higher temperature region than a masking temperature which is determined by H_B.

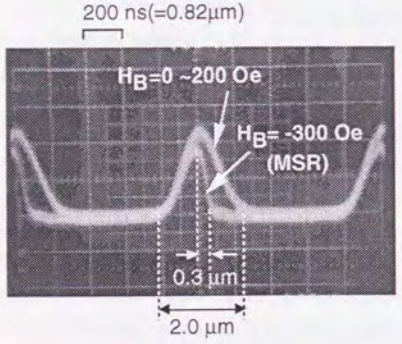

Fig. 4.7 The disk structure, which is a typical structure for MSR detection.

4.3.4 Domain collapse model

In order to obtain a good explanation to the rapid change in the signal, we proposed a domain collapse model. Generally, each magnetic film has a minimum domain radius. In this case, since domains are on the readout layer, we analyzed the minimum domain radius of the multilayer system.

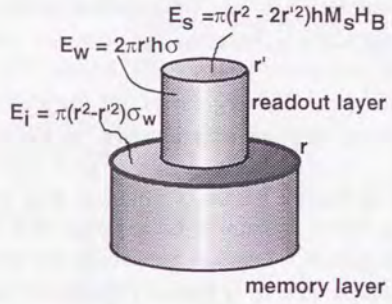

Fig. 4.8 A cylindrical domain model for evaluating the total magnetic energy of the multilayer with a single domain.

Figure 4.8 shows a cylindrical domain model for evaluating the total magnetic energy of the multilayer. Here, we suppose that a domain on the memory layer shows no change, that a domain on the readout layer shrinks or expands with a cylindrical shape, that the demagnetization field from each layer is sufficiently low and that thickness of domain walls and the switching layer is sufficiently small.

The magneto-static energy E_S, the interface wall energy between the memory and the readout layer E_i, the domain wall energy in the readout layer E_W and the total magnetic energy E_t are expressed as follows.

$$E_S=-2\pi r'^2 h M_S H_B+\pi(r^2-r'^2)h M_S H_B \quad (4.1)$$

$$E_i=\pi(r^2-r'^2)\sigma_W \quad (4.2)$$

$$E_W=2\pi r' h\sigma \quad (4.3)$$

$$E_t(r')=E_S+E_i+E_W=-2\pi h\sigma/r_c(r'-r_c/2)^2+\text{const} \quad (4.4)$$

$$r_c=2h\sigma/(\sigma_W+2hM_S H_B) \quad (4.5)$$

were, r, r', σ_W (0 ~ 0.004 J/m^2 {0 ~ 4 erg/cm^2}) and H_B denote the domain radius on the memory layer, the domain radius on the readout layer, the interface wall energy density between the memory and the readout layers, and the bias field, respectively. M_S (~200 kA/m {200 emu/cm^3}), h (30 nm) and σ (~4×10^{-3} J/m^2 {~4 erg/cm^2}) are the magnetization, the thickness and the domain wall energy density of the readout layer, respectively.

Since Eq. (4.4) is a convex parabola function with a maximum at $r'=r_c/2$ as shown in Fig. 4.9, a domain with the radius of $r_c/2$ shrinks and collapses. In the case of $r_c/2<r<r_c$, though the energy at $r'=r$ is larger than the energy at $r'=0$, a domain with r_c is partially stable because the energy has a barrier (maximum) between $r'=0$ and $r'=r$. Therefore, the minimum stable domain radius for this system is r_c and a domain smaller than $r_c/2$ collapses rapidly.

Since the estimated minimum domain radii $r_c/2$ of the disk at room temperature and at the masking temperature are 0.06 μm and 0.5 μm, respectively, smaller domain than the radius of 0.5 μm can not exist stably and collapses rapidly. Therefore, when a smaller domain than the minimum radius comes within the heated area where the exchange force disappears, the domain collapses as shown in Fig. 4.10(a).

The speed of the collapse phenomenon is determined by the domain wall velocity. For GdFeCo film, the domain wall velocity is higher than the linear velocity of the disk. Therefore, the collapse speed is faster than the linear velocity of the disk.

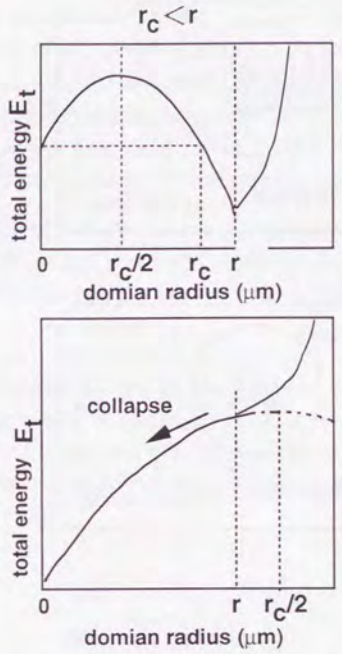

Fig. 4.9 Relationship between the total energy of the multilayer system and the domain radius on the readout layer. If the domain radius on the memory layer r is smaller than rc/2, the domain on the readout layer collapses.

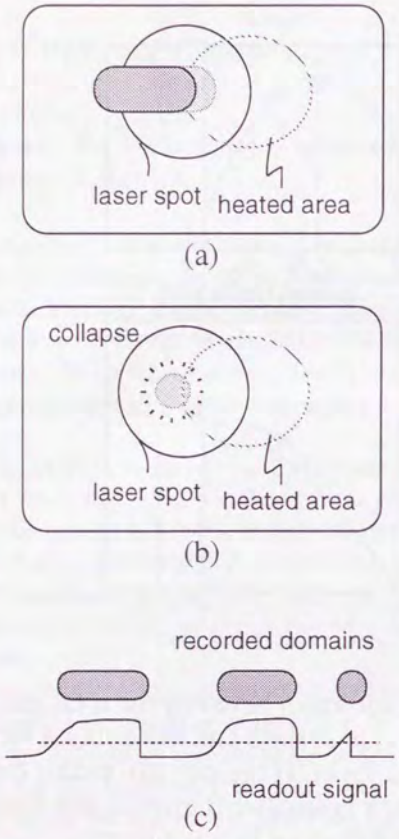

Fig. 4.10 Origin of a rapid change in the readout signal. collapsing of a small domain when the domain comes into the heated area, (b) shrinking of a long domain, (c) rapid decreases of the trailing edges in the readout signal.

When a long domain comes into the laser spot (heated area) as shown in Fig. 4.10(b), a portion of the domain is masked and the domain is shorten. After the domain is shorten, the left small domain collapses.

As a result of the domain collapse, the rapid change in the signal is observed at the end of the domain as shown in Fig. 4.10(c). However, front edge signal is not steepened and the asymmetric signal is observed.

4.3.5 New readout technique using domain collapse

The rapid change is used to detect the precise position of the domain or the domain wall. This detection is very effective in reducing random noise such as shot noise as shown in Fig. 4.11.

The readout signal contains random noise such as shot noise. The noise swings the readout signal mainly in the vertical direction in the figure. Therefore, when the signal is sliced by a slice level, jitter for the rapid trailing edge is reduced compared with the leading edge.

Figure 4.12 shows the differentiated signals under the various bias fields.

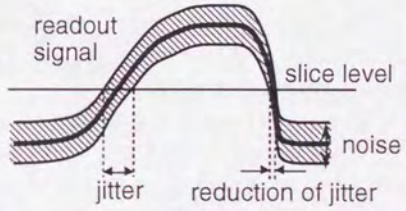

Fig. 4.11 Reduction of domain edge jitters by domain collapse detection technique.

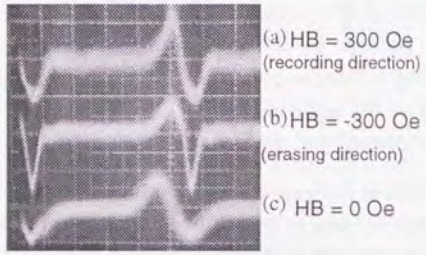

Fig. 4.12 Differentiated readout signals for (a) reverse collapse, (b) normal collapse and (c) non-MSR detection.

When the bias field H_B is 0 kA/m, the differentiated signal is small and noisy as shown in Fig. 4.12(c). This is the non-MSR detection.
When H_B is -24 kA/m {-300 Oe} at which the MSR occurs, the differentiated signal of the trailing edge is larger and less noisy as shown in Fig. 4.12(b). This is the result of the domain collapse and it shows that the noise was reduced.

When H_B is +24 kA/m {+300 Oe} at which the MSR occurs, the differentiated signal of the leading edge is larger, which means the leading edge is steepened, and less noisy as shown in Fig. 4.12(a). This phenomenon is explained by the domain deformation as follows.

In this case, the MSR mask is formed as a domain on the readout layer. Therefore, when the recorded domain is absorbed by the mask domain, the combined domain tends to become round shape to minimize the domain wall energy. At the instant of the domain deformation, the rapid leading edge is observed. Additionally, the first portion of the leading edge is not steepened because the domain deformation occurs after the recorded domain comes within the laser spot.

The result implies the applicability of the collapse technique to the mark edge recording because it improves rapidity of both leading and trailing edges.

Further, the domain collapse is suitable for mark position recording because it improves precision of the mark position detection due to the high SNR of the differentiated signal. The collapse enables a high-density recording with narrow window channel such as variable five modulation (VFM) [4.11].

Figure 4.13 shows an eye-pattern for the combination of the collapse technique and the VFM channel with mark position recording. The bit density and the detection window length $\mathbf{T}_w$ are 0.5 μm/bit and 0.2 μm, respectively, 0.5-μm-diameter domains are recorded with variable intervals ($\mathbf{n} \times \mathbf{T}_w$) by using the magneto-optical drive with 680 nm laser at the liner velocity of 7.5 m/s. The minimum domain interval is 131.3 nsec, which coincides 5 times the Tw of 26.3 nsec. A very clear eye-pattern is observed.

Figure 4.14 shows the detection jitters of the sliced signal. With 10^5 samples, the relative jitter of 90 % was observed. Since the measurement was performed without any equalization or signal processing, a smaller jitter and a higher density recording are expected if the appreciate equalization is applied.

With this condition, SNR of the minimum interval domains measured by a spectrum analyzer was 22 dB in route mean square with the band width of 0 to 10 MHz. The detection jitter is relatively good compared with the expectation value from the SNR, which coincides 170 %. This means that the collapse readout technique enlarges the effective SNR and reduces jitters.

In summary, a rapid change in the readout signal of the MSR detection was observed. This rapid change is the result of domain collapse on the readout layer. The rapid change improves the SNR of the differentiated signal and enables the high-density recording with narrow detection window. Relative detection jitter of 90 % was obtained with a 0.5-μm/bit linear density, which is half of the jitter for conventional detection. A higher density recording is obtainable if an appreciate equalization is applied.

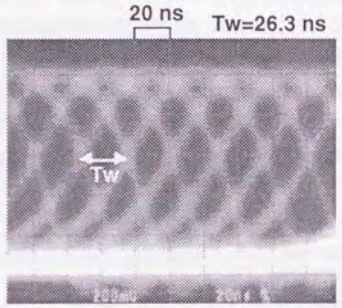

Fig. 4.13 Eye-pattern of the collapse readout technique with a combination of mark position recording and VFM channel.

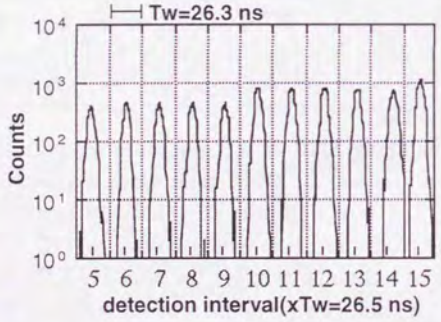

Fig. 4.14 Detection jitters of 10^5 samples using the collapse readout technique with a combination of mark position recording and VFM read/write channel.

4.4 Conclusion

To achieve high-density recording, small-domain recording and small-domain readout are important. As examples of small-domain recording and readout, magnetic-field modulation overwriting with multiple laser-pulse irradiation, and magnetic super-resolution technique were studied.

Magnetic-field modulation with pulsed-laser irradiation showed good characteristics for recording small domains because it does not require strict control of the laser power as a result of its overwritability. That is, the partial erasure of the domain by the following laser pulse enables the stable recording of domains smaller than the optical laser spot.

In magnetic super-resolution readout, a rapid change in the readout signal is observed. It is due to the domain collapse in the readout layer. The introduced readout technique using domain collapse showed good characteristics for reading out small domains because it reduces the effect of shot noise by using the rapid response of the readout signal.

Experimental and simulation results showed that combining these two techniques can double the recording density of an MO disk. Furthermore, a higher-density is likely if a short-wavelength laser is applied with an adequate readout layer for the wavelength. For example, a Pt/Co multilayer [4.12], [4.13] which has a high Kerr rotation angle at a wavelength of about 400 nm, is applicable as a readout layer.

References

[4.1] M. Takahashi, H. Sukeda, M. Ojima, and N. Ohta, J. Appl. Phys. **63**, 3838 (1988).

[4.2] Y. Yamanaka, Y. Hirose, H. Fujii, and K. Kubota, Appl. Opt. **29**, 3046 (1990)

[4.3] A. Fukumoto, S. Masuhara, and K. Aratani, Tech. Digest of Symp. Opt. Memory '94, 41 (1994)

[4.4] T. Maeda, H. Sugiyama, A. Saitoh, K. Wakabayashi, H. Miyamoto, and H. Awano, SPIE **2514**, Optical Data Storage '95, 70 (1995)

[4.5] K. Aratani, A. Fukumoto, M. Ohta, M. Kaneko, and K. Watanabe, SPIE, **1499**, Optical Data Storage '91, 209 (1991)

[4.6] A. Fukumoto, and S. Kubota, Jpn. J. Appl. Phys., **31**, 529 (1992)

[4.7] Y. Murakami, N. Iketani, J. Nakajima, A. Takahashi, K. Ohta, and T. Ishikawa, J. Magn. Soc. Jpn., **17**, Suppl. **S1**, 201 (1993)

[4.8] S. Yonezawa and H. Miyamoto, Digest of Symp. on Opt. Memory 1994 (SOM'94), 65 (1994)

[4.9] H. Miyamoto, K. Andoo, H. Saga, H. Sukeda, and M. Ojima, J. Magn. Soc. Jpn., **19**, Suppl. No. **S1**, 425 (1995)

[4.10] T. Maeda T. Toda, H. Ide, F. Kirino, S. Mita, and K. Shigematsu, IEEE Trans. Magn. **29**, 3787 (1993)

[4.11] N. Eguchi and Y. Akiyama, Jpn. J. Appl. Phys., Part 1, **32**, 5307(1993)

[4.12] M. Takahashi, J. Nakamura, T. Niihara, and K. Tatsuno, J. Magn. Soc. Jpn. **15**, Suppl. **S1**, 49 (1991)

[4.13] J. Nakamura, H. Awano, H. Miyamoto, M. Takahashi, and M. Ojima, J. Magn. Soc. Jpn., **17**, 809 (1993) (Japanese)

5 Summary and Conclusion

Multilayered magneto-optical (MO) media were studied in order to achieve high-speed, high-density MO recording. The relationship between the recording characteristics and the structure of the multilayered MO disk was analyzed from the viewpoints of the three kinds of physical properties: thermal, magnetic, and optical properties. The analysis was performed both numerically and experimentally.

In §5.1, §5.2, and § 5.3, the discussions in the previous chapters are summarized. In §5.4 and §5.5, the thesis concludes with the most suitable form of MO recording as developed by this study.

5.1 Optical and thermal structure of MO media

Two optical properties, Kerr rotation and reflectivity, were studied through optical simulation and experiment. The enhancement effect of the Kerr rotation in a multilayered MO disk has been simulated by using a multiple-reflection model of magnetically induced circular dichroism. The simulated results were consistent with the experimental ones. From the optical point of view, the most suitable structures for MO media are a quadrilayered structure with a metal (aluminum) reflective layer, and a magnetic bilayer with a readout magnetic layer. In the quadrilayered disk, the figure of merit (FOM) and the reflectivity are independently controlled by changing the structure. Furthermore, the Kerr ellipticity, which degrades the SNR, can be completely eliminated. In the magnetic bilayer, use of a magnetically soft readout layer, which has good MO characteristics, provides a good FOM.

The thermal properties of MO disks were studied by the analyzing the relationship between the recording characteristics and the thermal structure of the media for magnetic-field modulation overwriting (MMO). Thermal simulation combined with a domain-formation model showed the relationship between the media structure, the recording characteristics, and the recorded domain shape. From the thermal point of view, the most suitable thermal structure for MO media is a quadrilayered structure with a thermal-diffusive metal layer. The quadrilayered disk reduces the length of

the "tail" in the domain recorded by MMO, thus eliminating the overlap between domains and increasing the signal intensity and quality.

Fortunately, the quadrilayered structure has both good optical the thermal properties. To maintain consistency between the optical and thermal properties, the optical properties should be controlled by changing the thicknesses of the two dielectric layers and of the MO film, and the thermal properties should be controlled by changing the thermal conductivity of the heat-sink (metal) layer. Changing the composition of the metal film greatly affects the thermal conductivity.

5.2 Magnetic multilayer

In light-intensity modulated overwriting (LMO), there are many problems to be solved. Basically, these problems are because LMO requires two levels of laser power for overwriting and because LMO uses magnetic exchange-coupling between layers. The former results in a narrow power margin and thermal crosstalk. The latter results in initialization noise and degradation after repetitive overwriting.

An application of domain transfer (magnetic printing) was studied in order to expand the readout power margin. It was found that the domain-transfer process expands the readout power margin, although a slight increase in the noise level was observed when the readout power was high.

The thermal crosstalk caused by light-intensity modulated magneto-optical overwriting, which results in the erasure of domains recorded on adjacent tracks, was also analyzed. Use of comb-shaped laser pulses and disk with a thick layer having moderate thermal conductivity on the top, effectively reduced the thermal crosstalk .

Noise increase ΔN after initialization was detected for LMO with exchange-coupled magnetic films. Detailed analysis revealed that the applied initializing field destroyed domains recorded on the memory layer to induce the noise increase. Use of the transition-metal dominant memory layer having large *effective* coercivity eliminated the noise increase after initialization.

The overwrite repeatability of LMO media with an exchange-coupled multilayer was studied by using Arrhenius analysis. The thermal diffusion

layer in an overwritable disk was found to be less effective for extending the repeatability than that in a non-overwritable disk. The origin of a degradation mode characteristic of the overwritable disk, which has a lower activation energy than that of a non-overwritable disk, was found to be an initialization noise due to the degradation of the memory layer. Use of a TM dominant memory layer with high domain wall coercivity suppressed the degradation mode and provided an overwrite repeatability of more than 10^6.

Mark-edge recording , a high-density recording technique, was applied to an LMO disk. An LMO disk with 2-GB capacity on a 130-mm-diameter disk was obtained with a sufficient jitter margin. The write-laser waveform is common to both non-overwritable and LMO disks.

In summary, to achieve high-performance LMO, high-coercive-force, transition-metal dominant memory layer is needed to reduce the noise level before and after repetitive overwriting, and a multipulsed laser waveform is needed to eliminate the thermal crosstalk and to form precise marks.

5.3 High-density technology

Small-domain readout and small-domain recording are required for high-density recording. As examples of small-domain recording and readout, MMO with multiple laser-pulse irradiation, and magnetically induced super-resolution (MSR) were studied.

MMO with pulsed-laser irradiation is good for small-domain recording because it does not require strict control of the laser power as a result of its overwritability. That is, the partial erasure of the domains by the following laser pulse enables the stable recording of domains smaller than the optical laser spot.

MSR shows a rapid change in the readout signal, which results from the domain collapse in the readout layer. The introduced readout technique using domain collapse is good for reading out small domains because it reduces the effect of shot noise by using the rapid response of the readout signal.

Experiment and simulation results showed that combining the two techniques can double the recording density of an MO disk. Furthermore,

higher-density is likely if a short-wavelength laser is applied with an adequate readout layer for the wavelength. For example, a Pt/Co multilayer, which has a high Kerr rotation angle at a wavelength of 400 nm, is applicable as a readout layer.

5.4 Conclusion

Magnetic multilayers provide useful functions, such the light-intensity modulated overwriting and magnetically induced super-resolution. However, magnetic multilayers are inconsistent with a quadrilayered disk having a single-layered magnetic film, which has good optical and thermal characteristics. Therefore, it is necessary to discuss what is needed to obtain high-speed, high-capacity MO recording from the viewpoints of three physical properties.

From the optical point of view, a quadrilayered structure and a magnetic bilayer with a readout layer show good performance. Although the quadrilayered structure is inconsistent with magnetic multilayers, the magnetic bilayer is consistent.

From the thermal point of view, the heat flow is controlled by the improved laser waveform. In other words, the thermal properties are improved by not only the media structure but also by the laser waveform. Short-pulsed laser irradiation heats the media up to a temperature profile that is approximately the same as the laser intensity profile. In this condition, the thermal properties of the media show very little effect.

From the magnetic point of view, magnetic multilayers have several useful functions, such as LMO and MSR. MSR, especially, is essential for achieving high density MO recording because it overcomes the optical-resolution limit.

Abstracting the essential functions, high-speed, high-density MO recording requires overwriting and super-resolution. In addition, the applicability of a short-wavelength laser needs to be considered for the future.

These requirements lead to the conclusion presented in chapter 4: a combination of MSR with a readout layer for a short-wavelength laser and MMO with pulsed-laser irradiation are needed for high-speed, high-density

MO media. Overwriting is achievable by MMO for any type of media; the MMO should be accompanied by pulsed-laser irradiation to achieve small domain-formation. MSR is easily combined with pulsed-laser-irradiated MMO. The readout layer for a short-wavelength laser is also applicable to the readout layer for MSR.

In conclusion, the most suitable form for a high-density, high-speed magneto-optical disk is a combination of magnetically induced super-resolution using the readout layer for a short-wavelength laser and magnetic-field modulation overwriting with pulsed-laser irradiation.

Acknowledgments

I am grateful for the guidance and encouragement of Prof. Ryoichi Ito in writing this thesis.

I also thank all those at Hitachi's Central Research Laboratory, who gave me the opportunity to perform this study. Above all, I express my sincere gratitude to Dr. Masahiro Ojima for his clear guidance and patient support. I also thank Dr. Norio Ohta, Dr. Ryo Suzuki, Dr. Fumio Kugiya and Dr. Masahiko Takahashi for their continuing guidance and support. I am also grateful to Dr. Kazuo Shigematsu, Dr. Takeshi Maeda, and Dr. Seiji Yonezawa for their helpful suggestions and discussions.

I wish to express special thanks to Dr. Toshio Niihara, who has been my supervisor and colleague, for his sincere guidance and fruitful discussions.

I had many discussions with my colleagues, Mr. Hirofumi Sukeda, Mr. Keikichi Andoo, Mr. Makoto Miyamoto, Mr. Takeshi Nakao, Mr. Tsuyoshi Toda, Mr. Hiroshi Ide, Mr. Atsushi Saito, and Mr. Hideki Saga, whose contributions to this thesis were very great, and I take pleasure in acknowledging the important part played by them.

I also thank Dr. Yoshio Suzuki, Dr. Fumiyoshi Kirino, Ms. Yumiko Anzai, Ms. Junko Ushiyama, Dr. Kimio Nakamura, Mr. Norio Ogihara, and Dr. Hiroyuki Awano for their considerable assistance and suggestions.

I am indebted to Dr. Jun Saito, Mr. Hiroyuki Matsumoto, Mr. Tetsuo Hosokawa, and Dr. Hideki Akasaka of Nikon Corporation for providing the direct overwrite media and for this fruitful discussions.

I thank Dr. Yasutsugu Takeda, Dr. Hisashi Horikoshi, Dr. Michiharu Nakamura, Dr. Yasuo Suganuma, Dr. Katsumi Miyauchi, Dr. Yoshito Tsunoda, Dr. Yoshihiro Shiroishi, and Dr. Ryo Imura for their continuing support.

Finally, I wish to thank my wife, for without her help and support none of this would have been possible.

List of Publications

Most of the study presented in this thesis is based on the publications in the following lists.

Chapter 2 consists of the study presented in [1]. Chapter 3 consists of the studies presented in [2]-[6]. Sections 3.1, 3.2, 3.3, 3.4, and 3.5 are based on [2], [3], [4], [5], and [6], respectively. Chapter 4 consists of the study presented in [7].

Papers [8]-[12] are related to Chapter 2, papers [13]-[18] are related to Chapter 3, and papers [19]-[21] are related to Chapter 4.

Publications

[1] H. Miyamoto, T. Niihara, H. Sukeda, M. Takahashi, T. Nakao, M. Ojima and N. Ohta, "Domain and Write-read Characteristics for Magnetic Field Modulated Magneto-optical Disk with High Data Transfer Rate"; J. Appl. Phys. **66**, 6138 (1989)

[2] H. Miyamoto, K. Andoo, T. Niihara, T. Toda, T. Maeda, and M. Ojima, "Application of Domain Duplication to Magneto-optical Recording : Domain Stabilization During Readout on Direct Overwrite Disk"; Jpn. J. Appl. Phys. **35**, 5326 (1996)

[3] H. Miyamoto, T. Toda, H. Ide, A. Saito, K. Andoo, T. Niihara, and M. Ojima, "Thermal Cross-talk on Light Intensity Modulated Magneto-optical Overwriting"; J. Magn. Soc. Jpn. **17**, Suppl. **S1**, 179 (1993)

[4] H. Miyamoto, M. Miyamoto, K. Andoo, T. Niihara, and M. Ojima, "Stabilization of Recorded Domains on Light Power Modulated Magneto-optical Disk with Exchange-coupled Films"; J. Magn. Soc. Jpn. **15**, Suppl. S1, 343 (1991)

[5] H. Miyamoto, K. Andoo, T. Niihara, and M. Ojima, "Overwrite Repeatability of Magneto-optical Exchange-coupled Multilayer"; J. Appl. Phys., **77**, 265 (1995)

[6] H. Miyamoto, M. Ojima, T. Toda, T. Niihara, T. Maeda, J. Saito, H. Matsumoto, T. Hosokawa, and H. Akasaka, "2 GB/130 mm Capacity Direct-Overwrite Magneto-Optical Disk"; Jpn. J. Appl. Phys., **32**, 5457 (1993)

[7] H. Miyamoto, K. Andoo, H. Saga, H. Sukeda, and M. Ojima, "New Readout Technique using Domain Collapse on Magnetic Multilayer"; J. Magn. Soc. Jpn., **19**, Suppl. No. **S1**, 425 (1995).

Related publications and oral presentations

[8] H. Miyamoto, T. Niihara, M. Takahashi, H. Sukeda, M. Ojima, and N. Ohta, "Simulation of Write-Read Characteristics of Overwritable Magneto-Optical Disk"; Dig. Symp. Opt. Memory '88, 49 (1988) (Japanese)

[9] T. Niihara, H. Miyamoto, and R. Suzuki, "Magnetic and Write/Read Properties of NdTbFeCo/TbFeCo Double-layered Film"; Digest of 14th Annual Conf. of Magn. Soc. Jpn., 364 (1990). (Japanese)

[10] T. Niihara, M. Takahashi, H. Miyamoto, F. Kirino, N. Ogihara, an N. Ohta, "Thermomagnetic Recording Mechanism on TbFeCo Disks"; J. Magn. Magn. Materials, **88**, 177 (1990)

[11] H. Sukeda, T. Kaku, T. Niihara, T. Nakao, M. Kasai, H. Miyamoto, K. Akagi, Y. Miyamura, N. Ohta, M. Ojima, F. Tanaka, S. Tanaka, Y. Sasano, K. Ono, and S. Suzuki, Int. Symp. Opt. Memory '89, "Advanced Magneto-optical Disk Drive"; Post-deadline papers Tech. Digest, 28B-22, Sep. (1989).

[12] M. Ojima, H. Sukeda, T. Niihara, T. Nakao, M. Kasai, T. Kaku, H. Miyamoto, K. Akagi, Y. Miyamura, and N. Ohta, "Performance and Reliability of Advanced Magneto-optical Disk Drive"; SPIE, **1316**, 95 (1990).

[13] H. Miyamoto, T. Toda, H. Ide, A. Saitoh, K. Andoo, T. Niihara, and M. Ojima, "Thermal Cross-talk on Light Intensity Modulated Magneto-optical Overwriting"; Tech. Report of IEICE, **MR92-93** (1993) (Japanese)

[14] H. Miyamoto, M. Ojima, T. Toda, T. Niihara, T. Maeda, J. Saito, H. Matsumoto, T. Hosokawa, and H. Akasaka, "2GB/5.25-inches Overwritable Magneto-optical Disk"; Elec. Soc., **MAG-93-176** (1993) (Japanese)

[15] H. Miyamoto, T. Niihara, T. Toda, and R. Suzuki, "Stabilization of Recorded Domains in Reading Process on Light Modulated Overwriting with Exchange Coupled Magnetic Films"; Elec. Soc., **MAG-91-21** (1991) (Japanese)

[16] M. Miyamoto, H. Miyamoto, T. Niihara, K. Andoo and M. Ojima, "Relationship between Laser Power Margin and Thermal Stability of Overwritable Exchange-Coupled MO-Media"; J. Magn. Soc. Jpn., Vol. **17**, Suppl. No. **S1** (1993) p. 339

[17] R. Malmhäll, M. Ojima, H. Awano, T. Niihara, H. Miyamoto, and M. Miyamoto, "Magnetic Spin Directions in Direct Overwrite Exchange-coupled MO Disk"; SPIE, **1663**, 204 (1992)

[18] R. Malmhäll, T. Niihara, H. Miyamoto, and M. Ojima, "Spin Directions in Exchange-Coupled Rare-Earth Transition Metal Double Layer Films with In-Plane Magnetic Intermediate Layer"; Jpn. J. Appl. Phys, **31**, 1050 (1992)

[19] H. Miyamoto, H. Saga, H. Sukeda, K. Andoo, and M. Ojima, "High-density Readout Method using Domain Collapse"; Elec. Soc., **MAG-94-231** (1994) (Japanese)

[20] S. Yonezawa and H. Miyamoto, "Pulsed Laser Irradiated Magnetic Field Modulation Method for High Density Magneto-Optical Disk"; Digest of Symp. on Opt. Memory '94 (SOM'94), 65 (1994)

[21] J. Nakamura, H. Awano, H. Miyamoto, M. Takahashi, and M. Ojima, "Write/Erase Cyclability of Pt/Co Magneto-Optical Disks"; J. Magn. Soc. Jpn., **17**, 809 (1993) (Japanese)